Enclosure 2

MFN 06-229, Supplement 6

Research Report No. VTT-R-04413-06
Estimation and Modeling of Effective Fission Product Decontamination Factor for ESBWR Containment
Part 1, October 2006
and
Part 2, December 2006

Public Versions

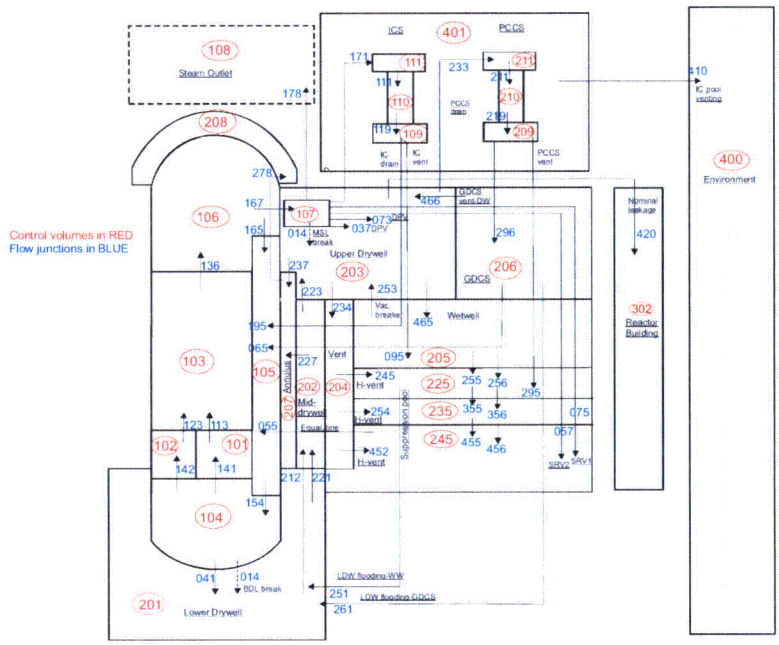

Estimation and Modeling of Effective Fission Product Decontamination Factor for ESBWR Containment – Part 1

Authors

Ilona Lindholm, Ari Auvinen, Yuko Enqvist, Karri Penttilä, Tuomo Sevón, Riitta Zilliacus

Confidentiality

Report's title

Estimation and Modeling of Effective Fission Product Decontamination Factor for ESBWR Containment

Customer, contact person, address	Order reference
GE Nuclear Energy Wayne Marquino 3901 Castle Hayne Road M/C L60 Cube AE-5039 Wilmington, NC 28402 U.S.A.	4431005566
Project name Fission Product/Aerosol Removal model for ESBWR	Project number/Short name 4664/Fission/aerosol removal
Author(s) I. Lindholm, A. Auvinen, Y. Enqvist, K. Penttilä, T. Sevón, R. Zilliacus	Pages 123
Keywords ESBWR, Severe accidents, Source term	Report identification code VTT-R-04413-06

Summary

For assessment of fission product retention in a PCCS a separate 1-D model to calculate particle deposition in tube flow was developed and validated against 1-tube heat exchanger experiments. Both the experimental and modeling results showed that more than 90% of particles can be deposited in PCC, if the steam mass flow rate is low. MELCOR models were also assessed against the 1-tube heat exchanger models and were observed to give conservative estimates in terms of condensation and fission product removal.

A Bottom Drain Line Break scenario with successful depressurization of RCS and reflooding at 6083 s (and a second variation run with reflooding at 7400 s) was calculated to 16 hrs, after which the calculation terminated to fatal convergence error. The value for containment decontamination factor ranges from 1.4 to 3467 on the basis of MELCOR calculation.

The GDCS pool turn acidic at about 12.5 h into the accident due to continuous addition of HCl from the cables and simultaneous loss of water mass due to RPV injection. The pool in the Lower Drywell remains basic due to buffer drainage from the RPV and Suppression Pool remains basic due to sufficient amount of CsOH.

Confidentiality

Espoo 16.10. 2006

Signatures

Ilona Lindholm	Eija Karita Puska	Seppo Vuori
Senior Research Scientist	Senior Research Scientist	Deputy Technology Manager

VTT's contact address

VTT Technical Research Centre of Finland, P.O.Box 1000, FI-02044 VTT, Finland

Distribution (customer and VTT)

GE (customer 2 copies)
VTT (1 copy)

Preface

This report is proprietary report of General Electric Nuclear under the GE Purchase Order No. 4431005566. The contact persons at GE were Mr. Wayne Marquino, Mr. Chris Pratt, Mr. Gilbert Hwang and Mr. Erik Kirsten.

Espoo 16.10.2006

I. Lindholm,
A. Auvinen
Y. Enqvist
K. Penttilä
T. Sevón
R. Zilliacus

Contents

Nomenclature

A	Cross-sectional flow area	[m^2]
C_m, C_s, C_t	constants in Eq. (33), C_m=1.14, C_s=1.17, C_t=2.18	[-]
Cn	Cunningham slip correction factor	[-]
c_p	Heat capacity	[J/kg K]
D	Diffusion coefficient	[m^2/s]
d	Diameter	[m]
d_h	Hydraulic diameter of the heat exchanger tube	[m]
Dep	Total deposition in a tube	[%]
f	Friction factor	[-]
g	Gravitational acceleration	[m/s^2]
H	Enthalpy	[J/kg]
K	Coefficient in Eqs. (32) and (35)	[-]
Kn	Knudsen number, $Kn = \lambda_g / r_p$	[-]
k	Thermal conductivity	[W/m K]
LW	Latent heat	[J/kg]
M	Molecular weight	[g/mol]
mf	Mass fraction	[-]
$\dot{m}$	Mass flow rate	[kg/s]
$\dot{m}_{TL}$	Lower limit of the transition flow regime	[kg/s]
$\dot{m}_{TH}$	Upper limit of the transition flow regime	[kg/s]
$\dot{m}^*_{TL}$	Effective lower limit of the transition flow regime	[kg/s]
$\dot{m}^*_{TH}$	Effective upper limit of the transition flow regime	[kg/s]
$\dot{M} = \begin{bmatrix} 1 \\ \dot{m} \end{bmatrix}$	Steam mass flow rate vector for correlation model	[kg/s]
$\dot{M}^*$	Effective steam mass flow rate vector	
Nu	Nusselt number	[-]
P	Perimeter of the heat exchanger tube	[m]
Pr	Prandtl number	[-]
p	Pressure	[Pa]
q^m_w	Condensation mass flux	[kg/s m^2]
q^T	Heat flux due to the sensible cooling of the gas	[W/m^2]
q^{TS}	Heat flux from the interface to the wall	[W/m^2]
q^{TC}	Heat flux from the wall to the coolant	[W/m^2]
Ra	Rayleigh number	[-]
Re	Reynolds number	[-]
R_g	Gas constant	[N m/mol K]
r	Radius	[m]
Sc	Schmidt number	[-]

Sh	Sherwood number	[-]
$Stef$	Stefan flow correction factor, $Stef = 1/(1-0.5\cdot(\min(mf_w + mf_{ws}, 2 - mf_w - mf_{ws})))$	[-]
T	Average gas temperature	[K]
$\vec{T}$	Average inlet gas temperature vector for correlation model	[K]
T_l	Average liquid film temperature	[K]
T_{ls}	Interface temperature between the gas and the liquid film	[K]
T_{ref}	Reference temperature, $T_{ref} = 273.15$	[K]
T_s	Wall temperature	[K]
T_b	Steam condensation temperature at atmospheric pressure, $T_b = 373.15$	[K]
U	Gas velocity	[m/s]
VF_{H_2O}	Steam volume fraction	[-]
$\overrightarrow{VF}_{H_2O}$	Steam volume fraction vector	[-]
$W = \begin{bmatrix} w_1 \\ w_2 \end{bmatrix}$	Multipliers for the effective steam mass flow rate	
u_p	Particle deposition velocity	[m/s]
u^+	Dimensionless deposition velocity	[-]
x	Mole fraction or tube length	[-] or [m]

Greek symbols

α	Ratio of gas to particle thermal conductivities, $\alpha = k_g / k_p$	[-]
β	Structural diffusion volume	[cm^3/mol]
δ	Liquid film thickness	[m]
γ	Coefficient matrix for steam volume fraction correlation	[-]
Λ	Coefficient matrix for gas temperature and steam mass Flow rate correlation	[-]
λ	Mean free path	[m]
μ	Viscosity	[N/s m^2]
ν	Kinematics viscosity	[m^2/s]
ρ	Density or mass concentration	[kg/m^3]
ρ_w	Mass concentration of water vapor in the gas	[kg/m^3]
ρ_{ws}	The equilibrium vapor mass concentration at the film interface temperature T_{ls}	[kg/m^3]
σ	Surface tension	[N/m]
τ^+	Dimensionless relaxation time	[-]
ζ	Volumetric thermal expansion coefficient	[1/K]

Subscripts

D	based on diameter
g	gas mixture
l	liquid water

m	mixture
n	nitrogen gas
p	particle
w	water vapor
L	laminar flow case
T	turbulent flow case

Superscripts

DPH	diffusiophoresis
TPH	thermophoresis
TUR	turbulent impaction

1 Executive Summary

The purpose of this work is to investigate the capacity of Passive Containment Coolant System Condensers (PCCS) to remove airborne fission products from the containment atmosphere. A specific goal is to determine the decontamination factor of the PCCS units and validate the model against existing experiments. Further aim is to perform source term calculations with the integral MELCOR code in selected accident cases. For minimization of formation of volatile iodine compounds during the severe accidents a high pH in the containment pools is preferable. The estimation of pH in the containment with consideration of buffer injections is being performed with a dedicated analytical equilibrium chemistry tool.

The studied ESBWR plant has a rated power of 4590 MWt and the Reactor Coolant System (RCS) and Containment design is according to ESBWR Design Control Document Tier 1 and 2 rev 1. As to the containment passive safety systems, four double-module units of Isolations Condensers are capable of providing coolant injection to the RCS at high pressure and a total of 6 double-module PCCS provide long term pressure control of the containment. In addition to that an attractive feature of the PCCS is the potential for fission product retention to the heat exchanger tubes and to condensate flow.

The applied MELCOR version is 1.8.6 YK that was released in May 2006. The new features in MELCOR 1.8.6 comprise a more detailed lower head model addressing better the creep rupture failure of lower head. The core melt blockage and relocation model have been enhanced and a stratified molten pool model for lower head has been included. Also more output variables have been added for fission product transport and release results.

The first task was to update existing MELCOR input of ESBWR for the latest MELCOR version 1.8.6YK. The MELCOR model was updated to incorporate the current ESBWR design parameters for this report. The key modifications are the updating of COR input to be compatible with the new models, checking and upgrading of most of the RCS and containment volumes, flow junction and heat structure input, building up of RN package input for radionuclide calculations.

For assessment of fission product retention in a PCCS a separate 1-D model to calculate particle deposition in tube flow was developed as task 2. The model was validated against 1-tube heat exchanger experiments conducted previously at VTT. The model can calculate heat transfer as well as particle deposition by diffusiophoresis and thermophoresis reasonably accurately. Diffusiophoresis and thermophoresis were expected to be the main deposition mechanisms also in the case of PCCS.

Both the experimental and modeling results suggest that deposition by diffusiophoresis could remove as much as 50% of particles from the gas flow. However, aerosol did not accumulate to the heat exchanger. In all experiments condensed water rinsed deposited particles from the tube walls even though particle mass concentration was increased up to 6 g/m^3 (NTP). If steam mass flow rate through the PCCS is 10 kg/s, such concentration would correspond approximately to 75 g/s mass flow rate of particles. Based on experiments conducted at VTT the assumption that deposited particles are entirely rinsed from PCCS by the condensed water is justified.

Particle deposition in a PCC tube was calculated with the developed 1-D model using a wide range of values for steam mass flow rate, gas temperature, pressure, and steam volume fraction and particle size. In the modeling work it was assumed that ICS/PCCS pool would be at boiling temperature around the tubes and steam would be saturated in PCC. The results showed that more than 90% of particles can be deposited in PCC, if the steam mass flow rate is low. In turbulent flow the maximum deposition could be observed to be about 40%.

The aerosol retention models of MELCOR 1.8.6 were also tested against the heat exchanger experiments conducted at VTT. The result was that MELCOR generally underestimated heat transfer and steam condensation rates in the heat exchanger tubes. This is probably the reason why also the aerosol retention was underestimated in comparison to the measured values. In addition, the MELCOR results were compared to the 1-D aerosol deposition model developed in task 2. The 1-D model gives better results for the experiments that involve steam condensation, but MELCOR is better at predicting the aerosol retention in the dry experiments.

A Bottom Drain Line Break scenario with successful depressurization of RCS and reflooding at 6083 s (and a second variation run with reflooding at 7400 s) was calculated to 16 hrs, after which the calculation terminated to fatal convergence error.

The fission product release from the core was for noble gases about 82 %, for Cs 75 % and CsI 82 % of the whole core inventory. The modeled single-hole leakage for containment nominal leakage resulted in release fractions of noble gases, CsOH and CsI to the reactor building to be $5.71 \cdot 10^{-5}$, $1.65 \cdot 10^{-5}$ and $1.68 \cdot 10^{-5}$ of the core release, respectively. At 15.8 h into the accident 13 % of the CsI released from the core was in the Lower Drywell pool, 25 % in the Suppression Pool and 4 % in the water inside the Reactor Pressure Vessel (RPV). A total of 51 % of released CsI was deposited on structures.

When approximating the decontamination factor of CsI aerosol in the PCCS from MELCOR results by dividing the airborne mass entering the PCCS by the airborne mass exiting the PCCS one obtains a decontamination factor varying between 4.4 and 17 during the bulk of the accident time.

The CsI decontamination factor for the whole containment can be defined as the ratio of total CsI released from the RPV divided by the total airborne mass of CsI in the containment. The value for containment decontamination factor ranges from 1.4 to 3467 on the basis of MELCOR calculation.

The pH of the containment pools was calculated with ChemSheet code with the history of mass flow rates and pool masses obtained from MELCOR results and given as boundary conditions to ChemSheet. The formation of HCl due to radiolytical release of Cl from the cable insulations was estimated as a function of dose rate with the method presented in NUREG/CR-5950. The sensitivity of pH to HCl release rate was examined by varying the HCl release rate. The drainage of CsOH with the PCCS condensate flow through the PCCS Drain Line keeps the water in GDCS alkaline in the beginning of the accident as CsOH is highly soluble to water and a strong base. But as the amount of airborne CsOH in the Upper Drywell reduces and GDCS water mass decreases due to injection to the RPV the pH in GDCS is also decreases due to acidic flow from Upper Drywell/PCCS containing soluble HCl. The time range when pH in the GDCS turns to acidic depends on the formation rate of HCl. In the Base Case with a total HCl release of 430 moles, the GDCS shifts from alkaline to acidic at about 12.5 h. In the base case all other pools (Lower Drywell, Wetwell and RPV) remain alkaline.

In the sensitivity runs with the total HCl formation of 131 moles (release rate 0.0015 mol/s) the GDCS shifts from alkaline to acidic at around 11 h with the pH being already 3.95 after 15 h. With the HCl release being 532 moles (release rate of 0.0060 mol/s) the shift from basic to acidic takes place at about 8 h with the pH being 3.31 at 15 h. The initial pH (being neutral or 5.3) seemed to have a negligible effect.

Also with the HCl formation rate of 0.0060 mol/s the water in reactor becomes acidic at around 11 h and with 0.0038 mol/s around 13 h. This is due to high flow rate of acidic water from GDCS.

In all sensitivity runs the pH in Lower Drywell stayed alkaline after buffer solution injection is started (at 6080 s) and the pH in Wetwell was alkaline due to sufficient amount of CsOH.

2 Introduction

The studied ESBWR plant has a rated power of 4590 MWt and the Reactor Coolant System (RCS) and Containment design is according to ESBWR Design Control Document Tier 1 and 2 rev 1. As to the containment passive safety systems, four double-module units of Isolations Condensers are capable of providing coolant injection to the RCS at high pressure and a total of 6 double-module Passive Containment Coolant System Condensers (PCCS) provide long term pressure control of the containment. In addition to that an attractive feature of the PCCS is the potential for fission product retention to the heat exchanger tubes and to condensate flow.

3 Goal

The purpose of this work is to investigate the capacity of PCCS condenser to remove airborne fission products from the containment atmosphere. A specific goal is to determine the decontamination factor of the PCCS units and validate the model against existing experiments. Further aim is to perform source term calculations with the integral MELCOR code in selected accident cases. For minimization of formation of volatile iodine compounds during the severe accidents a high pH in the containment pools is preferable. The estimation of pH in the containment with consideration of buffer injections is being performed with a dedicated analytical equilibrium chemistry tool.

4 Description of ESBWR plant model for MELCOR 1.8.6

The applied MELCOR version is 1.8.6 YK that was released in May 2006. The new features in MELCOR 1.8.6 comprise a more detailed lower head model addressing better the creep rupture failure of lower head. The core melt blockage and relocation model have been enhanced and a stratified molten pool model for lower head has been included. Also more output variables have been added for fission product transport and release results.

4.1 Reactor Core

The reactor core nodalization is depicted in Figure 1. The core region is divided into 6 radial rings and 14 axial levels. The radial rings in the active core region have equal cross-section area. The ring 6 is for lower head modeling and the ring 6 cells above the elevation of the bottom of downcomer (=1.544 m) are dummy. The lower head model is a new feature in MELCOR version 1.8.6. Tables 1, 2 and 3 collect the applied parameters in the COR model. The full core decay heat curve is given as a tabular function power vs. time and represents the situation of a full core at the end of cycle.

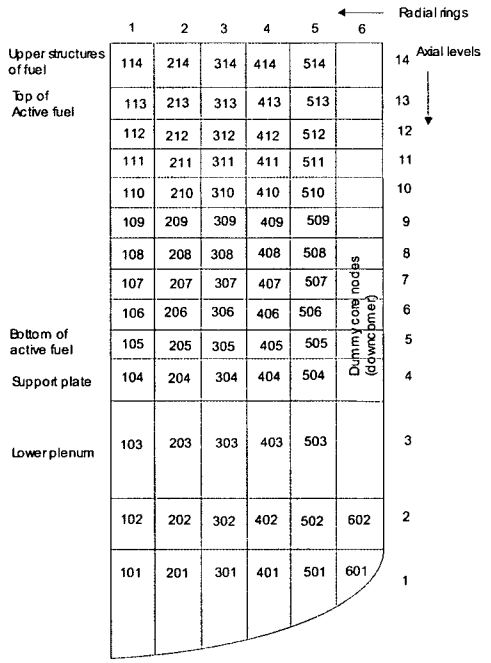

Figure 1. *Schematic description of the COR model.*

Table 1. *Applied ESBWR core data in the MELCOR 1.8.6 code*

Item	Data in the MELCOR 1.8.6 input	Data source
Outer radius of fuel pellet	[[ ]]	MELCOR input (2001)
Outer radius of cladding	[[ ]]	MELCOR input (2001)
Thickness of gap between the pellet and the cladding	[[ ]]	MELCOR input (2001)
Center-to-center spacing of fuel rods	[[ ]]	MELCOR input (2001)
Thickness of canister wall	[[ ]]	MELCOR input (2001)
Outer radius of core region	[[ ]]	DRF 0000-0037-2687
Radius of curvature of inside of the lower head	[[ ]]	DRF 0000-0037-2687
Inner radius of RPV cylinder	[[ ]]	DRF 0000-0037-2687
Thickness of cylindrical vessel wall	[[ ]]	DRF 0000-0037-2687
Thickness of lower head	[[ ]]	DRF 0000-0037-2687
Elevation of baffle plate	[[ ]]	DRF 0000-0037-2687
Elevation of (top of) lower core support plate	[[ ]]	DRF 0000-0037-2687
Elevation at top of active fuel	[[ ]]	DRF 0000-0037-2687
Elevation at top of core region	[[ ]]	DRF 0000-0037-2687
Total mass of UO_2	[[ ]]	ORIGEN calculation by GE
Total mass of Zircaloy (cladding)	[[ ]]	calculated from rod data
Total mass of Zircaloy (canisters)	[[ ]]	calculated from canister data, DCD Tier 2, chapter 1
Total mass of stainless steel in active core	[[ ]]	
Total mass of B_4C	[[ ]]	
Mass of core support plate	[[ ]]	estimated from DRF 0000-0037-2687 data
Mass of control rod guide tubes	[[ ]]	MELCOR 2001 input
Support plate thickness	[[ ]]	DRF 0000-0037-2687

Table 2. *Core radial data.*

Core ring	Outer radius of ring (m)	Data source	Power peaking factor	Data source
1	[[ ]]	calculated*	[[ ]]	DCD Tier 2, Chapter 4
2	[[ ]]	calculated*	[[ ]]	DCD Tier 2, Chapter 4
3	[[ ]]	calculated*	[[ ]]	DCD Tier 2, Chapter 4
4	[[ ]]	calculated*	[[ ]]	DCD Tier 2, Chapter 4
5	[[ ]]	DRF 0000-0037-2687	[[ ]]	DCD Tier 2, Chapter 4
6	[[ ]]	DRF 0000-0037-2687	[[ ]]	DCD, Tier 2, Chapter 1

* The assumption that A1=A2=A3=A4=A5

Table 3. *Axial core input data.*

Axial level	Elevation at the bottom of cell (m)	height of cell (m)	Channel flow area per ring (m^2)	Bypass flow area per ring (m^2)	Axial power peaking factor	Data source
1	[[					MELCOR 2001 input, DCD Tier 2, Chapter 4
2						MELCOR 2001 input, DCD Tier 2, Chapter 4
3						MELCOR 2001 input, DCD Tier 2, Chapter 4
4						MELCOR 2001 input, DCD Tier 2, Chapter 4
5						MELCOR 2001 input, DCD Tier 2, Chapter 4
6						MELCOR 2001 input, DCD Tier 2, Chapter 4
7						MELCOR 2001 input, DCD Tier 2, Chapter 4
8						MELCOR 2001 input, DCD Tier 2, Chapter 4
9						MELCOR 2001 input, DCD Tier 2, Chapter 4
10						MELCOR 2001 input, DCD Tier 2, Chapter 4
11						MELCOR 2001 input, DCD Tier 2, Chapter 4
12						MELCOR 2001 input, DCD Tier 2, Chapter 4
13						MELCOR 2001 input, DCD Tier 2, Chapter 4
14					]]	MELCOR 2001 input, DCD Tier 2, Chapter 4

4.2 Reactor Coolant System volumes and flow paths

The reactor coolant system and containment nodalization of ESBWR for MELCOR 1.8.6 input are depicted in Fig. 2. The total volume of reactor pressure vessel nodes in the MELCOR 1.8.6 input is 942.126 m^3. The total volume of RPV in (Figure 5.1-1 in [1]) is 959 m^3. Tables 4, 5 and 6 gather the key input data for RCS nodalization and flow paths. The operation logic of valves connected to different flow paths is discussed in Chapter 4.6 of this report.

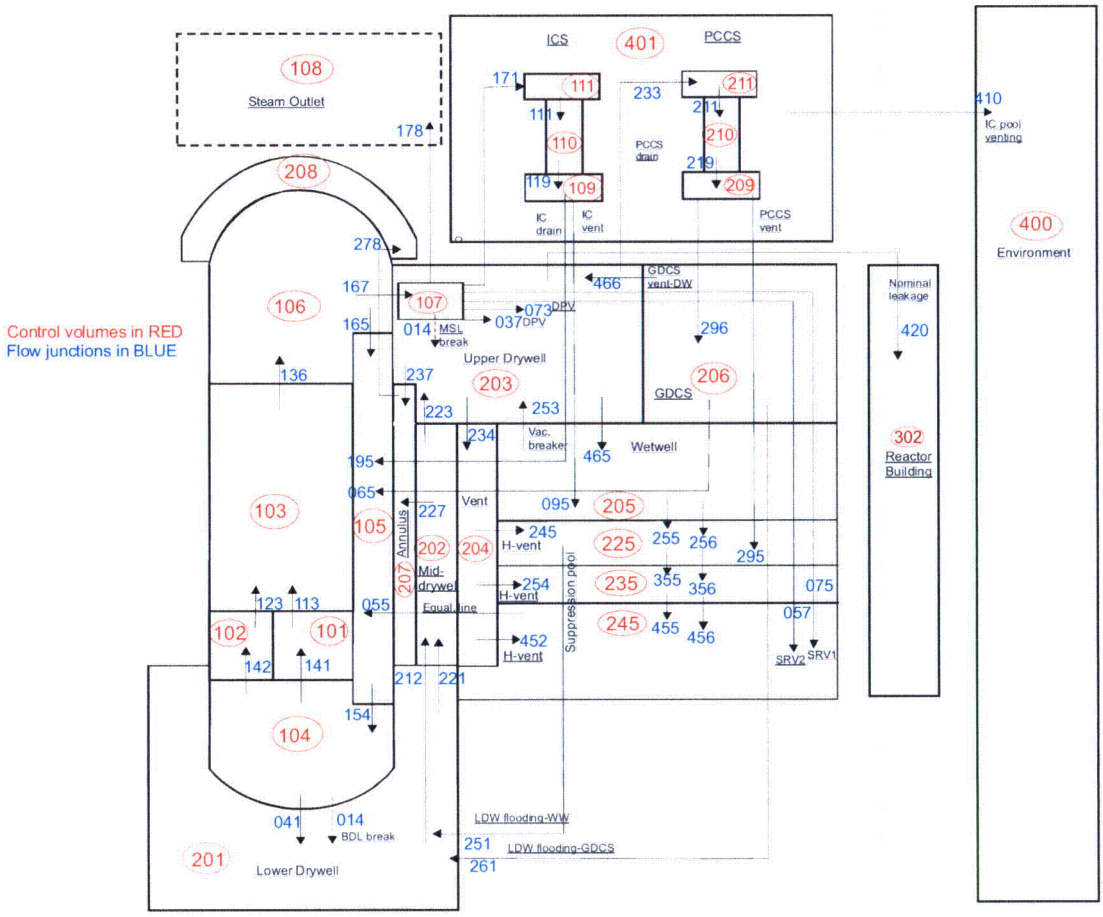

Figure 2. *MELCOR 1.8.6 control volume and flow junction scheme of ESBWR model.*

Table 4. *Control volumes of reactor coolant system.*

Control volume name	Control volume node	Elevation vs. volume of node		Volume of pool (m^3)	Initial temperature		Initial pressure (MPa)	Data source
		elev. (m)	vol. (m^3)		T_{atm}(K)	T_{pool}(K)		
Core	101	7.896 7.4533 4.405	59.46681 42.9312 0.0	43.0	sat.	sat.	7.21	DRF 0000-0037-2687 & ESBWR DCD Tier 2, Ch. 6 rev1
Bypass	102	7.896 7.4533 4.405	54.138 39.08414 0.0	54.138	-	551.82	7.21	DRF 0000-0037-2687 & ESBWR DCD Tier 2, Ch. 6 rev1
Chimney	103	16.51 7.896	255.6355 0.0	66.79	sat.	sat.	7.21	DRF 0000-0037-2687 & ESBWR DCD Tier 2, Ch. 6 rev1
Lower plenum	104	4.405 4.0105 2.365 0.0	136.0938 123.6317 71.65127 0.0	136.09	-	550.9	7.21	DRF 0000-0037-2687 & ESBWR DCD Tier 2, Ch. 6 rev1
Downcomer	105	22.276 19.540 16.365 7.896 2.365	147.0625 135.2081 115.1544 39.2945 0.0	147.0625	sat.	488.8	7.21	DRF 0000-0037-2687 & ESBWR DCD Tier 2, Ch. 6 rev1
Upper plenum	106	27.56 25.24 19.5278 16.51	289.7294 226.2726 54.8177 0.0	26.862	sat.	sat.	7.17	DRF 0000-0037-2687 & ESBWR DCD Tier 2, Ch. 6 rev1
Main steam line	107	23.58 22.08	27.25 0.0	-	sat.	-	7.0881	DRF 0000-0037-2687 & ESBWR DCD Tier 2, Ch. 6 rev1
Steam outlet (*	108	30.0 20.0	$1 \cdot 10^8$	-	sat.	-	2.0	

(* steam outlet is an arbitrarily large volume representing turbine bypass

Table 5. *Isolation condenser system (ICS) control volumes.*

Control vol. name	Control vol. number	Elevation vs. volume table		Volume of pool (m^3)	Initial temperature		Initial pressure (MPa)	Data source
		Elev. (m)	Vol. (m^3)		T_{atm}(K)	T_{pool}(K)		
IC steam box	111	29.95 29.185	4.01 0.0	4.01	sat.	sat.	7.088	MFN 05-122 & MFN 06-003
IC tubes	110	29.185 27.385	2.173 0.0	2.0	sat.	sat.	7.088	MFN 05-122 & MFN 06-003
IC water box	109	27.385 26.755	4.077 0.0	4.075	sat.	sat.	7.088	MFN 05-122 & MFN 06-003

Table 6. *Flow paths between RCS volumes*

Flow path no	From volume	To volume	from elevation (m)	To elevation (m)	Flow area (m^2)	length (m)	fraction open	Data source
RPV flow paths								
113	core	chimney	7.896	7.896	S0: 9.48 S1: 15.858	0.914 1.356	1.0	MELCOR 2001 input and DCD, Chapter 4
123	bypass	chimney	7.896	7.896	8.503	1.649	1.0	MELCOR 2001 input and DCD, Chapter 4
136	chimney	upper plenum	16.51	16.51	S0: 32.94 S1: 49.253 S2: 7.761 S3: 11.533 S4: 38.114	8.008 1.156 3.381 0.779 5.141	1.0	MELCOR 2001 input and DCD, Chapter 4
165	upper plenum	downcomer	21.91	21.91	S0: 20.388 S1: 33.977	2.845 2.470	1.0	MELCOR 2001 input and DCD, Chapter 4
154	downcomer	lower plenum	2.365	2.365	S0: 6.647 S1: 6.647 S2: 8.191 S3: 7.522	5.118 2.890 1.815 4.272	1.0	MELCOR 2001 input and DCD, Chapter 4
141	lower plenum	core	4.405	4.405	S0: 0.317 S1: 11.835	0.094 1.142	1.0	DCD, Ch. 4 & 6
142	lower plenum	bypass	4.405	4.405	S0: 26.83 S1: 0.166 S2: 8.503	2.145 1.327 1.649	1.0	DCD, Ch. 4 & 6
167	upper plenum	main steam line	22.83	22.83	S0: 0.3932 S1: 1.283	2.129 5.128	1.0	DCD, Ch. 4 & 6
178	main steam line	steam outlet	22.83	22.83	0.4276	7.543	valve (CF178)	DCD, Tier 2, Ch. 6
ICS flow paths								
195	IC water box	downcomer	26.755	13.025	0.1004	32.5	valve (CF195)	MFN 05-122
171	upper plenum	IC steam box	21.91	29.95	0.3936	31.5	1.0	MFN 05-122
111	IC steam box	IC tubes	29.29	29.185	1.207	0.8	1.0	MFN 05-122
119	IC tubes	IC water box	27.385	27.385	1.207	0.8	1.0	MFN 05-122
ECCS injection flow paths								
065	GDCS pool	downcomer	17.8	8.453	0.0912	10.57	valve (CF265)	DCD, Tier 2, Ch. 6
055	Suppression pool bottom	downcomer	8.453	8.453	0.0912	2.89	valve (CF070)	DCD, Tier 2, Ch. 6
RPV pressure control flow paths								
075	main steam line	suppression pool bottom	22.83	6.494	0. 0673	14.795	valve (CF075)	DCD, Tier 2, Ch. 6
057	main steam line	suppression pool bottom	22.83	6.494	0.0673	14.795	valve (CF057)	DCD, Tier 2, Ch. 6
073	upper plenum	upper drywell	21.91	22.83	0.1224	0.2	valve (CF273)	DCD, Tier 2, Ch. 6
037	upper plenum	upper drywell	21.91	22.83	0.1224	0.2	valve (CF237)	DCD, Tier 2, Ch. 6
095	IC water box	Wetwell	27.355	9.533	0.00278	27.3	valve (CF095)	MFN 05-122
014	lower plenum	lower drywell	0.0	-0.212	$2.165 \cdot 10^{-3}$	0.3	valve (CF142)	model assumption
041	lower plenum	lower drywell	0.0	-0.212	1.0	0.212	valve (CF141)	model assumption

4.3 Containment

The total gas space volume of the containment in the MELCOR 1.8.6 model is 13 580 m^3 and water pool volume 6288 m^3. The detailed description of the containment control volumes is given in Tables 7 and 8.

Table 7. *Containment control volumes.*

Control vol. name	Control vol. number	Elevation vs. volume table		Volume of pool (m^3)	Initial temperature (K)		Initial pressure (MPa)	Data source
		elev. (m)	Vol. (m^3)		atm.	pool		
Lower drywell	201	7.443 -8.8	1190 0.0	-	330	-	0.1013	ESBWR DCD Tier 2, Ch. 6, rev 1
Central drywell	202	17.5 7.443	713.56 0.0	-	330	-	0.1013	ESBWR DCD Tier 2, Ch. 6, rev 1
Upper drywell	203	24.6 17.5	5302.44 0.0	-	330	-	0.1013	ESBWR DCD Tier 2, Ch. 6, rev 1
Vents	204	17.5 10.1 4.65	174.76 74.12 0.0	74.12	316	330.	0.1013	ESBWR DCD Tier 2, Ch. 6, rev 1
Wetwell	205	16.9 10.1 9.4	5991.3 559.3 0.0	559.3	300.	300.	0.1013	ESBWR DCD Tier 2, Ch. 6, rev 1
Suppression pool upper	225	9.4 8.1	1038.7 0.0	1038.7	-	300	0.1130	ESBWR DCD Tier 2, Ch. 6, rev 1
Suppression pool middle	235	8.1 6.7	1118.0 0.0	1118.6	-	300.	0.1238	ESBWR DCD Tier 2, Ch. 6, rev 1
Suppression pool bottom	245	6.7 4.65	1637.95 0.0	1637.95	-	300.	0.1374	ESBWR DCD Tier 2, Ch. 6, rev 1
GDCS	206	24.6 24.1 17.5	1999.4 1859.0 0.0	1859.0	300.	300.	0.1013	ESBWR DCD Tier 2, Ch. 6, rev 1
Annulus	207	21.85 7.443	349.46 0.0	-	340.	-	0.1013	ESBWR DCD Tier 2, Ch. 6, rev 1
Head	208	35.35 29.35 21.85	277.0 68.254 0.0	-	330.	-	0.1013	ESBWR DCD Tier 2, Ch. 6, rev 1

Table 8. *Passive Containment Cooling System (PCCS) control volumes.*

Control vol. name	Control vol. number	Elevation vs. volume table		Volume of pool (m^3)	Initial temperature		Initial pressure (MPa)	Data source
		Elev. (m).	Vol. (m^3)		T_{atm}(K)	T_{pool}(K)		
PCC steam box	211	30.22 28.90	12.96 0.0	-	300	-	0.1013	MFN 05-122 & MFN 06-003
PCC tubes	210	28.90 27.563	12.94 0.0	-	300.	-	0.1013	MFN 05-122 & MFN 06-003
PCC water box	209	27.563 26.243	12.96 0.0	-	300.	-	0.1013	MFN 05-122 & MFN 06-003

Table 9. *Containment flow paths.*

Flow path no	From volume	To volume	from elevation (m)	To elevation (m)	Flow area (m^2)	length (m)	fraction open	Data source
212	lower drywell	mid drywell	-8.256	7.443	0.01634	14.2	1.0	DCD Tier 2, Chapter 6, MELCOR 2001 input
221	lower drywell	mid drywell	6.4	7.443	7.98	1.0	1.0	DCD Tier 2, Chapter 6, MELCOR 2001 input
223	mid drywell	upper drywell	17.5	17.5	42.0	8.4	1.0	DCD Tier 2, Chapter 6, MELCOR 2001 input
227	mid drywell	annulus	9.379	9.379	6.92	0.15	1.0	DCD Tier 2, Chapter 6, MELCOR 2001 input
234	upper drywell	vent	17.5	17.5	9.05	9.56	1.0	DCD Tier 2, Chapter 6, MELCOR 2001 input
237	upper drywell	annulus	21.85	21.85	8.04	0.15	1.0	DCD Tier 2, Chapter 6, MELCOR 2001 input
465	upper drywell	Wetwell	21.05	15.0	0.0001	6.05	1.0	DCD Tier 2, Chapter 6
466	GDCS	upper drywell	24.45	24.45	17.63	1.0	1.0	MFN 05-122
245	vent	suppression pool-upper	8.493	8.493	S0: 11.31 S1: 3.85	1.21	1.0	DCD Tier 2, Chapter 6
254	vent	suppression pool-middle	7.123	7.123	S0: 11.31 S1: 3.85	1.68	valve (CF358)	DCD Tier 2, Chapter 6
452	vent	suppression pool-bottom	5.753	5.753	S0: 11.31 S1: 3.85	2.14	valve (CF458)	DCD Tier 2, Chapter 6
255	Wetwell	suppression pool-upper	9.91	9.4	600.0	1.6	1.0	model assumption
256	Wetwell	suppression pool-upper	9.71	9.2	600.	1.6	valve (CF259)	model assumption
355	suppression pool-upper	suppression pool-middle	8.75	8.1	600.	1.6	1.0	model assumption
356	suppression pool-upper	suppression pool-middle	8.55	7.9	600.	1.6	valve (CF365)	model assumption
455	suppression pool-middle	suppression pool-bottom	7.4	6.7	600.	1.6	1.0	model assumption
456	suppression pool-middle	suppression pool-bottom	7.2	6.5	600.	1.6	valve (CF465)	model assumption
251	suppression pool upper	lower drywell	8.45	-6.565	0.01634	13.56	valve (CF253)	model assumption
253	Wetwell	upper drywell	16.9	17.5	1.13	1.61	valve (CF255)	DCD Tier 2, Ch. 6
261	GDCS	lower drywell	17.8	-6.565	0.01634	23.68	valve (CF263)	DCD Tier 2, Ch. 6
278	annulus	upper head	21.85	21.85	$1 \cdot 10^{-4}$	0.1	1.0	
PCC flow paths								
296	PCC water box	GDCS pool	27.01	21.538	0.10603	11.0	1.0	MFN 05-122 & MFN 06-003
295	PCC water box	Wetwell	27.67	9.350	0.3040	24.5	1.0	MFN 05-122 & MFN 06-003 & comm. with GE
233	upper drywell	PCC steam box	24.6	30.88	0.2945	S0:8.15 S1: 2.9	1.0	MFN 05-122 & MFN 06-003
211	PCC steam box	PCC tubes	29.56	29.56	6.81	0.8	1.0	MFN 05-122 & MFN 06-003
219	PCC tubes	PCC water box	28.33	28.33	6.81	0.8	1.0	MFN 05-122 & MFN 06-003

4.4 Reactor building and environment volumes

The current MELCOR model has one control volume representing the whole reactor building. It is defined to be an artificially large volume to provide constant down stream thermal hydraulic conditions. Refueling pool volume is presented as a separate control volume. The water pool housing ICS and PCCS condensers is modeled as single large pool. The environment is modeled as a large control volume for purposes of being a heat sink to containment outer walls and a receiving volume for possible source term.

Table 10. *Reactor building and environment control volumes.*

Control vol. name	Control vol. number	Elevation vs. volume table		Volume of pool (m^3)	Initial temperature		Initial pressure (MPa)	Data source
		Elev. (m)	Vol. (m^3)		T_{atm} (K)	T_{pool} (K)		
Refuel floor	301	45.695 33.505 33.205 26.6	15540. 758.24 725.3 0.0	725.3	300	300	0.1013	MELCOR 2001 input
Reactor building	302	50.0 -10.3	$1 \cdot 10^8$ 0.0	-	300.	-	0.1013	model assumption
Environment	400	50.0 -20.0	$1 \cdot 10^8$ 0.0	-	300.	-	0.1013	model assumption
IC pool	401	33.7 28.65 26.0	6100. 3180. 0.0	4900.	300.	300.	0.1013	DCD, Tier 2, Ch. 6

Table 11. *Reactor building and environment flow paths.*

Flow path no	From volume	To volume	from elevation (m)	To elevation (m)	Flow area (m^2)	length (m)	fraction open	Data source
410	ICS pool	environment	33.7	40.0	1.131	30.0	1.0	Estimated from DCD, Tier 2, Ch. 6 data
420	Upper drywell	reactor building	24.0	24.0	$1.949 \cdot 10^{-6}$	1.0	1.0	area calculated from Bernoulli's equation (0.5 % of containment volume per day at 310 kPa)

4.5 Heat structures

The heat structures act as heat sinks according to their material characteristics and as deposition surfaces for fission product aerosols according to their geometric alignment.

Table 12. *Reactor coolant system and containment heat structures.*

Heat structure number	name	bottom elevation (m)	top elevation (m)	area (m^2)	thickness (m)	material	type/ orientation	
10002	shroud level 2	4.0105	4.405	7.86	0.05	SS	vertical cylinder	DCD Tier 2, Ch. 4,5,6 and model assumptions
10003	shroud level 3	4.405	4.7437	6.74825	0.05	SS	vertical cylinder	same as above
10004	shroud level 4	4.7437	5.0824	6.74825	0.05	SS	vertical cylinder	same as above
10005	shroud level 5	5.0824	5.4211	6.74825	0.05	SS	vertical cylinder	same as above
10005	shroud level 6	5.4211	5.7598	6.74825	0.05	SS	vertical cylinder	same as above
10007	shroud level 7	5.7598	6.0985	6.74825	0.05	SS	vertical cylinder	same as above
10008	shroud level 8	6.0985	6.4372	6.74825	0.05	SS	vertical cylinder	same as above
10009	shroud level 9	6.4372	6.7759	6.74825	0.05	SS	vertical cylinder	same as above
10010	shroud level 10	6.7759	7.1146	6.74825	0.05	SS	vertical cylinder	same as above
10011	shroud level 11	7.1146	7.4533	6.74825	0.05	SS	vertical cylinder	same as above
10012	shroud level 12	7.4533	7.896	8.8203	0.05	SS	vertical cylinder	same as above
10305	chimney shroud	7.896	16.51	171.625	0.05	SS	vertical cylinder	same as above
11003	top guide ring 1	7.896	8.076	6.285	0.18	SS	horizontal slab	same as above
12003	top guide ring 2	7.896	8.076	6.285	0.18	SS	horizontal slab	same as above
13003	top guide ring 3	7.896	8.076	6.285	0.18	SS	horizontal slab	same as above
14003	top guide ring 4	7.896	8.076	6.285	0.18	SS	horizontal slab	same as above
15003	top guide ring 5	7.896	8.076	6.285	0.18	SS	horizontal slab	same as above
RCS to containment heat structures								
10001	shroud level 1	2.365	4.0105	32.785	0.05	SS	vertical cylinder	same as above
15207	vessel	7.443	20.259	285.865	0.154	SS	vertical cylinder	same as above
16208	vessel head	22.84	23.84	79.452	0.154	SS	upper hemisphere	same as above
ICS heat structures								
11041	IC tubes	27.385	29.185	0.28727 x 810	0.0023	SS	vertical cylinder manifold (810 tubes)	MFN 06-003

Containment heat structures								
25160	GDCS floor	16.9	18.5	234.2	1.6	concrete	horizontal slab	MELCOR 2001 input and estimation from DCD, Tier 2, Chapter 6
25130	Upper drywell floor	16.9	18.5	484.25	1.6	concrete	horizontal slab	same as above
26130	GDCS wall	17.5	23.55	338.32	0.2	concrete	vertical cylinder	same as above
22170	Lower biological shield	7.443	17.5	302.68	0.016	SS	vertical cylinder	same as above
23170	central biological shield	17.5	21.85	130.92	0.016	SS	vertical cylinder	same as above
25220	vent wall 1	10.443	16.9	267.77	1.6	concrete	vertical cylinder	same as above
25221	vent wall 2	9.4	10.4	41.47	1.6	concrete	vertical cylinder	same as above
26210	GDCS ceiling	24.6	26.6	50.64	2.0	concrete	horizontal slab	same as above
23210	Upper drywell ceiling	24.6	26.6	781.4	2.0	concrete	horizontal slab	same as above
28220	Drywell head	26.6	32.76	226.195	0.16	SS	upper hemisphere	same as above
25310	SP-RB wall	9.4	20.4	103.67	2.0	concrete	vertical cylinder	same as above
25311	WW-RB wall	10.44	16.9	669.72	2.0	concrete	vertical cylinder	same as above
25313	WW floor	2.65	10.75	633.63	2.35	concrete	horizontal slab	same as above
33401	LDW-HCU wall	-8.8	2.6	637.49	2.0	concrete	vertical cylinder	same as above
25320	LDW floor	-8.8	-6.8	116.9	2.0	concrete	horizontal slab	added (ESBWR DCD Tier 2)
25321	MID-DW floor	7.443	9.443	70.9	1.0	concrete	horizontal slab	added (ESBWR DCD Tier 2)
25323	Shield ann. floor	7.443	8.043	24.2	0.6	concrete	horizontal slab	added (ESBWR DCD Tier 2)
PCCS heat structures								
21041	PCC tubes top	28.2315	28.90	0.10669 (x3360)	0.00165	SS	vertical cylinder manifold (3360 tubes)	MFN 06-003 & MFN05-122
21042	PCC tubes bottom	27.563	28.2315	0.10669 (x3360)	0.00165	SS	vertical cylinder manifold (3360 tubes)	MFN 06-003 & MFN05-122

4.6 Engineered Safety Features

4.6.1 Isolation condenser system (ICS)

ICS drain line is modeled with valve operation. ICS drain line opens fully when Main Steam Line Valve has closed (in 4.2 s following a scram signal). ICS vent line is modeled to remain closed until a user-specified time is reached.

4.6.2 Passive Containment Cooling System (PCCS)

PCCS Drain Line has a loop seal at the pipe end in the GDCS pool. The Drain Line is modeled with a normal vertical flow junction.

The PCCS Vent line is modeled as vertical flow junction between the PCCS water box and the Suppression Pool. [[

]]

4.6.3 GDCS injection to RPV Downcomer

Coolant injection from the GDCS pool is modeled to start at a user-specified time. In the calculation of scenario 1 the start of reflooding was set initially set to 7400 s and in a second run variation to 6083 s. The GDCS line opening fraction can be varied, in the Scenario 1 calculation it was defined to be 100 % of full area.

4.6.4 Equalization line injection from Suppression pool to RPV downcomer

The opening of Equalization Line is modeled to occur after a user-specified time delay has the beginning of the core oxidation and the boiled-up water level in the downcomer of the Reactor Pressure Vessel (RPV) has fallen below level L1 (11.0 m from the bottom of RPV). In the Bottom Drain Line Break scenario, the opening of Equalization Line was set to occur simultaneously with the start of GDCS injection.

4.6.5 Safety Relief Valves (SRV#1 and SRV #2)

Two separate Safety Relief Valve Lines (SRV) are modeled. The SRV #1 and SRV #2 open when the pressure in the Upper Plenum of the RPV exceeds 8.723 MPa and closes when Upper Plenum Pressure decreases below 8.045 MPa. If the water level in the downcomer is below level L1, SRV#1 opens fully and stays open in 10 s and SRV#2 in 55 s, respectively. The flow areas of both SRV junctions are equal. [[

]]

4.6.6 Depressurization Valves (DPV#1 and DPV#2)

Two separate RPV Depressurization Lines are modeled. The DPV#1 opens fully with a 100-s delay from the level L1 signal. DPV#2 opens respectively with 145-s delay from the level L1 signal. The flow areas of the two valves are equal.

4.6.7 Lower Drywell Flooding from Wetwell and GDCS Pool

The Lower Drywell flooding from the Wetwell and GDCS Pool start, when the gas temperature in the Lower Drywell exceeds 533 K.

4.6.8 Vacuum Breakers

The Vacuum Breakers open fully when the Wetwell pressure exceeds the Drywell pressure by 3445 Pa. In addition to Vacuum Breakers the Wetwell airspace is connected to the Drywell airspace via a small leakage flow path ($A=1\cdot10^{-4}$ m^2).

4.7 Decay heat

The operating power of the reactor is defined in the input to be $4.59\cdot10^9$ W, which is 102 % of the rated power. The decay heat is defined as a Tabular Function of power vs. time through input (Table 13). MELCOR interpolates the values of power between the given time points. The reactor shutdown time is currently determined to be at time 0.

Table 13. *Decay heat vs. time used in MELCOR input for ESBWR.*

Time from scram (s)	Decay heat (W)
0.0	$4.5900\cdot10^9$
0.1	$4.5097\cdot10^9$
0.6	$2.6806\cdot10^9$
1.0	$1.5298\cdot10^9$
6.0	$2.6314\cdot10^8$
10.0	$2.2592\cdot10^8$
60.0	$1.5946\cdot10^8$
100.0	$2.4367\cdot10^8$
600.0	$1.0148\cdot10^8$
1000.0	$8.9872\cdot10^7$
2000.0	$7.3624\cdot10^7$
4000.0	$5.8981\cdot10^7$
6000.0	$5.2051\cdot10^7$
8000.0	$4.7920\cdot10^7$
10000.0	$4.5083\cdot10^7$
20000.0	$3.9635\cdot10^7$
40000.0	$3.3530\cdot10^7$
60000.0	$3.0252\cdot10^7$
86400.0	$2.7416\cdot10^7$
100000.0	$2.6314\cdot10^7$
150000.0	$2.3340\cdot10^7$
172800.0	$2.2326\cdot10^7$

All default fission product classes in the MELCOR 1.8.6 are used in the ESBWR model. The total masses of fission products in each class are defined to be the default values of MELCOR. The initial masses of the fission product classes were updated according to ORIGEN calculations for ESBWR specific core.

Iodine and Cesium are assumed to form CsI following the release from the fuel. The excess Cs is assumed to be as CsOH. Table 14 shows the distribution different radionuclide elements into default radionuclide classes used for fission product transport and deposition models.

Table 14. *Applied default classification of fission product elements and Initial fission product class masses.*

Fission product class	Representative class element	Initial mass (kg)	Elements in the class
1	Xe	827.4	He, Ne, Ar, Kr, Xe, Rn, H, N
2	Cs	496.4	Li, Na, K, Rb, Cs, Fr, Cu
3	Ba	363.0	Be, Mg, Ca, Sr, Ba, Ra, Es, Fm
4	I	37.27	F, Cl, Br, I, At
5	Te	77.6	O, S, Se, Te, Po
6	Ru	555.4	Ru, Rh, Pd, Re, Os, Ir, Pt, Au, Ni
7	Mo	662.8	V, Cr, Fe, Co, Mn, Nb, Mo, Tc, Ta, W
8	Ce	1227.6	Ti, Zr, Hf, Ce, Th, Pa, Np, Pu, C
9	La	1019.7	Al, Sc, Y, La, Ac, Pr, Nd, Pm, Sm, Eu, Gd, Tb, Dy, Ho, Er, Tm, Yb, Lu, Am, Cm, Bk, Cf
10	U	136 000	U
11	Cd	5.07	Cd, Hg, Zn, As, Sb, Pb, Tl, Bi
12	Sn	24.7	Ga, Ge, In, Sn, Ag
13	B	0	B, Si, P
14	H_2O	0	H_2O
15	concrete	0	--
16*	CsI	0	CsI

* when all iodine is assumed to combine with Cs to form CsI, the equivalent whole core inventory of CsI is 76.3 kg.

4.8 Fission product release and transport

The release of fission products from the fuel is calculated with CORSOR-M model with multiplication with surface-to-volume ratio. The default number (10) of aerosol size sections are used in the calculation. The hygroscopicity model is activated.

Fission products were assumed to be initially evenly distributed in the fuel in the core rings. The fission product release in the gap in the beginning of the calculation was 5% for noble gases (class 1), Cs (class 2) and I (class 4). For the other classes the initial gap release was 0. The initial gap inventory is according to the specification for BWR core inventory gap release in [2]. The fission product release to the reactor coolant system begins, when the specified failure temperature (1173 K) is reached in the cladding. Once the failure temperature is reached at any axial level of a core radial ring, the whole airborne inventory in that radial ring is released.

All heat structures act as deposition surfaces according to their defined orientation. The PCCS tube walls were modeled as cylindrical heat structures and a floor heat structure was defined for PCC water box. PCC steam box and the tube volume have no horizontal heat slabs. An aerosol settling area equal to the total cross section area of the tube bundle is defined for aerosol settling by gravitation from steam box volume to tube volume and from tube volume to water box, respectively.

The fission product pool scrubbing model (SPARC) is activated in the SRV Lines, in the IC Drain Line in the IC Vent Line in the Horizontal Vent Lines in the Lower Drywell flooding lines and in the PCC Drain Line and in the PCC Vent Line flow junctions.

5 Model for fission Product Removal in Passive Containment Cooling System Modules

A detailed, specific model for fission product removal in PCCS was developed. The model was validated against 1-tube heat exchanger experiments performed at VTT. The model was then applied to full scale PCCS geometry to evaluate the effect of key modeling parameters to fission product retention. A decontamination factor for PCCS was estimated. Further, easily usable correlation models were developed.

Also the 1-tube experiments were calculated with MELCOR using the same type of input as applied in the ESBWR model, i.e. describing the operation of a PCCS with control volume, flow path and heat structure input (not the CND model). The results were compared to the measured values.

The theoretical basis of the separate, detailed fission product modeling is given in the next.

5.1 The description of the modeling principles

5.1.1 Heat and mass transfer

The heat and mass fluxes of the system were estimated using a simple plug flow balance model with appropriate Nusselt (*Nu*) and Sherwood (*Sh*) numbers, [3]. The energy balance for the gas and the water film are expressed as:

$$\frac{d\left(\dot{m}_w H_w + \dot{m}_n H_n\right)}{dx} = -P\left(q_w^m H_w + q^T\right) \tag{1}$$

and

$$\frac{d\left(\dot{m}_l H_l\right)}{dx} = P\left(q_w^m H_w + q^T - q^{TS}\right) \tag{2}$$

where

$$\left(\dot{m}_w H_w\right) = \dot{m}_w\left(\int_{T_{ref}}^{T_b} c_{pl}\,dT + LW_{T_b} + \int_{T_b}^{T} c_{pw}\,dT\right)$$

$$\approx \dot{m}_w\left(c_{pw,T}T - c_{pw,T_b}T_b + LW_{T_b} + c_{pl,T_b}T_b - c_{pl,T_{ref}}T_{ref}\right), \tag{3}$$

$$\left(\dot{m}_n H_n\right) = \dot{m}_n\left(\int_{T_{ref}}^{T} c_{pn}\,dT + \right) \approx \dot{m}_n\left(c_{pn,T}T - c_{pn,T_{ref}}T_{ref}\right), \tag{4}$$

$$(\dot{m}_l H_l) = \dot{m}_l \left(\int_{T_{ref}}^{T_l} c_{pl} dT \right) \approx \dot{m}_l \left(c_{pl} T_l - c_{pl,T_{ref}} T_{ref} \right), \quad (5)$$

LW_{T_b} is the latent heat of condensation at T_b=373.15 K [J/kg].

The heat fluxes from gas to the film of condensed water q^T and through the water film q^{TS} [W/m^2] are calculated from:

$$q^T = Nu \cdot k_g \frac{T - T_{ls}}{d_h}, \quad (6)$$

and

$$q^{TS} = k_l \frac{T_{ls} - T_s}{\delta}. \quad (7)$$

The assumption of the linear temperature profile across the liquid film satisfies:

$$T_l = \frac{T_{ls} + T_s}{2} \quad (8)$$

The liquid film thickness δ [m] can be approximated by [6]:

$$\delta = \left(\frac{3 \mu \dot{m}_l}{\rho_l^2 g d_h} \right)^{1/3}, \quad (9)$$

Besides the energy balance equations, the mass balances are also formulated for solving a solution of the system simultaneously. For the nitrogen $\dot{m}_n$, water vapor $\dot{m}_w$ and liquid water $\dot{m}_l$ mass flow rates [kg/s] we obtain:

$$\frac{d\dot{m}_n}{dx} = 0, \quad (10)$$

$$\frac{d\dot{m}_w}{dx} = -P q_w^m, \quad (11)$$

$$\frac{d\dot{m}_l}{dx} = P q_w^m. \quad (12)$$

The water vapor condensation mass flux q_w^m [kg/s m^2] is calculated from:

$$q_w^m = Stef \cdot Sh \cdot D \cdot \frac{\rho_w - \rho_{ws}}{d_h}, \quad (13)$$

The diffusion coefficient of the steam in the mixture can be approximated by:

$$D_{w,m} = \frac{1}{\frac{x_n}{D_{w,n}} + \frac{x_w}{D_{w,w}}}, \tag{14}$$

where the binary diffusion coefficients for water vapor - nitrogen pair and for water vapor - water vapor pair are estimated by [9], respectively:

$$D_{w,n} = 0.0101 \frac{T^{1.75}\left(\frac{1}{M_w} + \frac{1}{M_n}\right)^{0.5}}{p \times 10^5 \left[\beta_w^{1/3} + \beta_n^{1/3}\right]^2}, \tag{15}$$

and

$$D_{w,w} = 0.0101 \frac{T^{1.75}\left(\frac{1}{M_w} + \frac{1}{M_w}\right)^{0.5}}{p \times 10^5 \left[\beta_w^{1/3} + \beta_w^{1/3}\right]^2} \tag{16}$$

β is the structural diffusion volume, β_w=12.7 and β_n =17.9 [cm^3/mol].

The mass concentration and mass flux are related to the following:

$$\dot{m}_w = \rho_w U A \tag{17}$$

For the laminar flow regime (Re<2300) the expression of Nusselt and Sherwood numbers are:

$$Nu = 3.66, \tag{18}$$
$$Sh = 3.66. \tag{19}$$

For the turbulent flow regime (3000<Re<5×10^6) the corresponding equations are [8],

$$Nu = \frac{(f/8)(Re - 1000)Pr}{1 + 12.7(f/8)^{1/2}\left(Pr^{2/3} - 1\right)} \qquad 0.5<Pr<2000, \tag{20}$$

$$Sh = \frac{(f/8)(Re - 1000)Sc}{1 + 12.7(f/8)^{1/2}\left(Sc^{2/3} - 1\right)} \qquad 0.5<Sc<2000. \tag{21}$$

In the intermittent regime (2300≤Re≤3000), Nusselt and Sherwood number increase linearly between the two correlations.

The friction factor f depends on Re in the following way [3]:

$$f = \frac{64}{Re}, \tag{22}$$

$$f = 0.316Re^{-0.25} \qquad 2300<Re<20000, \tag{23}$$

$$f = 0.184Re^{-0.2} \qquad Re>20000. \tag{24}$$

The pressure drop associated with the flow was calculated using

$$\frac{dp}{dx} = -f\frac{\rho_g U^2}{2d_h} \tag{25}$$

In addition to previously presented equations, heat transfer from the tube wall to the coolant was modeled in the PCC calculations. Heat flux to the coolant was assumed to be equal to the heat flux through the liquid film (Eq. 7):

$$q^{TS} = q^{TC} \tag{26}$$

Pool was assumed to be boiling around the PCC tubes. For free convection boiling mode, mean Nusselt number $\overline{Nu}$ was approximated from the correlation for an isothermal cylinder [10]:

$$\overline{Nu}_d = \left\{0.60 + \frac{0.387Ra_d^{1/6}}{\left[1+(0.559/Pr)^{9/16}\right]^{8/27}}\right\}^2 \qquad Ra_d \le 10^{12}, \tag{27}$$

where

$$Ra_d = \frac{\rho_l c_{pl} g\zeta_l (T_s - T_b)d^3}{\nu_l k_l}. \tag{28}$$

The heat flux to the coolant was then calculated by:

$$q^{TC} = \frac{k_l}{d}\overline{Nu}_d (T_s - T_b) \tag{29}$$

On the other hand, for the nucleate boiling mode, the heat flux to the coolant was expressed by the following correlation [11]:

$$q^{TC} = \mu_l LW\left[\frac{g(\rho_l - \rho_w)}{\sigma}\right]^{1/2}\left(\frac{c_{pl}(T_s - T_b)}{C_{s,f}LWPr_l^{n}}\right)^3 \tag{30}$$

where the coefficient $C_{s,f}$ and the exponent n depend on the surface-liquid combination. For the case of water-stainless steel, $C_{s,f}$ =0.0130 and n=1.0, respectively.

5.1.2 Particle deposition

In addition to steam condensation, the model includes the particle deposition onto the heat exchanger tube wall. The deposition mechanisms considered in the validation work were: diffusiophoresis, thermophoresis, and the turbulent eddy impaction. As the model for turbulent impaction seemed to contain relatively high uncertainties, only diffusiophoresis and thermophoresis were taken into account in PCC calculations.

The diffusiophoretic deposition velocity of particles onto the walls u_p^{DPH} [m/s] is directly proportional to the water vapor condensation rate q_w^m [kg/m^{2}s] [4]:

$$u_p^{DPH} = \frac{x_w\sqrt{M_w}}{x_w\sqrt{M_w} + x_n\sqrt{M_n}} \frac{q_w^m}{\rho_w} \tag{31}$$

The thermophoretic deposition velocity is calculated using a generally accepted formula over a wide range of particle diameters [5]:

$$u_p^{TPH} = -K\frac{\nu_g}{T}\nabla T, \tag{32}$$

where

$$K = 2C_s \frac{(\alpha + C_t Kn)Cn}{(1+3C_m Kn)(1+2\alpha+2C_t Kn)}. \tag{33}$$

Kn is the Knudsen number, $Kn = \lambda_g / r_p$, which is the ratio of the gas mean free path to the particle radius. The gas mean free path is calculated by:

$$\lambda_g = \frac{\mu_g}{0.499p \cdot \sqrt{8\left(M_g \cdot 10^{-3}\right)/\pi R_g T}} \tag{34}$$

Because thermophoresis is proportional to the temperature gradient, it is closely related to heat transfer. The actual value for the temperature gradient at the surface, which is required for calculating the thermophoretic deposition velocity u_p^{TPH}, can be obtained using the heat transfer correlations for the Nusselt number Nu, which is the dimensionless temperature gradient at the surface. Consequently, we obtain the following simple equation:

$$u_p^{TPH} = -K\nu_g Nu\frac{T - T_{ls}}{Td_h} \tag{35}$$

Turbulent impaction is an important deposition mechanism for large particles, when the boundary layer between the surface and the host flow is turbulent. Inside the turbulent boundary layer turbulent eddies have a velocity component, which is normal to the main flow. Eddies may give enough momentum for particles to cross the laminar sub layer and finally to deposit on the wall.

At present there is no generally accepted mechanistic model available for turbulent deposition. Rough predictions can be made by using experimental correlations. The experimental deposition rate is usually given in such a way that the dimensionless deposition velocity u^+ is plotted as a function of the dimensionless relaxation time τ^+. The dimensionless relaxation time τ^+ characterizes the ability of the particles to react to sudden changes of the fluid. In constant conditions it depends on particle size and other flow variables in the following way:

$$\tau^+ = \frac{1}{36}\frac{\rho_p}{\rho_g}\left(\frac{d_p}{d_h}\right)^2 \mathrm{Re}^2 f_c(\mathrm{Re}), \tag{36}$$

where f_c is the Fanning friction factor.

The non-dimensional deposition velocity u^+ is the actual velocity, with which the particles deposit, normalized with "wall variables" [7]:

$$u^+ \triangleq \frac{u_p^{TUR}}{U\sqrt{\frac{f}{2}}}, \tag{37}$$

Submicron range particles ($\tau^+ < 0.2$) tend to follow the streamlines of fluid motion. This means that in the absence of thermophoresis Brownian motion is the mechanism mainly responsible for deposition. Therefore it is assumed that u^+ is independent of τ^+ and is a function of Schmidt number only:

$$u^+ = 0.065 Sc^{-2/3}. \tag{38}$$

However, when τ^+ is greater than 0.2, the deposition velocity becomes independent of *Sc*. Particles in this range diffuse towards the wall due to radial velocity fluctuations (turbulent diffusion) and then deposit onto the wall by a free-flight mechanism through the viscous sub layer. This is caused by the inability of the particles to follow the turbulent eddies in the vicinity of the wall. This inability can be conveniently described by the concept of a stopping distance. In this range, the experimental deposition data can be roughly correlated using the following equation:

$$u^+ = 3.5 \cdot 10^{-4} \tau^{+2}. \tag{39}$$

Neither of the correlations above work properly, however, as the particle relaxation time increases beyond $\tau^+ > 30$. After this point the particles are too large to respond to the fluid fluctuations, and the $u^+(\tau^+)$ curve levels off to an approximately constant value 0.18 (see [12] for details). This is also approximately the point, where gravitation starts to play an increasingly important role in particle depositions dynamics.

Finally, by combining the different deposition velocities the reduction in the particle mass flux $\dot{m}_p$ [kg/s], due to deposition can be obtained from:

$$\frac{d\dot{m}_p}{dx} = -\left\{P\rho_p\left(u_p^{DPII} + u_p^{TPII} + u_p^{TUR}\right)\right\}, \tag{40}$$

5.1.2.1 Diffusiophoresis

Diffusiophoresis is flow of aerosol particles down the concentration gradient of gas or vapor due to bombardment of particles by the gas or vapor molecules as they diffuse down the gradient. To maintain a constant total pressure near a condensing surface, the concentration gradient of vapor is balanced by an equal and opposite concentration gradient of non-condensable gas. The effect of gas molecules diffusing away from the surface on the transport of aerosol particles is however cancelled out by an aerodynamic flow of gas towards the surface (Stefan flow). Therefore the diffusiophoretic deposition velocity of particles onto the walls u_p^{DPII} [m/s] is directly proportional to the water vapor condensation rate q_w^m [kg/m^{2}s]:

$$u_p^{DPII} = \frac{x_w\sqrt{M_w}}{x_w\sqrt{M_w} + x_n\sqrt{M_n}}\frac{q_w^m}{\rho_w}, \tag{41}$$

where x_w and x_n are the mole fractions and M_w and M_n the molecular weights of water and nitrogen [g/mol], respectively and ρ_w is the mass concentrations of water [kg/m^3] in the gas flow. Diffusiophoresis is approximately independent on particle size.

5.1.2.2 Thermophoresis

Thermophoresis is the result of the temperature gradients. On the hotter side, gas molecules colliding with particles carry on average a higher momentum than on the colder side, thus, causing a net transport in the direction of colder temperature. The thermophoretic deposition velocity is calculated using a generally accepted formula over a wide range of particle diameters [5]:

$$u_p^{TPII} = -K\frac{\nu}{T}\nabla T \tag{42}$$

where

$$K = 2C_s\frac{(\alpha + C_t Kn)Cn}{(1+3C_m Kn)(1+2\alpha+2C_t Kn)}. \tag{43}$$

Here C_s=1.147, C_t=2.20, C_m=1.146, Cn is the Cunningham slip correction factor, ν the kinematic viscosity [m^2/s], T temperature [K], $\alpha = \lambda_g/\lambda_p$ is the ratio of gas to particle thermal conductivities, and Kn the Knudsen number. The Knudsen number $Kn = l_g/r_p$ is the

ratio of the gas mean free path to the particle radius. In above equations, the thermophoretic velocity in the free molecular regime is interpolated with the corresponding expression in the continuum regime. Because thermophoresis is proportional to the temperature gradient, it is closely related to heat transfer. The actual value for the temperature gradient at the surface, which is required for calculating the thermophoretic deposition velocity u_p^{TPH}, can be obtained using the heat transfer correlations for the Nusselt number *Nu*, which is the dimensionless temperature gradient at the surface. Consequently, we obtain the following simple equation:

$$u_p^{TPH} = -K\nu Nu \frac{T - T_{ls}}{T d_h} \tag{44}$$

5.1.2.3 Gravitational settling

Gravitational settling is caused by the effects of gravity on the particles. Settling affects particle transport in PCC only, if the tubes are not vertical. For spherical particles of density ρ_{den_p} [kg/m^3] and diameter d_p [m] in the range of 1-100 μm, the gravitational deposition velocity can be calculated from [6]:

$$u_p^G = \frac{\rho_{den\_p} d_p^{\,2} \boldsymbol{g}}{18\mu} \cdot \boldsymbol{n}, \tag{45}$$

where $\boldsymbol{g}$ is the gravitational acceleration [m/s^2] and $\boldsymbol{n}$ the unit vector normal to the tube wall. For submicron particles gravitational deposition can be considered as negligible.

5.1.2.4 Turbulent impaction

Turbulent impaction is an important deposition mechanism for large particles, when the boundary layer between the surface and the host flow is turbulent. Inside the turbulent boundary layer turbulent eddies have a velocity component, which is normal to the main flow. Eddies may give enough momentum for particles to cross the laminar sub layer and finally to deposit on the wall.

At present there is no generally accepted mechanistic model available for turbulent deposition. Rough predictions can be made by using experimental correlations. The experimental deposition rate is usually given in such a way that the dimensionless deposition velocity u^+ is plotted as a function of the dimensionless stopping distance τ^+. The dimensionless stopping distance τ^+ characterizes the ability of the particles to react to sudden changes of the fluid. In constant conditions it depends on particle size and other flow variables in the following way:

$$\tau^+ = \frac{1}{36} \frac{\rho_{den\_p}}{\rho_{den\_g}} \left(\frac{d_p}{d_h} \right)^2 \mathrm{Re}^2 f(\mathrm{Re}), \tag{46}$$

where f is the Fanning friction factor. The deposition velocity u^+ is the actual velocity, with which the particles deposit, normalized with "wall variables" [7]:

$$u^+ = \frac{u_p^{TUR}}{U\frac{f}{2}} \tag{47}$$

Submicron range particles ($\tau^+ < 0.2$) tend to follow the streamlines of fluid motion. This means that in the absence of thermophoresis Brownian motion is the mechanism mainly responsible for deposition. Therefore it is assumed that u^+ is independent of τ^+ and is a function of Schmidt number only:

$$u^+ = 0.086Sc^{-0.7}. \tag{48}$$

($Sc = \nu/D$, where ν is the kinematic viscosity of the fluid [m^2/s] and D the Brownian diffusivity [m^2/s])

However, when τ^+ is greater than 0.2, the deposition velocity becomes independent of *Sc*. Particles in this range diffuse towards the wall due to radial velocity fluctuations (turbulent diffusion) and then deposit onto the wall by a free-flight mechanism through the viscous sub layer. This is caused by the inability of the particles to follow the turbulent eddies in the vicinity of the wall. This inability can be conveniently described by the concept of a stopping distance. In this range, the experimental deposition data can be roughly correlated using the following equation:

$$u^+ = 3.5 \cdot 10^{-4}\tau^{+2}. \tag{49}$$

Neither of the correlations above work properly, however, as the particle stopping distance increases beyond $\tau^+ > 30$. After this point the particles are too large to respond to the fluid fluctuations, and the $u^+(\tau^+)$ curve levels off to an approximately constant value 0.17 (see [7] for details). This is also approximately the point, where gravitation starts to play an increasingly important role in particle depositions dynamics.

The reduction in the particle mass flux $\dot{m}_p$ [kg/s], due to deposition can be obtained from:

$$\frac{d\dot{m}_p}{dx} = -\left\{P\rho_p\left(u_p^{DPII} + u_p^{TPII} + u_p^{G} + u_p^{TUR}\right)\right\}, \tag{50}$$

where ρ_p is the particle mass concentration [kg/m^3] in the gas flow.

5.2 Experimental studies with 1-tube heat exchangers

5.2.1 Experimental facility

Aerosol deposition within a heat exchanger tube has been experimentally studied in two previous projects. In both projects mass concentration of aerosol was measured before and after a 1-tube heat exchanger using tapered element oscillating microbalance (TEOM). The size distribution of aerosol in the system was characterized as well using Berner type Low

Pressure Impactor (BLPI). Essentially the same facility was applied in both projects. A schematic figure of the facility used in the latter project is presented in figure 3.

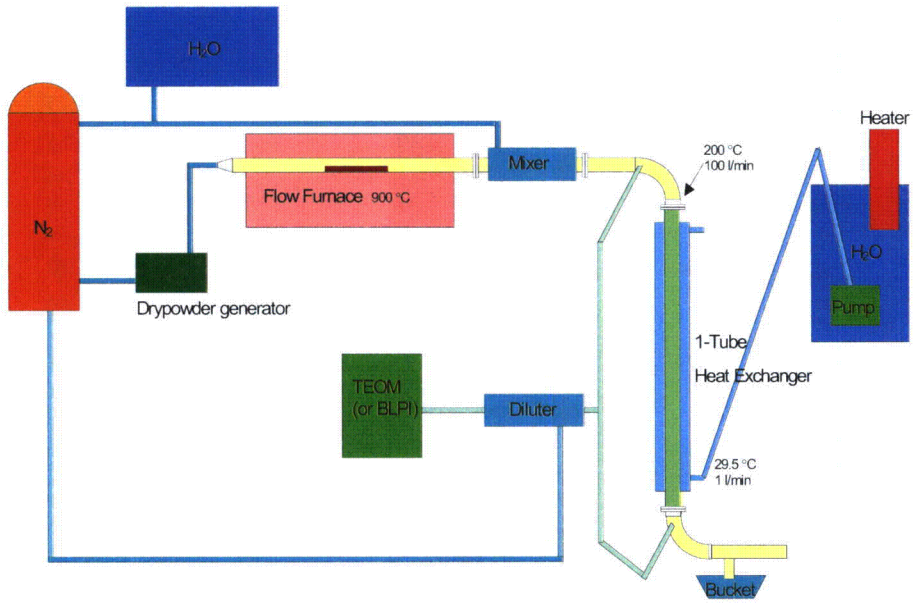

Figure 3. *Experimental facility for the study of aerosol deposition in a 1-tube heat exchanger.*

5.2.2 Aerosol generation and main flow channel

In the first experimental series Ag and Ag-CsOH aerosol mixtures were produced from liquid precursors using an ultrasonic nebulizer. Aerosol flow was conducted trough a high temperature furnace, in which the produced droplets formed aerosol particles by spray drying method. As shown in the figure, Cu aerosol was produced in the second set of experiments using a dry powder generator. In those experiments NaCl-particles were produced in the furnace by vaporization-condensation method.

In all experiments the aerosol flow was mixed after the furnace with the main gas flow so that the total flow rate was 100 l/min (NTP). The main flow was either nitrogen or a mixture of steam and nitrogen. Both steam and nitrogen flows were controlled with proper critical orifices. Steam for the experiment was produced with VEIT 2365 steam generator. A 50 cm long straight tube was placed between the mixer and the heat exchanger in order to allow the particles to mix uniformly in the turbulent gas flow. The temperature of the flow was measured at the inlet of the heat exchanger with K-type thermocouple to be close to 200°C. Temperature of the flow at the outlet of the heat exchanger was measured with K-type thermocouple as well.

The vertical heat exchanger models one tube of the PCC. The heat exchanger was built in such a way that the inner tube was removable. The total length of the removable tube was 100 cm and the length of the cooled area was 80 cm. The inner diameter of the tube was 22 mm and wall thickness was 1.5 mm. The inner tube was changed after every experiment for possible later examination.

The deposition tube was cooled by water flowing upward between the deposition tube and an outer tube. The thickness of flow channel between the tubes was 5 mm. In the first set of experiments the flow rate of cooling water varied between 2.8 and 3.0 l/min. The temperature of the coolant was measured at the heat exchanger inlet and outlet, but the temperature was not controlled. In the second experimental series the flow rate of the cooling water was 1.0 l/min. The flow rate was controlled with an Aquarius 600 submersible pump. Cooling water was preheated to 30°C in a 60 liter tub with HAAKE DL30 circulator heater. At the inlet water temperature was measured with Pt100 resistance type detector (RTD). The temperature gradient of the cooling water was measured as well with three Pt100 RTDs attached on the outer wall of the deposition tube. Temperature of outlet water was measured from one outlet with one Pt100 RTD and with a T-type thermocouple. In both experimental series a bucket was placed below the heat exchanger in order to collect the condensed water.

As reported in [12], a third set of experiments were conducted in order to determine the effect of particle deposition on the heat transfer characteristics of the heat exchanger. In those experiments the length of the vertical inner tube of the heat exchanger was increased to 152 cm, of which 45 cm was placed before the heat exchanger inlet. The cooled length of the tube was increased to 85 cm. A condensation pool was placed at the outlet of the heat exchanger as well. Otherwise the experimental facility was similar to the one used in the second set of deposition studies. Because the heat loss from the condensation pool had previously been measured as a function of time and temperature, the heat loss in the heat exchanger could accurately be determined just by measuring the temperature of the pool.

5.2.3 Aerosol sampling and dilution

In order to determine the deposition of the particles, the flow was sampled from the beginning and from the end of the heat exchanger. The sampling nozzles were stainless steel tubes with an inner diameter of 4.0 mm. Both sample lines were made out of a 1/2 inch tube and they were approximately of the same length, which made the diffusion losses similar. Due to their placing in the laboratory the difference in the length of the lines was 6 cm. The sample lines were heated up to 200°C in order to avoid condensation and thermophoretic deposition before the sample diluter.

The sample flow had to be quenched for the aerosol measurements, because the instruments could not withstand high temperatures. For this reason, the sample flow was diluted with ambient nitrogen in a porous tube diluter, which prevented deposition during the quenching process. The dilution ratio was selected so that water would not condense into the tubes, even if they were not heated. As the pressure in the system was constant, the sample flow rate and the dilution ratio could be controlled by adjusting the dilution flow. This was done with a mass flow controller.

5.2.4 Aerosol measuring instruments

The particle size distribution was measured with a Berner Low Pressure Impactor (BLPI). It is an 11 stage cascade impactor, which is capable of classifying small particles down to 0.0324 μm of diameter, because of the low pressure applied in the last stages. An impactor stage is composed of circular nozzles and a flat plate placed perpendicular to the flow path. Each impactor stage has a characteristic cut-off diameter D_{50}. Particles, which have an aerodynamic diameter larger than the cut-off diameter, can not follow the gas stream lines and collected to the stage. In a cascade impactor smaller particles are passed on to the successive stages. When the impactor stages are weighted after the collection, an aerosol mass size distribution based on the aerodynamic diameter of the particles is obtained.

Tapered Element Oscillating Microbalance (TEOM) is an aerosol mass monitoring device by Rupprecht and Patashnick Co. In TEOM gas flows through an oscillating tapered element, which have a particle collection filter placed on the top. TEOM monitors the changes of the element frequency and thus the mass collected to the filter on-line. TEOM 1400a has a built-in mass flow meter, which allows the flow to be set between 0.5 and 5 l/min (NTP). In these experiments a flow rate of 3 l/min was selected. The gas flow was heated to 50°C in order to avoid condensation to the particles and to the filter. With this method the mass concentration of dry particles could be measured.

5.3 Aerosol deposition experiments and model validation

In total, 16 aerosol deposition experiments were carried out using 1-tube heat exchanger facilities. The experimental matrix is presented in table 1. The deposition of particles was studied in three different environments: dry, low steam volume fraction and high steam volume fraction conditions. Aerosol materials used were Ag together with CsOH in the first and NaCl together with Cu in the second set of experiments. Aerosol mass concentrations varied between 0.25 – 0.9 g/m^3 (NTP) in NaCl experiments, between 0.3 – 0.4 g/m^3 (NTP) in copper experiments and between 0.06 – 0.17 g/m^3 (NTP) in silver experiments. Concentration was rather low, because aerosol measurement instrumentation requires fairly dilute sample flow. Excess dilution of the sample would have increased the uncertainty related to dilution

ration. Moreover, aerosol concentration does not have an influence on deposition velocity or decontamination factor. The first and second experimental series were applied in the validation of particle deposition modeling.

In the third set of experiments the retention of radioactive copper particles into the heat exchanger tube was measured instead of the deposition rate. Because aerosol instrumentation was not applied in that study, the mass concentration could be increased to 6 g/m^3 (NTP). With 10 kg/s steam mass flow rate through PCCs such concentration would correspond to 75 g/s mass flow rate of particles or more than 130 kg of aerosol in 30 minutes. After the radiotracer experiment about 6% of the injected aerosol mass remained in the heat-exchanger tube although approximately 50-60% of the particles deposited during the experiment. The rate of aerosol accumulation also decreased all through the experiments. More than half of the deposit could be found within 10 cm from the tube inlet. Aerosol accumulation did not seem to be significant in a section, where the whole surface was covered by water film. It is thus very likely that in a longer tube the removal of deposited material by condensed water would be even more efficient. Since aerosol mass concentration was not measured in the third set of experiments, these tests could not be applied in the validation of the deposition models. However, the experiments enabled validation of heat transfer modeling.

5.3.1 Particle mass size distribution measurements

The effect of deposition on particle size distribution was studied in experiments 1 – 4 of the first test series. In each of these experiments two impactor samples were taken both from the inlet and outlet of the heat exchanger. Results from impactor measurements 1-3 are graphically presented in figures A.1 – A.12 in appendix A.

It was assumed that the particle mass size distribution can be represented as log-normal size distribution. Parameters of the distribution, aerodynamic mass median diameter (AMMD) and geometric standard deviation (σ_g), estimated in different samplings are presented in table 2. The estimated log-normal distributions agree fairly well with the measured distributions as can be seen in Figures A.1 – A.12 in Appendix A. As can be seen in Table 16, aerosol deposition did not influence the particle size distribution. Any variation in AMMD is well within the experimental uncertainty. Such result was expected, because the main deposition mechanism, diffusiophoresis, does not depend on particle size. Deposition in dry conditions due to thermophoresis was so limited that it did not have an effect on the distribution either.

Table 15. *Experimental matrix of aerosol deposition studies with 1-tube heat exchangers.*

Series	Test No	Aerosol material	H_2O flow [mol/min]	N_2 flow [l/min] (NTP)	H_2O / N_2 Volume ratio	Measuring Instruments
1	1	Ag	-	100	0 / 100	BLPI
1	2	Ag	1.02	75	23 / 75	BLPI
1	3	Ag	3.36	33	75 / 33	BLPI
1	4	Ag + CsOH	3.36	25	75 / 25	BLPI
1	5	Ag	-	100	0 / 100	TEOM
1	6	Ag	1.02	75	23 / 75	TEOM
1	7	Ag	3.36	25	75 / 25	TEOM
1	8	Ag + CsOH	3.36	25	75 / 25	TEOM
2	1	NaCl	-	100	0 / 100	BLPI
2	2	Cu	-	100	0 / 100	BLPI
2	3	NaCl	-	100	0 / 100	TEOM
2	4	NaCl	1.02	75	23 / 75	TEOM
2	5	NaCl	3.36	25	75 / 25	TEOM
2	6	Cu	3.36	25	75 / 25	TEOM
3	1	-	3.97	32.7	89 / 33	TH – exp.
3	2	Cu	3.97	32.7	89 / 33	γ-tracer exp.

Mass size distribution in the fourth experiment of the first test series was bi-modal, with Ag particles forming the larger mode and CsOH particles the smaller. For this reason the distribution could not be approximated with log-normal distribution and was not applied in the validation work either.

In the second test series particle mass size distribution was measured for NaCl in the first and for Cu in the second experiment. Two impactor samplings were conducted in both experiments from the inlet of the heat exchanger. Results from the samplings are graphically presented in Figures A.13 – A.16 in Appendix A. As before NaCl particle mass size distributions were approximated with log-normal size distributions using parameters given in table 16. The mass size distribution of Cu particles was bi-modal. It was approximated both one log-normal distribution and a sum of two log-normal distributions. As can be seen in Figures A.15 and A.16 the sum distribution fits the measured data very well. Nevertheless, parameters for both unimodal distribution and a sum distribution are given in Table 16. The value presented in parentheses after the AMMD denotes the mass fraction of particles belonging to each log-normal distribution.

As evident in Table 16, different particle generation methods produced fairly constant particle size distribution. The distribution depended only on the aerosol material. In the validation work particle mass size distributions were assumed to be log-normal. Parameters for different aerosol materials were taken directly from Table 16.

Table 16. *Aerosol characteristics assuming log-normal particle mass size distribution.*

Series	Test No	Aerosol material	Sampling duration [min]	Sampling location	AMMD [μm]	σ_g
1	1	Ag	30	inlet	1.02	2.54
			27	outlet	1.28	2.26
			13	inlet	1.05	2.42
			14	outlet	1.00	2.47
1	2	Ag	25	inlet	1.07	2.49
			25	outlet	1.05	2.31
			25	inlet	1.07	2.29
			25	outlet	1.20	2.32
1	3	Ag	30	inlet	1.05	2.43
			30	outlet	0.97	2.68
			25	inlet	1.14	2.29
			25	outlet	0.95	2.61
2	1	NaCl	1.5	inlet	0.66	2.73
			2.5	inlet	0.76	2.40
2	2	Cu	1.5	inlet	7.23 (85%)	2.04
					0.65 (15%)	1.64
					or	
					5.01 (100%)	3.40
			5	inlet	6.17 (76%)	2.04
					0.71 (24%)	1.64
					or	
					3.69 (100%)	3.40

5.3.2 Particle deposition measurements and modeling results

Particle deposition was measured in experiments 5 – 8 of the first test series for Ag and CsOH aerosols and in experiments 3 – 6 of the second test series for NaCl and Cu aerosols. In addition to particle size and material, the main parameter modified in the experiments was volume fraction of steam in the gas flow. As condensation of steam induces particle deposition by diffusiophoresis, it was expected have a major influence on particle retention.

In each particle deposition experiment 8-10 samples were taken with the online mass monitor (TEOM) alternatively from the inlet and outlet of the heat exchanger. The duration of each sampling was approximately 10 minutes resulting about 300 measurement points. Mass concentration of particles in the sample was calculated averaging the measurements. Particle mass flow rate in the heat exchanger inlet and outlet were calculated by multiplying the measured result by dilution ratio and by volumetric flow rate of the gas in NTP conditions. Since volumetric flow rate of steam can not be defined in NTP conditions, the value was approximated by dividing the measured mass flow rate by the molar mass of water and multiplying the result with 22.4 l/mol (molar volume of ideal gas).

Results from experiments 5 – 7 of the first test series with Ag particles can be compared with the model calculations in table 3. The deposition of particles is also graphically presented in figure 2. In the modeling work the measured gas flow rate and temperature at the inlet were applied. The wall temperature at the inlet and outlet were assumed to be the same as the measured coolant temperature at those locations. Wall temperature between inlet and outlet was assumed to change linearly. The AMMD and geometric standard deviation of the distribution were assumed to be 1.05 μm and 2.42 correspondingly.

As is evident in Table 17 and in Figure 4, results calculated with the 1-D model agree fairly well with those of the experiments. Calculated flow outlet temperatures underestimate slightly the measured values. Such difference may be due to the fact that actual wall temperature inside the tube is higher than the measured coolant temperature. However, since the calculated temperature refers to average temperature of the flow, whereas the measured temperature is the centerline temperature, the difference may also be due to radial temperature gradient. In the experiments radial temperature gradient should have increased with steam volume fraction. In the case with highest steam mass flow rate, flow at the outlet was no longer turbulent due to significant condensation.

The calculated condensation rate of steam also seems to agree well with the measured values. This agreement is very important, because diffusiophoresis is considered to be the main deposition mechanism.

Finally, calculated deposition matches well with the measured values. This is especially true in experiments with steam flow. In those experiments deposition due to diffusiophoresis dominates and thermophoresis is a secondary mechanism. However, it should be kept in mind that uncertainty in the steam condensation rate directly influences the uncertainty in the experimental deposition rate. In dry conditions thermophoresis is the dominant deposition mechanism. Modeled thermophoresis seems to slightly over-estimate the experimental value, which is also true in all other experiments. In the dry case the deposition rate is however so low that the difference is not very significant. Turbulent impaction did not affect the deposition rate, because Ag particles were rather small. Deposition due to Brownian diffusion was not considered in the modeling work. Deposition due to diffusion only affects the smallest particles, which by definition should carry only negligible fraction of the mass released into the containment.

Results from the second test series are compared with the calculations in Table 18. The deposition of particles is presented in Figure 4. The results seem to be very similar to the first test series.

Table 17. *Comparison between experiments (exp) and simulations (sim) for the temperature decrease, steam condensation and deposition of silver particles.*

	Flow at inlet		Flow temp. [°C]		Wall temp. [°C]		Condensation [g/min]	Aerosol		Deposition [%]	
	N_2 [l/min] (NTP)	Steam [g/min]	inlet	outlet	inlet	outlet		mat.	AMMD [μm]		
exp	100	-	205	116	13.0	11.6	-	Ag	1.09	4.3	
sim	100	-	205	**115**	13.0	11.6	-	Ag	1.05	**7.4**	
										DiP=	-
										ThP=	**7.4**
										TI=	**0.0**
exp	75	18.4	207	129	14.0	11.6	9.5	Ag	1.10	17.3	
sim	75	18.4	207	**121**	14.0	11.6	**9.1**	Ag	1.05	**16.7**	
										DiP=	**9.4**
										ThP=	**7.3**
										TI=	**0.0**
exp	25	60.5	203	150	20.3	11.6	43.3	Ag	1.03	52.5	
sim	25	60.5	203	**135**	20.3	11.6	**37.4**	Ag	1.05	**48.0**	
										DiP=	**42.3**
										ThP=	**5.7**
										TI=	**0.0**

DiP – Diffusiophoresis; ThP – Thermophoresis; TI – Turbulent impaction. Calculated outputs of the simulations are **bolded** in the Table 17.

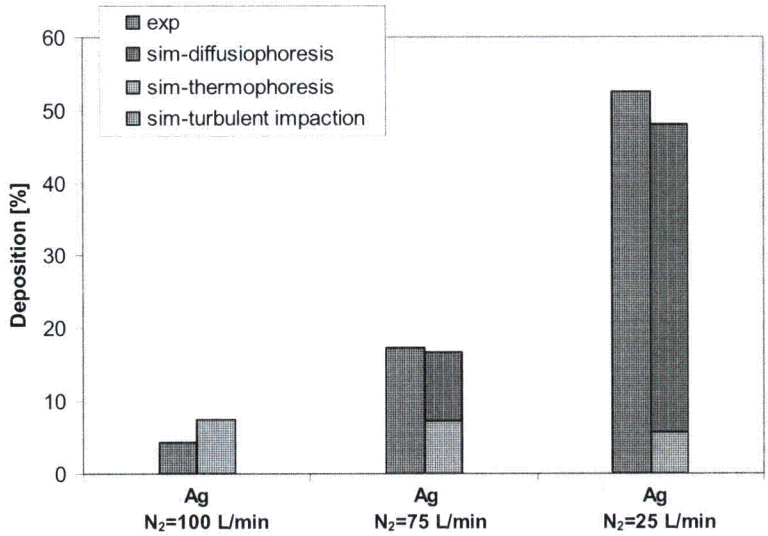

Figure 4. *Measured and calculated deposition [%] of silver particles in the heat exchanger at different nitrogen flow rates.*

Table 18. *Comparison between experiments (exp) and simulations (sim) for the temperature decrease, steam condensation and aerosol deposition for copper and sodium chloride particles.*

	Flow at inlet		Flow temp. [°C]		Wall temp. [°C]		Condensation [g/min]	Aerosol		Deposition [%]	
	N_2 [l/min] (NTP)	Steam [g/min]	inlet	outlet	inlet	outlet		mat.	AMMD [µm]		
ex	100	-	199	125	32.3	29.6	-	Cu	7.2 85% 0.7 15%	1.5	
sim	100	-	199	**121**	32.3	29.6	-	Cu	7.2	**10.7 (4.4)** DiP= ThP= TI=	- **4.4** **6.3**
exp	100	-	199	125	31.9	29.5	-	NaCl	0.71	3.8	
sim	100	-	199	**121**	31.9	29.5	-	NaCl	0.66	**6.2** DiP= ThP= TI=	- **6.2** **0.0**
exp	75	18.4	190	127	36.5	29.5	7.2	NaCl	0.71	11.7	
sim	75	18.4	190	**121**	36.5	29.5	**7.3**	NaCl	0.66	**13.4** DiP= ThP= TI=	**7.5** **5.9** **0.0**
exp	25	60.5	187	149	55.1	29.8	39.4	NaCl	0.71	56.4	
sim	25	60.5	187	**132**	55.1	29.8	**34.9**	NaCl	0.66	**44.3** DiP= ThP= TI=	**39.7** **4.6** **0.0**

DiP – Diffusiophoresis; ThP – Thermophoresis; TI – Turbulent impaction. The value in parenthesis shows the deposited mass in % without turbulent impaction. Calculated outputs of the simulations are **bolded** in the Table 18.

As in the first test series flow outlet temperature was slightly under-estimated. The difference also increased with the steam volume fraction. Again the calculated steam condensation rates agreed well with the experimental values. Due to higher cooling water temperatures, estimated deposition rates both by diffusion- and thermophoresis were slightly lower than in the first test series. This seemed to agree reasonably well with the measured values. With the high steam mass flow rate the difference between the model prediction and the measurement seems to be rather large. However, this is related to the fairly high uncertainty in the measurement of the condensation rate. Lastly, deposition of large Cu particles was significantly over-estimated. The over-estimation was mainly due to the fact that model predicted rather high deposition by turbulent impaction, whereas experiments showed no evidence of such. In the literature the estimates for turbulent impaction velocity in this flow regime differ approximately by three orders of magnitude. We concluded that the model for turbulent impaction is too unpredictable to be applied in this work. If only deposition by thermophoresis is considered, even Cu particle deposition could fairly accurately be estimated.

Particle mass concentration was not measured in the third test series. Thus those experiments could not be used in the validation of the deposition models. However, because the heat loss in the 1-tube heat exchanger could accurately be measured in these experiments, the results could be applied in the validation of our heat transfer modeling. Results from the experiment can be compared with the calculated values in Table 19.

Table 19. *Flow properties and the measured and the calculated heat balance due to the heat exchanger.*

		experiment	simulation
$\dot{m}_{w,\mathrm{in}}$	[g/min]	71.5	71.5
$\dot{m}_{n,\mathrm{in}}$	[g/min]	41.5	41.5
$T_{g,\mathrm{in}}$	[°C]	187	187
$T_{g,out}$	[°C]	142	**126**
$T_{w,\mathrm{in}}$	[°C]	38.3	38.3
$T_{w,high}$	[°C]	32.8	36.1
$T_{w,\mathrm{middle}}$	[°C]	31.2	33.9
$T_{w,bottom}$	[°C]	30.1	31.7
$T_{w,\mathrm{out}}$	[°C]	29.3	29.3
Q_{in}	[W]	3510	3510
Q_{loss}	[W]	2277	**2073**

(*) T_w is the cooling water temperature for the experiment and the wall temperature for the simulation, respectively. In the simulation, the wall temperature is assumed to decrease linearly, and is determined from the measured cooling water temperatures at inlet, $T_{w,\mathrm{in}}$, and outlet, $T_{w,\mathrm{out}}$.

(**) $T_{w,\mathrm{in}}$ and $T_{w,\mathrm{out}}$ are referred to the temperatures taken at the inlet and outlet of the heat exchanger, respectively. $T_{w,\mathrm{high}}$, $T_{w,\mathrm{middle}}$, and $T_{w,\mathrm{bottom}}$ are the temperatures at 21 cm, 42.5 cm and 64 cm from the inlet, respectively.
Calculated outputs of the simulations are **bolded** in the Table 19.

As in previous experiments the mass flow rate and temperature of the gas were taken from the experiments. Wall temperature at the inlet and outlet of the heat exchanger were assumed to be in the measured cooling water temperature. Wall temperature between these points was assumed to decrease linearly. As a result the wall temperature is slightly higher than the measure cooling water temperature. Similarly as before, the calculated flow temperature at the outlet is lower than the measured temperature. We believe that the difference is due to radial temperature gradient in the flow. Lastly, the calculated heat loss in the heat exchanger agrees remarkably well with the measured value. As a conclusion, the model should be able to accurately calculate steam condensation rate and particle deposition processes in the heat exchanger tube.

6 Validation of MELCOR Model Against VTT Experiments

The aerosol retention in 1-tube heat exchanger experiments, conducted at VTT, was calculated with MELCOR 1.8.6 and compared to the measured values [13]. The target of this effort is to estimate the suitability of the MELCOR aerosol retention models for use in the ESBWR PCCS simulations.

Figure 5 presents the geometry and nodalization of the heat exchanger tube. The cooled length of the tube was 80 cm, and it was divided into three control volumes. The uncooled parts at the ends were modeled as additional 10 cm long control volumes. The diameter of the tube was 22 mm. The tube was surrounded by a cooling tube that was also divided into three volumes. The thickness of the flow channel between the tubes was 5 mm. The outlet volumes of the both tubes were connected to a time-independent environment volume at pressure 0.1 MPa. The tubes were separated with three 1.5 mm thick heat structures, made of stainless steel. The walls of the uncooled inlet and outlet parts of the tube were modeled as heat structures that were insulated from the outside. The heat structures were defined to form a film-tracking network so that the condensed water film drains from the upper to the lower heat structures. An additional heat structure was defined to receive drainage from the lowest part of the aerosol tube and place it into the environment volume. This removed numerical instabilities that occurred when the lowest heat structure was first defined to drain to the lowest control volume of the tube, which caused a tiny amount of liquid water to appear and disappear from the volume. This additional heat structure was not defined as an aerosol deposition surface.

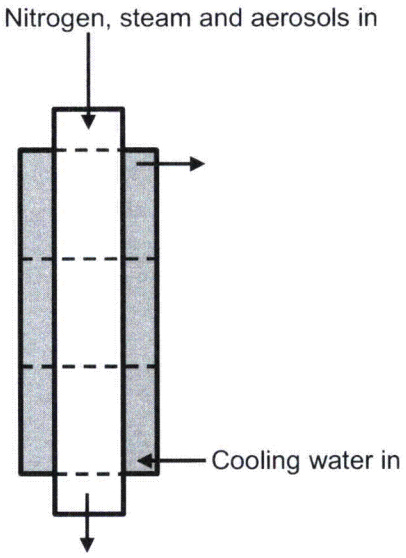

Figure 5. *Nodalization of the heat exchanger tube. The dashed lines mark control volume boundaries. The drawing is not in the right scale.*

The inflow of nitrogen, steam, aerosols and cooling water were modeled as mass, enthalpy and aerosol sources in the inlet volumes. The flow rates, inlet temperatures, aerosol aerodynamic mass median diameters and geometric standard deviations are presented in Table 20. The aerosol mass size distribution was assumed to be log-normal.

Table 20. *Flow rates, inlet temperatures and aerosol data of the simulated experiments. AMMD means aerodynamic mass median diameter.*

		Flow rates			Inlet temperatures (°C)		Aerosol data	
Test series	Test number	N_2 (l/min, NTP)	Steam (g/min)	Cooling water (l/min)	N_2 and steam	Cooling water	AMMD (μm)	Geometric standard deviation
1	5	100	0	2.9	205	11.6	1.05	2.42
1	6	75	18.4	2.9	207	11.6	1.05	2.42
1	7	25	60.5	2.9	203	11.6	1.05	2.42
2	2	100	0	1	199	29.6	7.2	2.04
2	3	100	0	1	199	29.5	0.66	2.73
2	4	75	18.4	1	190	29.5	0.66	2.73
2	5	25	60.5	1	187	29.8	0.66	2.73

The simulations were conducted with MELCOR 1.8.6 revision YK. The simulation was run for 10 minutes in order to let the temperatures reach their equilibrium values. The results are presented in 1 together with the measured values and those calculated with 1-D model. The boundary condition used in the calculations is a little different. In the 1-D model calculation it is assumed that the pipe inner surface is at the same temperature as the measured cooling water temperature. Conversely, in the MELCOR results only the cooling water inlet temperature was taken as a boundary condition, and the heat transfer from the water to the pipe and conduction in the pipe was calculated.

Table 21. *Results of the MELCOR simulations compared with the measured values and the data calculated with the 1-D Enqvist model.*

		Outlet temperature (°C)			Condensation (g/min)			Aerosol retention (%)		
Test series	Test number	Measured	Enqvist	MELCOR	Measured	Enqvist	MELCOR	Measured	Enqvist	MELCOR
1	5	116	115	141	0	0	0	4.3	7.2	3.5
1	6	129	121	145	9.5	9.1	6.6	17.3	16.5	8.2
1	7	150	135	154	43.3	37.4	33.5	52.5	47.8	36.1
2	2	125	121	143	0	0	0	1.5	4.3	1.9
2	3	125	121	143	0	0	0	3.8	6.1	3.1
2	4	127	121	138	7.2	7.3	5	11.7	13.2	6.6
2	5	149	132	148	39.4	34.9	27.9	56.4	44.1	30.2

It can be seen from the results that MELCOR overestimates the outlet temperature in all but one case. This means that MELCOR underestimates the heat transfer rate from the nitrogen and steam. Also the steam condensation rates are underestimated by about 20–30 %. MELCOR calculates too small aerosol retention in all cases except the one with larger 7.2 μm particles. The retention ratios are illustrated in Figure 14. The main reason for this underestimation is probably the underestimation of the steam condensation rate, which affects the aerosol deposition by diffusiophoresis. MELCOR output does not include the contributions of the different deposition mechanisms. The Enqvist model is better in predicting the aerosol retention in all the cases that involve steam condensation. On the other hand, the MELCOR results are better for the dry experiments.

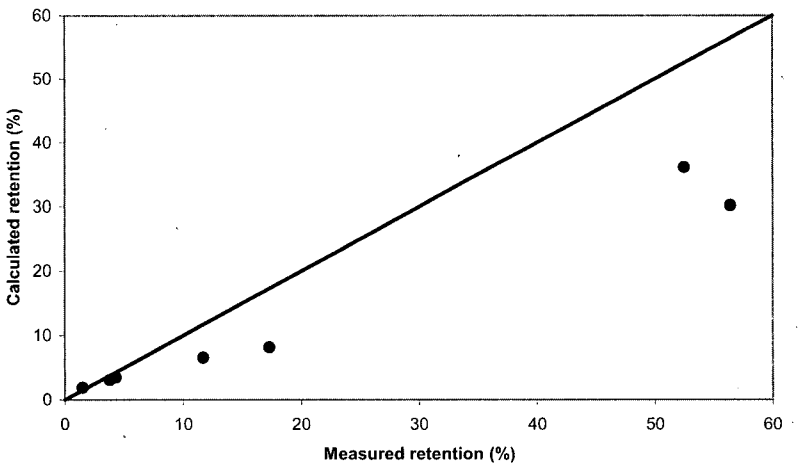

Figure 6. *Comparison of the measured aerosol retention and the estimate calculated with MELCOR 1.8.6 YK.*

7 Model to estimate pH in the containment sumps

7.1 Estimation of released HCl from the cables

The calculation of HCL production from cable insulators was performed in the way introduced in the NUREG/CR-5950 report [16]. According to this report, the amount of HCl produced from Hypalon used as the isolation material in electrical cables in the containment is estimated as 4.6×10^{-4} mol per lb of insulation per Mrad. This estimate is based on the model description of electrical cable and a radiation G value of 2.1. The extent of HCl production would depend on the total dose.

$$R = K \times M \times \Delta D/\Delta T \qquad (70)$$

R = production rate of the HCL due to the irradiation of the cable insulation inside the containment
$K = 4.6. \times 10^{-4}$ (mol_{HCl} Mrad h^{-1} lb^{-1}) [16]
M = mass of insulation material (lb)
$\Delta D/\Delta T$ = radiation dose rate (Mrad/h)

The cable insulation material in EBWR is Hypalon and mass of the cable insulation material in the containment of ESBWR is 7480 lbs according to the information received from GE. This is the same value used in the previous calculations for ABWR [18]. For ABWR the production of HCl was calculated to be 131 mol in 24 hours, 0.0015 mol/s.

In pH-case A the HCl release from estimated dose rates are calculated as shown in Table 22. The dose rates were calculated with RADTRAD by GE and were obtained using natural deposition coefficients for containment derived from MELCOR results. The decrease of the activities between time steps in Table 23 was approximated to be linear. The total dose is taken as a sum of β- and γ-doses. The HCl production was calculated using the Eq. (70). MELCOR results indicate that the fission product release starts at t ~ 2000s and HCl production from cables is assumed to start immediately after that. The pH calculation with ChemSheet was extended to 53000 s. When using the HCl production rate as in Table 22 and extending the release over the period of 2000 s – 53000 s one obtains for total HCl release of 430 mol.

Table 22. *Assumed radiation doses and respective total HCl release rates in pH case A.*

t_1, h	t_2, h	(t_1-t_2), s	(γ+β) Mrad TID	TID, Mrad (t_1-t_2)	HCl, mol (t_1-t_2)	HCl, mol/s (t_1-t_2)
0.44	0.83	988	0.932	0.932	3.2	0.0032
0.83	1.23	1440	3.11	2.178	7.5	0.0052
1.23	1.83	2160	10.07	6.96	23.9	0.0111
1.83	2.33	1800	18.32	8.25	28.4	0.0158
2.33	3	2412	28.46	10.14	34.9	0.0145
3	6	10800	65.6	37.14	127.8	0.0118
6	8.33	8388	85.3	19.7	67.8	0.0081
8.33	12	13212	110.5	25.2	86.7	0.0066
12	24.33	44388	176.1	65.6	225.7	0.0051

For sensitivity calculations two cases with radiation dose rates taken from the DCD Appendix 3H [19] were performed. The given value for radiation dose rate in the upper and lower dry well is 2.64E+7 R/h at t=0 [19]. At the time when fission product release to the containment commences the dose rate has decreased to 25 % of that of t=0 and further decreases to 20% at t=3600 and 10 % at t= 24 h of that of t=0 according to the decay heat curves [20]. The estimations of HCl production are made using these values (6.6 MR/h for t = 2000 s, 5.94 MR/h for t= 3600 s and 2.64 MR/h for t = 24 h) for the radiation dose rate.

In the pH-case B the HCl release was assumed to be 0.0015 mol/s, which is the same release rate for as in the reference calculated for ABWR [18].

In pH-cases C and E the radiation dose rate at t= 2000 s was estimated to be 25% of the dose at t = 0, 6.6 Mrad/h, 25 % of that of t=0. If this dose rate is used to evaluate the HCl release from the cables until t = 24 h, total dose is 155 Mrad and the total amount of HCL released during the first 24 hours is,

4.6 x10^{-4} mol lb^{-1} $Mrad^{-1}$ x 7480 lb x 155 = 532 mol of HCl, that gives the release rate of 0.006 mol/s.

The HCl release rate for pH-case D is obtained in the following way: The value 0.006 mol HCl/s is too high, because the activity decreases after t = 2000s. The decay heat curves after the reactor shut down show, that after 2000s the decay heat is about 25 % of the t=0 value and 10 % of the t =0 value after 24 hours [17]. If we make a rough estimation and evaluate the radiation dose to be 6.6 Mrad/h at the beginning of HCl release, 5.28 Mrad at t = 1 h, and 2.64 Mrad/h at t = 24 h, and activity decrease to be linear between these points, we get

4.6 x10^{-4} mol lb^{-1} $Mrad^{-1}$ x 7480 lb x (5.94 Mrad h^{-1} x 0.44h + 3.96 Mrad h^{-1} x 23h) = 322 mol of HCl the release rate is 0.0038 mol/s.

Because the HCl production is dependent of the total radiation dose that the insulation material is exposed to, the uncertainty in these calculations comes through the rough estimation of radiation dose. The linear decrease of radiation dose between 1-24 h gives 5-7 % increase in the release rate.

The overall amount of HCl produced by irradiation of insulation material is 9 - 25 % of the cable Cl inventory during the first 24 hours [18]. The total amounts of HCl used for ChemSheet calculations of this report (131, 322, 430, 532 and 606 mol of HCl during the first 24 hours) corresponds to 7.8 - 37 % of the total chlorine, 593 kg in the insulation material, if the Cl concentration in Hypalon is 17.5 % as assumed in reference [16].

7.2 Estimation of HNO3 production in Upper Drywell

Irradiation of water and air produces nitric acid into the water. According to the NUREG/CR-5950 report the radiation G value for nitric acid production is 0.007 molecules/100 eV and this value corresponds to 7.3 x 10^{-6}mol HNO_3/lb/ Mrad.

$$R = K \times M \times TID / t \quad (71)$$

R = production rate of the HNO_3 due to the irradiation of water
K = 7.3. x 10^{-6} (mol_{HNO3} Mrad h^{-1} lb^{-1}) [16]
M = mass of insulation material (lb)
TID = total integrated dose (Mrad)
t = irradiation time

The dose rates of pH-case A were applied to evaluate the HNO_3 production [23]. The decrease of the activities was estimated to be linear between given times. The total dose is taken as a sum of β- and γ-doses. The applied radiation doses and HNO_3 production rates are presented in Table 23.

Table_23. *Assumed dose rates and respective release rates of HNO3 in the Upper Drywell. pH cases A and E.*

t_1, h	t_2, h	(t_1-t_2), s	(γ+β) Mrad TID	TID, Mrad (t_1-t_2)	Water, kg average (t_1-t_2)	HNO_3, mol (t_1-t_2)	HNO_3, mol/s (t_1-t_2)
0.44	0.83	988	0.932	0.932	3007	0.020	2.07E-05
0.83	1.23	1440	3.11	2.178	3078.5	0.049	3.40E-05
1.23	1.83	2160	10.07	6.96	2363	0.120	5.56E-05
1.83	2.33	1800	18.32	8.25	3486.5	0.210	1.17E-04
2.33	3	2412	28.46	10.14	4450.5	0.329	1.37E-04
3	6	10800	65.6	37.14	3681.5	0.998	9.24E-05
6	8.33	8388	85.3	19.7	5764.5	0.829	9.88E-05
8.33	12	13212	110.5	25.2	8776	1.614	1.22E-04
12	15.8	13700	176.1	65.6	9863.5	1.483	1.08E-04

The total production of HNO_3 is according to this calculation only < 6 moles during 16 hours. The effect is not significant compared to the > 600 moles of HCl.

7.3 Sodium pentaborate

These reference values are from Eagle-Picher (http://www.eaglepicher.com/EaglePicherInternet) report on enriched sodium pentaborate products for BWR operators: http://www.eaglepicher.com/NR/rdonlyres/1183A34B-F387-4D85-A79A-C4C5F1FB806C/0/w_c_03.pdf

Table 24. *Physical properties of sodium pentaborate*

Form	White Crystals
Enrichment	To 99% at 1% ^{10}boron
Formula	$Na_2O{\cdot}5B_2O_3{\cdot}10H_2O$
Specific gravity	1.71 g/cm^3
Boron Content	17.21% at ^{10}boron

Table 25. *Solubility in water (natural isotopic composition)*

Temperature/C	% anhydrous salt by composition
0	6.28
10	8.10
20	10.55
30	12.20
40	17.40
50	21.80
60	26.90
70	32.25
80	37.84
90	43.80
100	50.30

7.4 Sodium diborate (common name Borax)

Borax ($Na_2O{\cdot}2B_2O_3{\cdot}10H_2O$) is the most common of sodium borate based buffer solutions. In this project it is used as a reference solution to validate the thermodynamic model as measured titration curves for it were found in the literature[1].

Table 26. *100 mL of 0.025 M Borax buffer solution titrated with 0.1 M HCl*[2]

HCl mL	pH
4.0	9.1
9.2	9.0
14.2	8.9
19.2	8.8
23.2	8.7
27.0	8.6
30.4	8.5
33.2	8.4
35.4	8.3
37.6	8.2
39.4	8.1
41.0	8.0

Table 27. *100 mL of 0.025 M Borax buffer solution titrated with 0.1 M NaOH*[2]

NaOH mL	pH
1.8	9.2
7.2	9.3
12.4	9.4
17.6	9.5
22.2	9.6
26.2	9.7
30.0	9.8

[1] Robinson, R. A., and Stokes, R. H., Electrolyte solutions, the measurement and interpretation of conductance, chemical potential, and diffusion in solutions of simple electrolytes, 2nd ed., rev. London, Butterworths, 1968

33.4	9.9
36.6	10.0
39.0	10.1
41.0	10.2
42.6	10.3

7.5 Thermodynamic System

The thermodynamic system used in pH calculation is shown below.

Table 28. *Thermodynamic system.*

Phase	Constituent	Components					
		B	Na	H	O	Cl	e
Gas	H_2O			2	1		
	HCl			1		1	
Water	H_2O			2	1		
	H+			1			-1
	OH-			1	1		1
	$B(OH)_3$	1		3	3		
	$B(OH)_4$-	1			2		1
	Cl-					1	1
	Na+		1				-1
NaCl	NaCl		1			1	
NaOH	NaOH		1	1	1		
$Na_2O{\cdot}2B_2O_3{\cdot}10H_2O$	$Na_2O{\cdot}2B_2O_3{\cdot}10H_2O$	4	2	20	17		
$Na_2O{\cdot}5B_2O_3{\cdot}10H_2O$	$Na_2O{\cdot}5B_2O_3{\cdot}10H_2O$	10	2	20	26		

Thermodynamic system consists of ideal gas phase (Gas), aqueous phase (Water) and condensed salts, NaCl, NaOH, sodium diborate (Borax) and sodium pentaborate. Aqueous phase is modeled using Pitzer formalism.

7.6 Calculation Results

Initial calculations were made with ChemSheet software using the thermodynamic system in Table 29. At this stage no calculation is made with any real or estimated process values. These calculations are used to verify the thermodynamic system and its applicability to pH calculations with sodium pentaborate and HCl systems in general.

First two reference calculations were made where results were compared against measured pH values with 0.025 M Borax buffer solution.

With low acid and base concentrations calculated and measured values are almost equal but especially with higher acid (HCl) concentration there is a clear difference but the result is still adequate.

Next calculation was made with sodium pentaborate solution where natural boron concentration is 1600 ppm (according to standby liquid control system specifications).

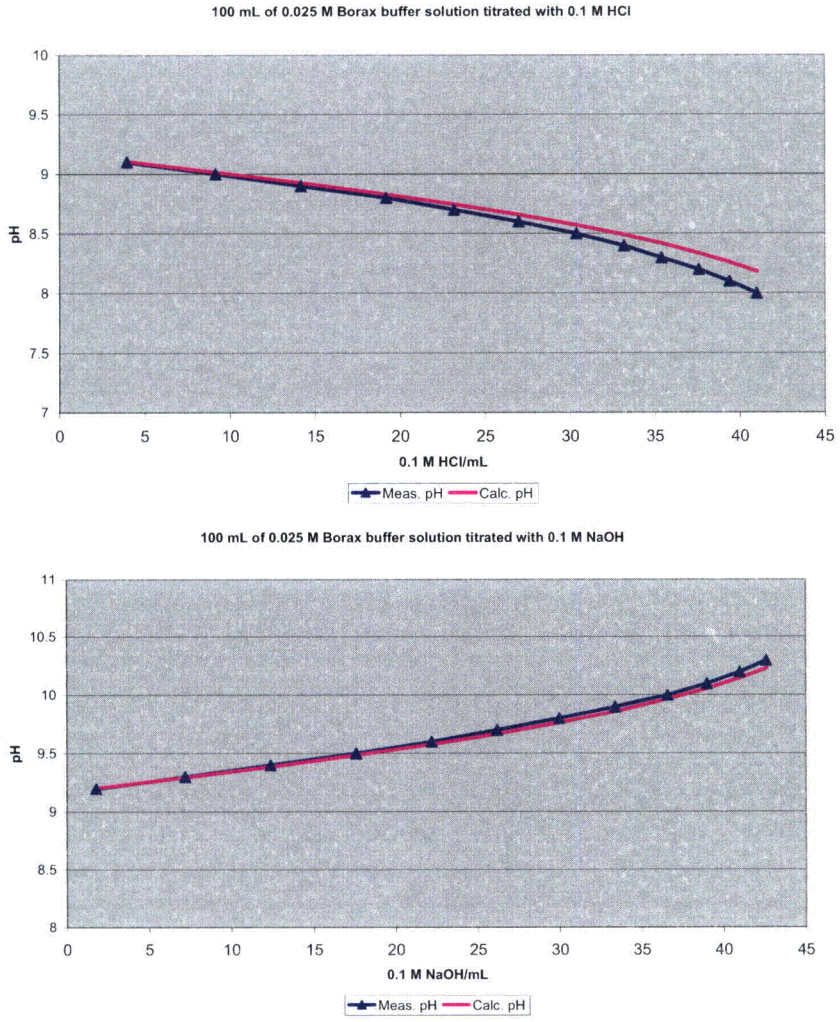

Figure 7. *Titration curves of 0.025 M Borax buffer solution with 0.1 M HCl (upper picture) and 0.1 M NaOH (lower picture).*

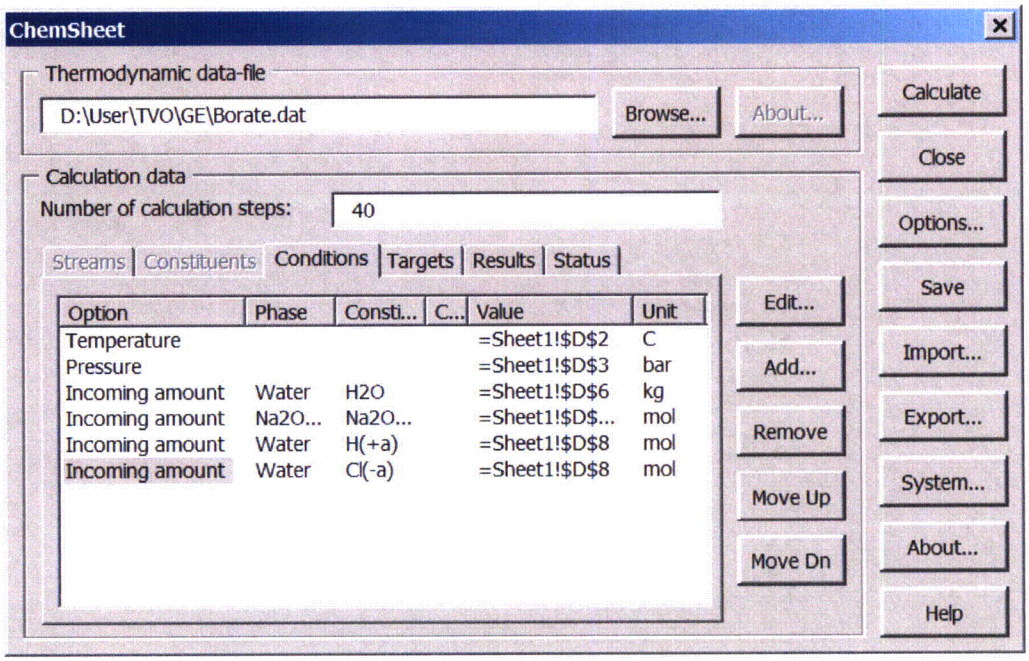

Figure 8. *ChemSheet dialog showing the initial conditions of pH calculation. Actual values were given in Excel worksheet cells.*

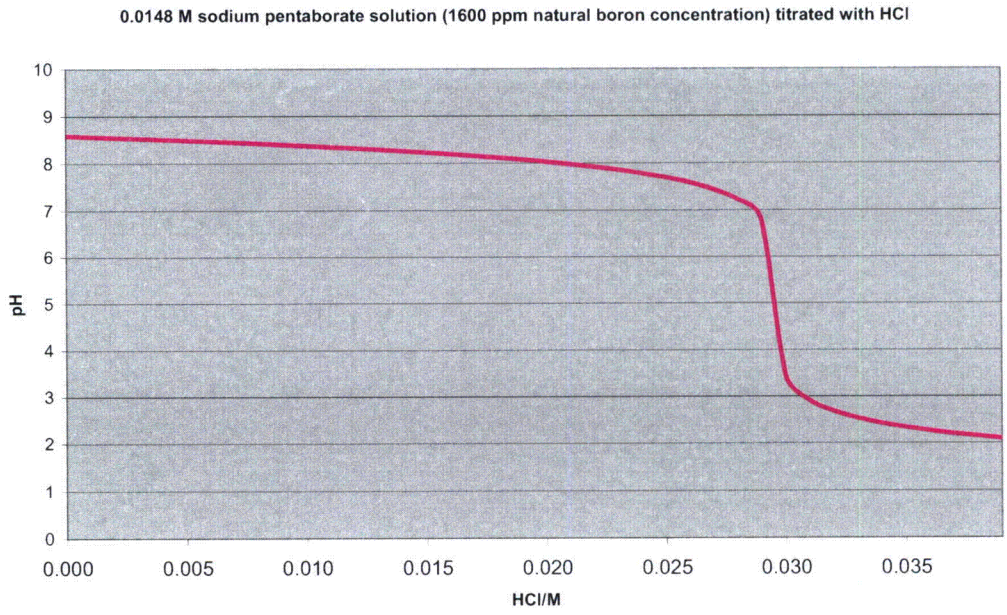

Figure 9. *Titration curve of 0.0148 M sodium pentaborate with HCl.*

It can be seen that pH changes to acidic when HCl concentration is greater than 0.029 mol/kg_{H2O}. This result is not verified yet (it is only based on calculation).

Similar titration curve was found for sodium diborate (Borax) at http://www.borax.com/detergents/pheffect.html.

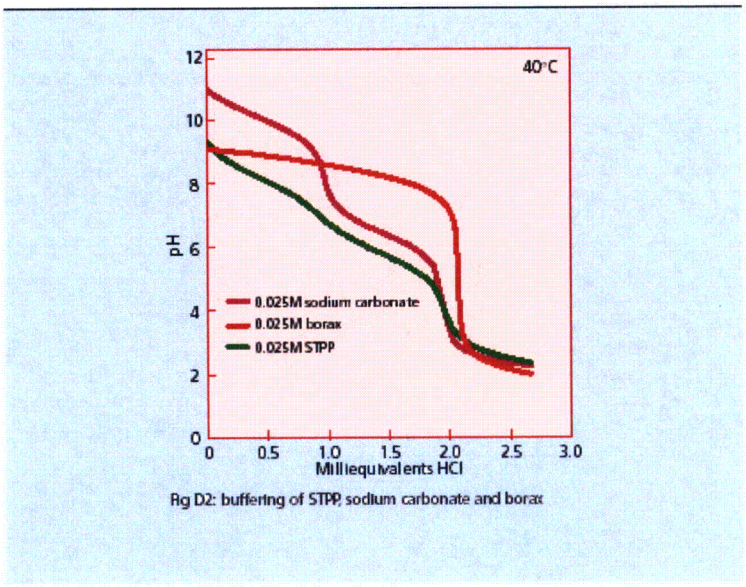

Figure 10. *Titration curve for 0.025 M Borax buffer solution found at http://www.borax.com/detergents/pheffect.html.*

The same titration curve was also calculated with ChemSheet.

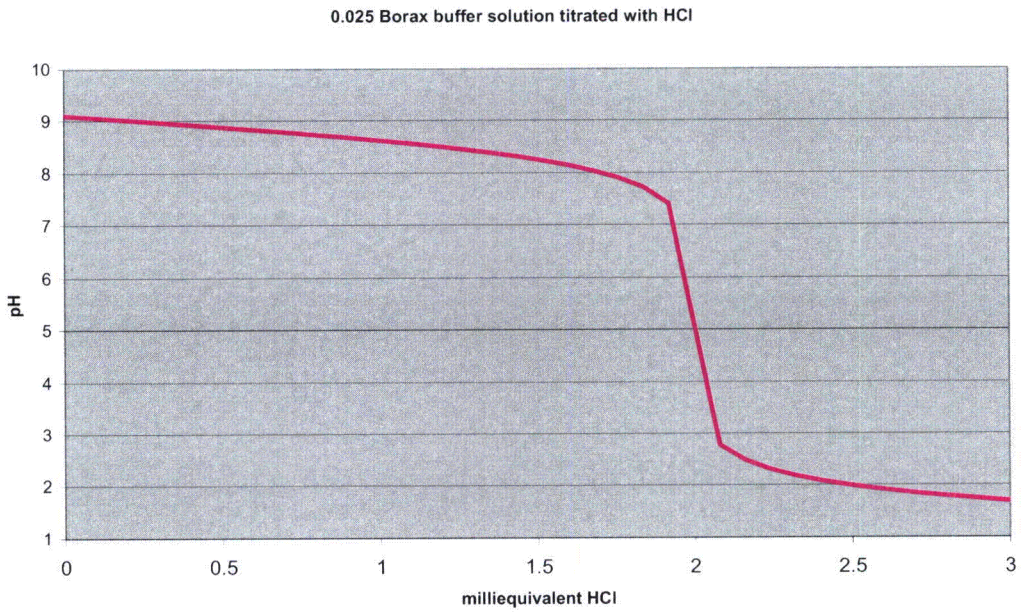

Figure 11. *Titration curve at 40 C for 0.025 M Borax buffer solution calculated with ChemSheet.*

It can be seen that the calculated titration curve is quite similar.

It can be concluded that the used thermodynamic data is applicable to pH calculations at temperature range between 25-50 degrees Celsius and at moderate pressure (1-5 atm). Probably it can be used at temperatures even close to boiling point of water (depending on the absolute pressure).

7.7 Updated Thermodynamic system

For ESBWR calculations a new thermodynamic system was prepared so that also cesium, iodine and necessary species for nitric acid are included.

Table 29. *Updated thermodynamic system.*

		Element								
Phase	Constituent	B	Cl	Cs	H	I	N	Na	O	e-
Vapour	H2O(g)				2				1	
	Cl2(g)		2							
	Cs(g)			1						
	Cs2(g)			2						
	CsH(g)			1	1					
	CsOH(g)			1	1				1	
	H(g)				1					
	H2(g)				2					
	HCl(g)		1		1					
	HI(g)				1	1				
	I(g)					1				
	I2(g)					2				
	ICl(g)		1			1				
	IO(g)					1			1	
	N2(g)						2			
	HNO3(g)				1		1		3	
	NH3(g)				3		1			
	NO(g)						1		1	
	NO2(g)						1		2	
	N2O(g)						2		1	
	O2(g)								2	
Water	H2O				2				1	
	B(OH)3(a)	1			3				3	
	B(OH)4(-a)	1			4				4	1
	Cl(-a)		1							1
	Cl2(a)		2							
	Cs(+a)			1						-1
	CsOH(a)			1	1				1	
	H(+a)				1					-1
	H2(a)				2					
	I(-a)					1				1
	I2(a)					2				
	Na(+a)							1		-1
	OH(-a)				1				1	1
	N2(a)						2			
	HNO3(a)				1		1		3	
	NH3(a)				3		1			
	NH4(+a)				4		1			-1
	NO2(-a)						1		2	1
	NO3(-a)						1		3	1
Solids	CsI			1		1				
	CsOH			1	1				1	
	Na2O*2B2O3*10H2O	4			20			2	17	
	Na2O*5B2O3*10H2O	10			20			2	26	
	NaCl		1					1		
	NaOH				1			1	1	

In ESBWR calculations cesium is given as CsOH which is highly soluble to water. CsOH(s) act as a strong base like NaOH(s) (it dissociates completely in aqueous solution)

Iodine is given as CsI, which is also soluble to water in basic pH range. As pH is lowered to acidic range iodine becomes volatile.

Formed HNO_3 is given as HNO_3 (a) which dissociates to H+ and NO_3^- ions (small fraction stays HNO_3 (a)). As an acid HNO_3 is comparable HCl.

It must mentioned that pH of neutral water is function of temperature. If temperature is increased from 25 °C then pH is lowered from 7.00 so that at 100 °C it is 6.14. This is the reason why there are small pH variations even with pure water if temperature is changed. Although pH of neutral water at elevated temperature is less than 7 it does not mean that it is acidic as there are as many hydrogen and hydroxide ions. So at 100 °C pH 6.14 marks neutral level on pH scale and pH 7 is already slightly alkaline.

7.8 ESBWR ChemSheet Model

An Excel model using ChemSheet and Excel macros and formulas was made for calculating pH in ESBWR system. Model is based on process flow diagram that was also used as basis in MELCOR simulation. The system is divided into six separate containers:

- SLCS Standby Liquid Control system buffer solution.
- RPV Reactor Pressure Vessel.
- LDW Lower drywell.
- UDW Upper drywell.
- GDSC GDCS pool.
- WW Wetwell.

Model contains a separate ChemSheet sub-model for each container. Each sub-model is stored in a separate worksheet. ChemSheet sub-models are used to calculate the thermodynamic equilibrium in containers. As a result of calculation the phase composition (vapor, liquid and solid phases) is determined (in this text liquid phase is same as aqueous phase). The pH is then calculated from H^+-ion activity in aqueous phase using simple formula ($-\log_{10}(Ac_{H+})$).

Vapor and liquid temperatures and vapor pressure in each container at different time steps are taken from MELCOR result file and used as input in each container's ChemSheet model. The phase equilibrium in a container is calculated using liquid temperature and vapor pressure.

Also the initial amounts of water, steam nitrogen and oxygen masses were taken from MELCOR.

MELCOR results contain amounts of steam and water flows between containers at each time step. These flow values are used to update the composition in containers. For example if water flow from RPV to LDW is 100 kg/s and length of time step is 1 s then 100 kg of liquid phase is removed from RPV and added to liquid phase in LDW. Or if steam flow from RPV to UDW is 10 kg/s and time step is 1 s then 10 kg of whole vapor phase is removed from RPV and added to vapor phase in UDW. This way every species in liquid or vapor phase is also transported from one container to other.

The whole calculation contains several thousands of time steps (from MELCOR). Each time step involves equilibrium calculation for phases in each container and then updating the amounts and the composition of phases based on inlet and outlet flow rates (from MELCOR).

A separate VBA macro was made that takes care of calling each container's ChemSheet model at each time step. Each ChemSheet model takes input values from certain worksheet range (containing values for temperature, pressure and phase composition). Also each model writes results from equilibrium calculation to certain worksheet range (containing equilibrium

phase composition). The values in input and output ranges are updated using Excel formulas between time steps according to inlet and outlet flow rates.

7.9 MELCOR Scenario 1

The ESBWR process flow diagram is shown in Figure 12. Grey arrows indicate connections that were not in use (but are included in the model in case they are used in other simulation).

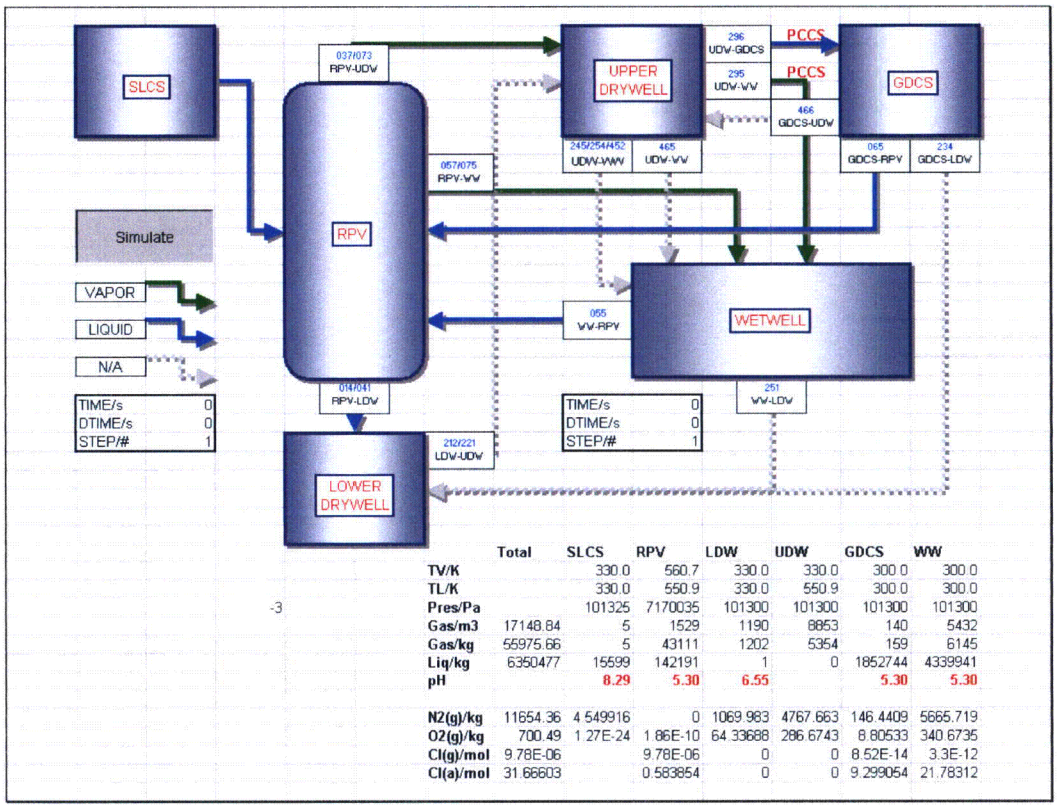

Figure 12. *ESBWR process flow diagram used in simulation.*

Containers are connected to each other according to respective MELCOR model.

- SLCS Connected to RPV (liquid flow).
- RPV Connected to LDW (liquid flow), UDW (vapor flow).
- UDW Connected to GDCS (liquid flow) and WW (vapor flow).
- GDCS Connected to RPV (liquid flow).
- WW Connected to RPV (liquid flow).

Flow amounts are negative if the flow direction is opposite (to directions given above). Each flow is divided into separate vapor and liquid flows so that vapor and liquid flow directions can be different.

PCCS was not included as data for it was not available when ChemSheet simulations were done. This means that flows to GDCS and WW were taken directly from UDW as vapor flows. This could underestimate HCl amount in the flow to GDCS. So even more HCl could be transported to GDCS than is now calculated. On the other hand the model is based purely

on equilibrium calculation – no transport mechanism like mass transfer from vapor to liquid phase is considered.

Input parameters used to initialize containers are shown in Table 30.

Table 30. *Initial values for ESBWR pH calculation of scenario 1.*

Parameter	RPV	LDW	UDW	GDCS	WW
T_V/K	560.69	330.00	330.00	300.00	300.00
T_L/K	550.90	330.00	550.90	300.00	300.00
Pres/Pa	7170035	101300	101300	101299.9	101299.9
H2O(g)/kg	21546.566*	67.255	299.676	3.584	138.648
N2(g)/kg	0.000	1069.983	4767.663	146.441	5665.719
O2(g)/kg	0.000	64.337	286.674	8.805	340.674
H2O(l)/kg	163755.7	0.0	0.0	1852744.0	4339939.9

**Amount of steam in RPV was not among MELCOR results and it was calculated from ideal gas law (pV=nRT), where volume of vapor in RPV was 942 m^3 – volume of water. Due to high pressure this value is not quite accurate.*

Mass fraction of sodium pentaborate was 12.5 % [8]. Volume of solution in SLCS was given as 15600 m^3. Density of soluble sodium pentaborate was estimated to be 1 kg/dm^3 and so amount of water in SLCS was set as 13650 kg and mass of sodium pentaborate as 1950 kg.

Amounts CsOH and CsI were calculated with MELCOR and given in results as masses in GDCS and WW. As the masses were only given at few time steps they were converted to linear formation rates so that it was easier to use them as source terms in ChemSheet model. The given rates are shown in Table 31 and Table 32.

Table 31. *Formation rates of CsOH and CsI in GDCS.*

GDCS (Data from MELCOR		
Time	CsOH	CsI
s	Rate/kg/s	Rate/kg/s
0	0	0
2000	0.0005	0.000075
3492	0.0075	0.001125
5388.7	0.075	0.01125
5881.3	0.004	0.0006
6080	0	0

Table 32. *Formation rates of CsOH and CsI in WW.*

WW (Data from MELCOR		
Time	CsOH	CsI
s	Rate/kg/s	Rate/kg/s
0	0	0
2000	0.0023	0.000345
5371.7	0.1	0.015
5831.3	0.022	0.0033
7200	0.0028	0.00042
10801	0.0002	0.00003
18001	0.00002	0.000003
25200	0	0

At each time step the given formation rate as [kg/s] was multiplied with time change (difference from previous time) to get formed CsOH and CsI amounts as [kg] and these values value were added to CsOH and CsI amounts from previous time step.

Different cases were calculated for HCl production from cable insulators. In ChemSheet model the HCl formation was given as source term in UDW (as gaseous HCl). At each time step the given formation rate as [mol/s] was multiplied with time change (difference from previous time) to get formed HCl amount as [mol] and this value was added to HCl amount from previous time step.

In cases where start pH is 5.3 appropriate amount of HCl was added to RPV (0.584 mol), GDCS (9.229 mol) and WW (21.783 mol).

Also for the Cases A and E the formation of HNO_3 in UDW was included. The total amount of formed HNO_3 is small if compared to the total amount of HCl and thus its effect on pH in GDCS is negligible in case E. Also in Case A HCl is still the main acid source.

HNO_3 formation was given as a source term in GDCS as it is added directly to the water phase and in UDW there is no liquid water present. Also the pH calculation has problems in absence of water.

Figure 13 shows temperature profiles that were calculated with MELCOR and used with ChemSheet models.

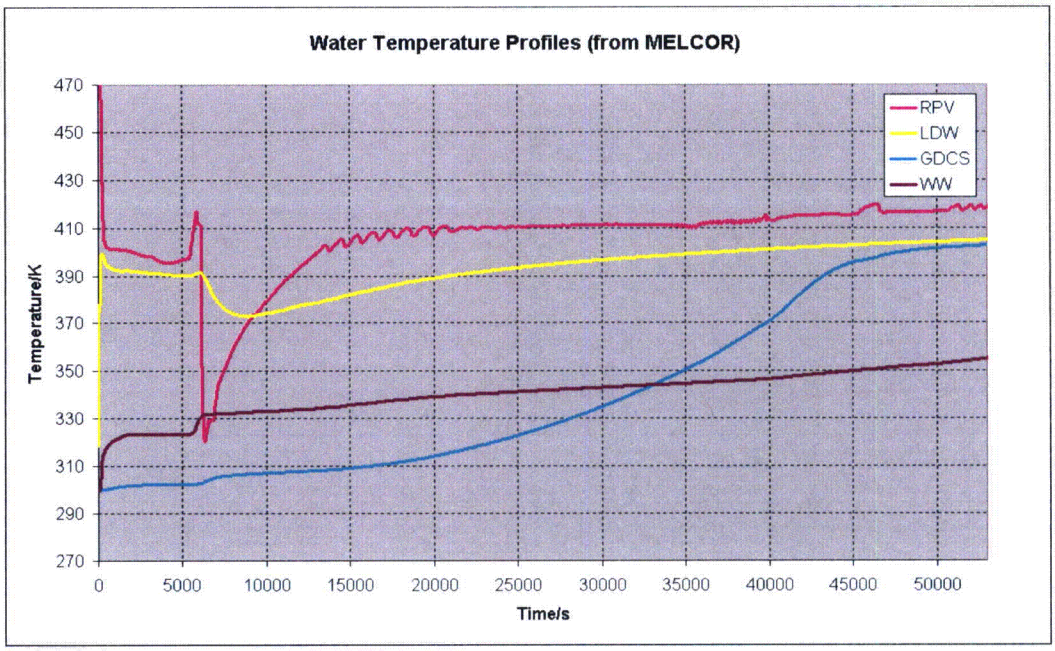

Figure 13. *Water temperature profiles from MELCOR.*

Figure 14 shows pressure profiles that were calculated with MELCOR and used with ChemSheet models.

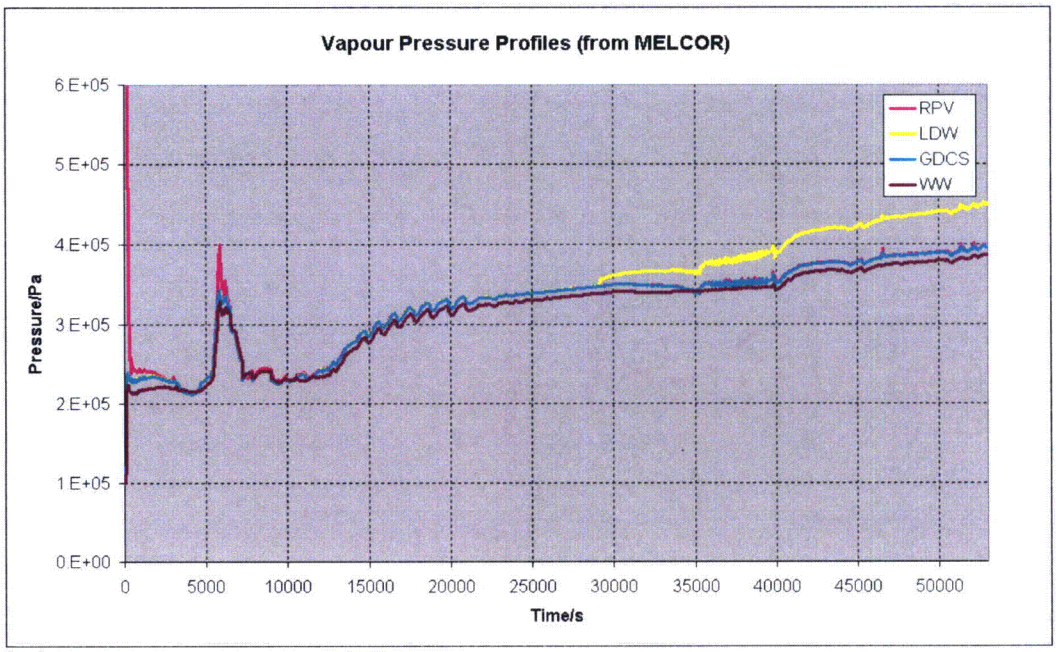

Figure 14. *Vapor pressure profiles from MELCOR.*

Figure 15 shows elementary Cs profiles that were calculated with MELCOR (in GDCS and WW) and used with ChemSheet model. Almost all Cs flows from GDCS through RPV to LDW.

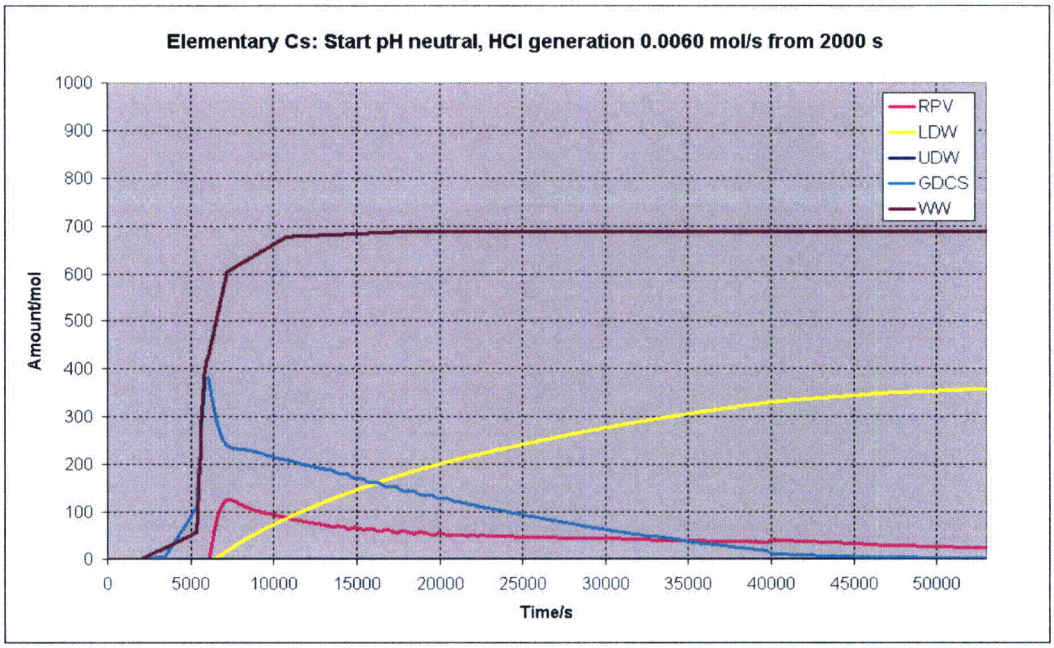

Figure 15. *Elementary Cs: same profiles in each pH case.*

Figure 16 shows flow rates to and from GDCS and mass of water in GDCS. It can be seen that mass of water in GDCS is decreased and at the same time flow from UDW (PCCS) containing HCl is slightly increasing. After formation of CsOH is stopped the acidic feed from PCCS decreases the pH in GDCS making it acidic. When this takes place depends on rate of HCl generation in UDW.

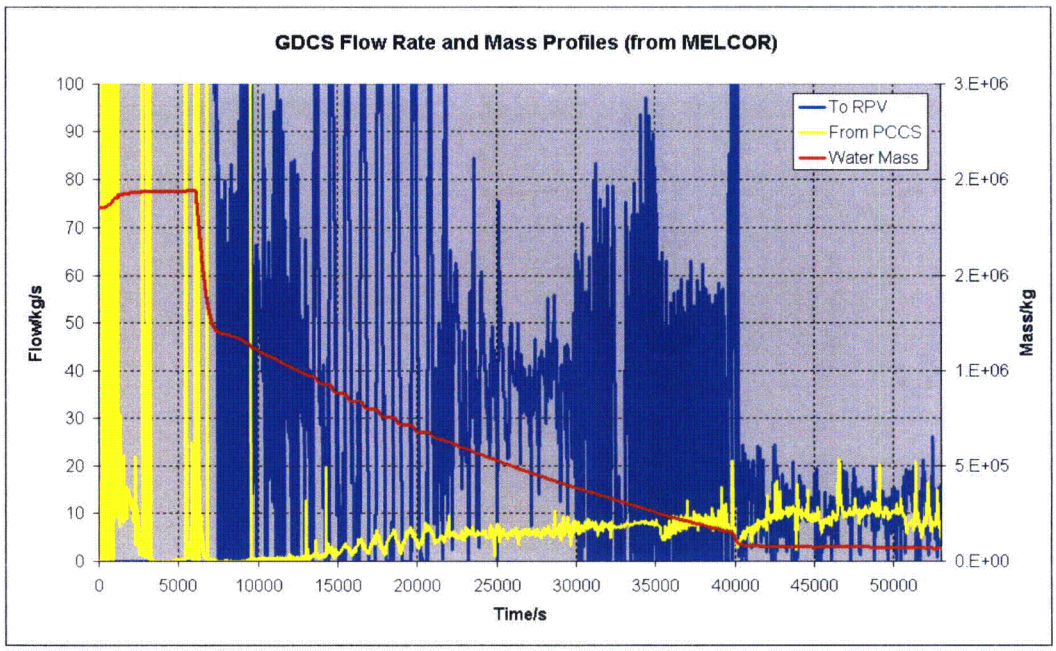

Figure 16. *GDCS flow rate and mass profiles from MELCOR.*

There are four figures from each pH case.

1. pH profiles. pH is calculated from H(+a) activity in water.
2. Elementary chlorine in water. If present then almost all chlorine in water is as Cl(-a).
3. Elementary iodine in vapor. If present then almost all iodine in vapor is as $I_2(g)$.
4. Elementary iodine in water. If present then almost all iodine in alkaline water is as I(-a) and more and more iodine is as $I_2(a)$ when water becomes more acidic.

Calculated iodine amounts in vapor phase (mainly in GDCS) at acidic conditions are result from equilibrium calculation using ideal data (no Pitzer interaction parameters were available for aqueous iodine species).

7.9.1 pH Case A

The case A can be considered as a base case for pH. In case A both HCl and HNO_3 production rates were accounted for. The HCl addition is distributed between Lower and Upper Drywell according to actual presence of cable material. About 92 % of all cables reside in the Lower Drywell and the rest is assumed to be in the Upper Drywell. HNO_3 was included though the total production of nitric acid is negligible in comparison to that of HCl.

Figures 17-20 show results from pH calculation with ChemSheet where start pH was set as 5.3 and total HCl generation was 430 mol (8 v-% in UDW and 92 v-% in LDW) and total HNO_3 generation was 5.2 mol (100 v-% in GDCS). These amounts correspond to the total formations of HCl and HNO_3 between 2000 s to 53 000 s. The pH in GDCS becomes acidic around 45 100 s. The pH in other containers stays alkaline. The rapid change from alkaline to acidic is typical for titration of strong bases (CsOH) with strong acids (HCl).

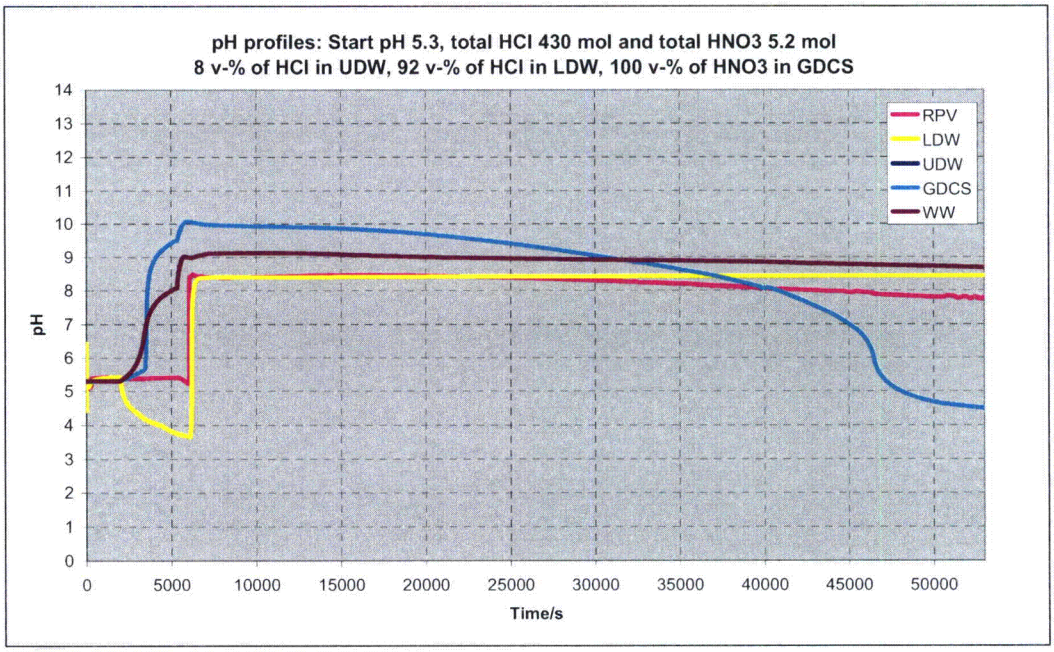

Figure 17. *pH profiles: start pH 5.3 and total HCl 430 mol and total HNO_3 5.2 mol. 8 v-% of HCl formation in UDW and 92 v-% in LDW, HNO_3 formation in GDCS.*

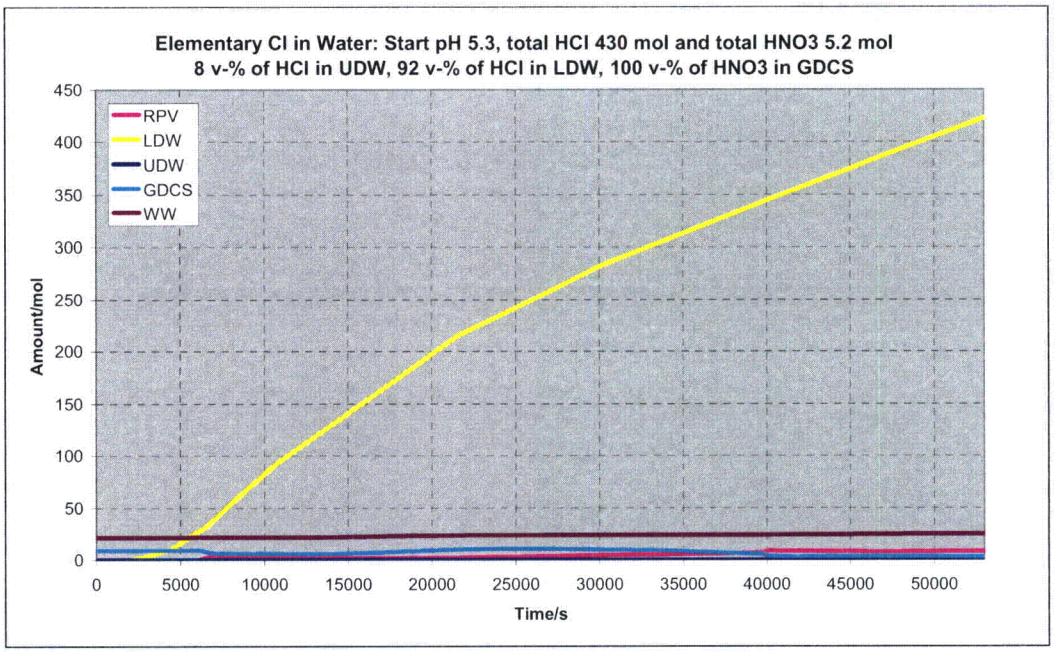

Figure 18. *Elementary Cl in water: start pH 5.3 and total HCl 430 mol and total HNO_3 5.2 mol. 8 v-% of HCl formation in UDW and 92 v-% in LDW, HNO_3 formation in GDCS.*

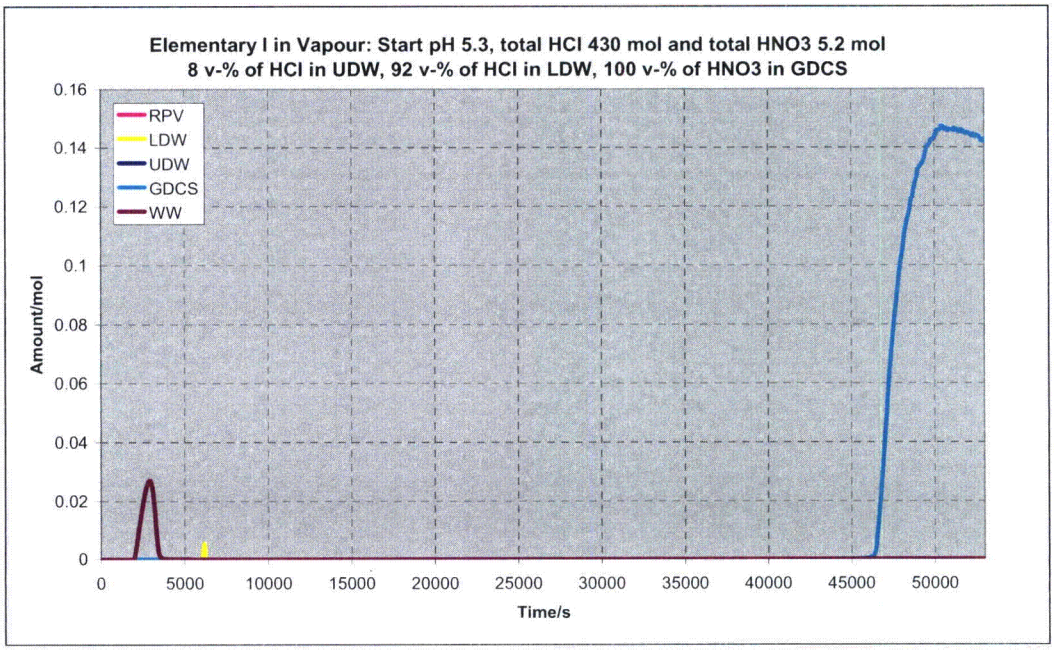

Figure 19. *Elementary I in vapor: start pH 5.3 and total HCl 430 mol and total HNO_3 5.2 mol. 8 v-% of HCl formation in UDW and 92 v-% in LDW, HNO_3 formation in GDCS.*

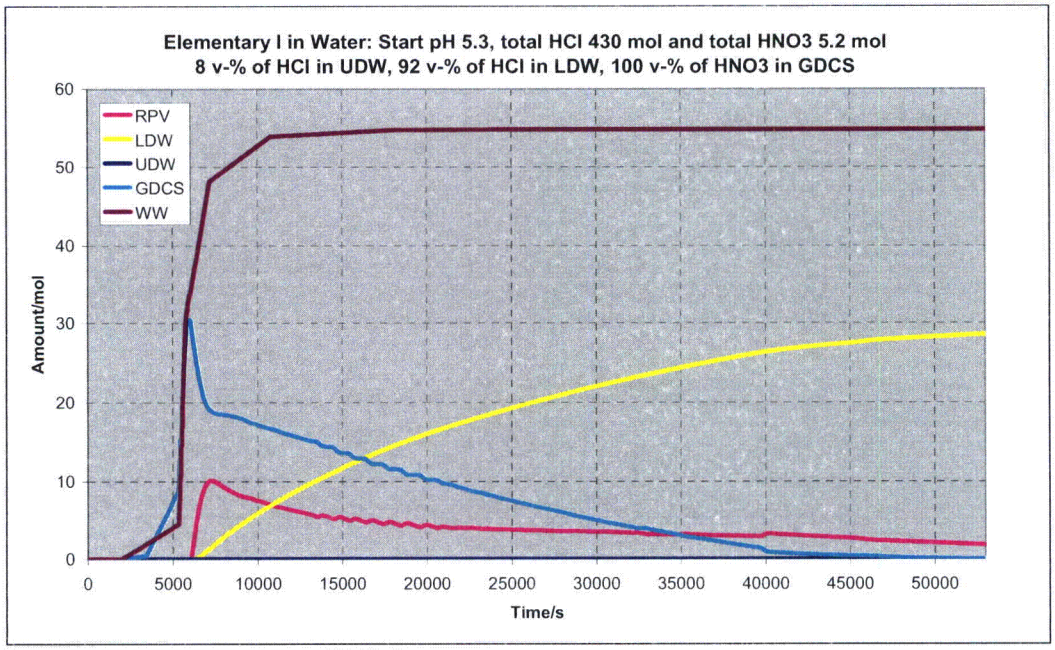

Figure 20. *Elementary I in water: start pH 5.3 and total HCl 430 mol and total HNO_3 5.2 mol. 8 v-% of HCl formation in UDW and 92 v-% in LDW, HNO_3 formation in GDCS.*

7.9.2 pH Case B Results

In the pH case B all HCl was assumed to be released in the UDW, no HNO_3 release was included. The release rate of HCl corresponded to that used for ABWR. Figures 21-24 show results from pH calculation with ChemSheet where start pH was set as 5.3 and HCl generation was set as 0.0015 mol/s from 2000 s. The pH in GDCS becomes acidic around 41 000 s. The pH in other containers stays alkaline.

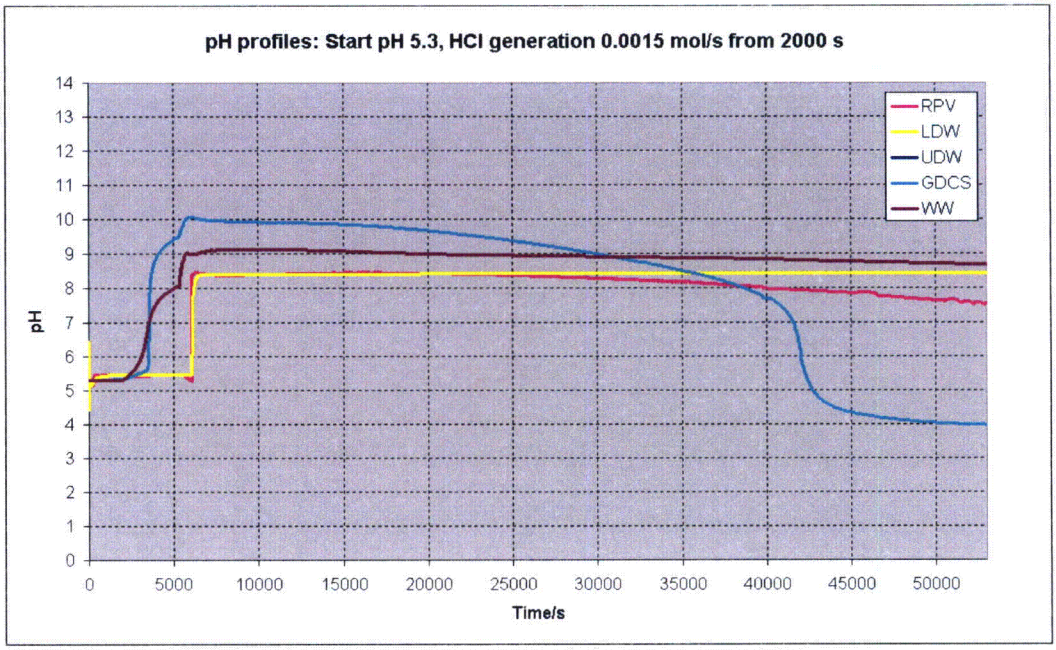

Figure 21. *pH profiles: start pH 5.3 and HCl generation 0.0015 mol/s.*

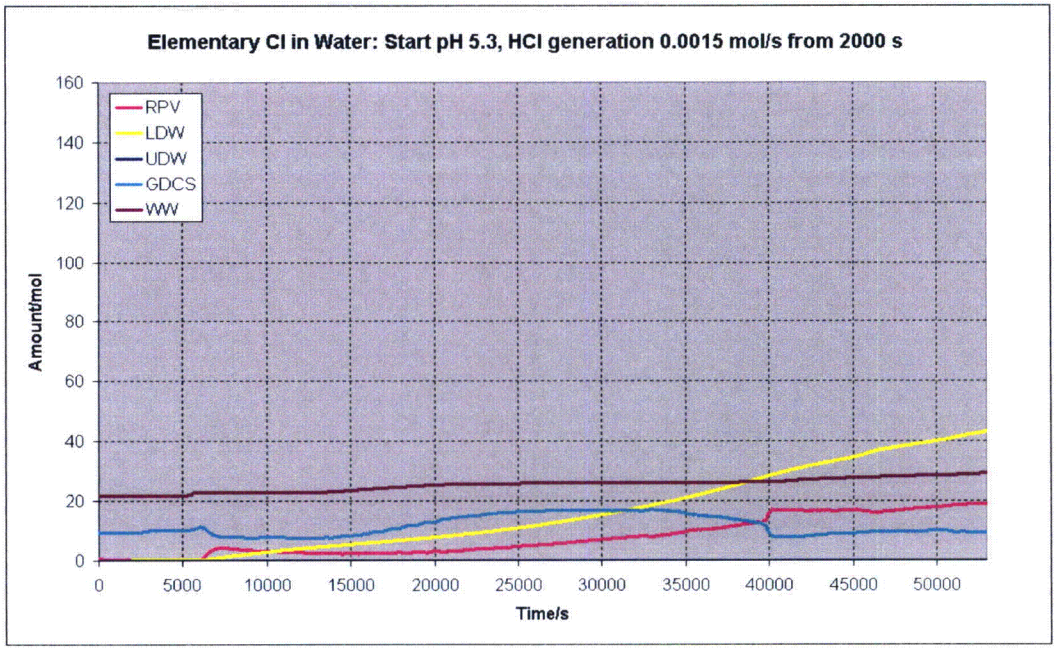

Figure 22. *Elementary Cl in water: start pH 5.3 and HCl generation 0.0015 mol/s.*

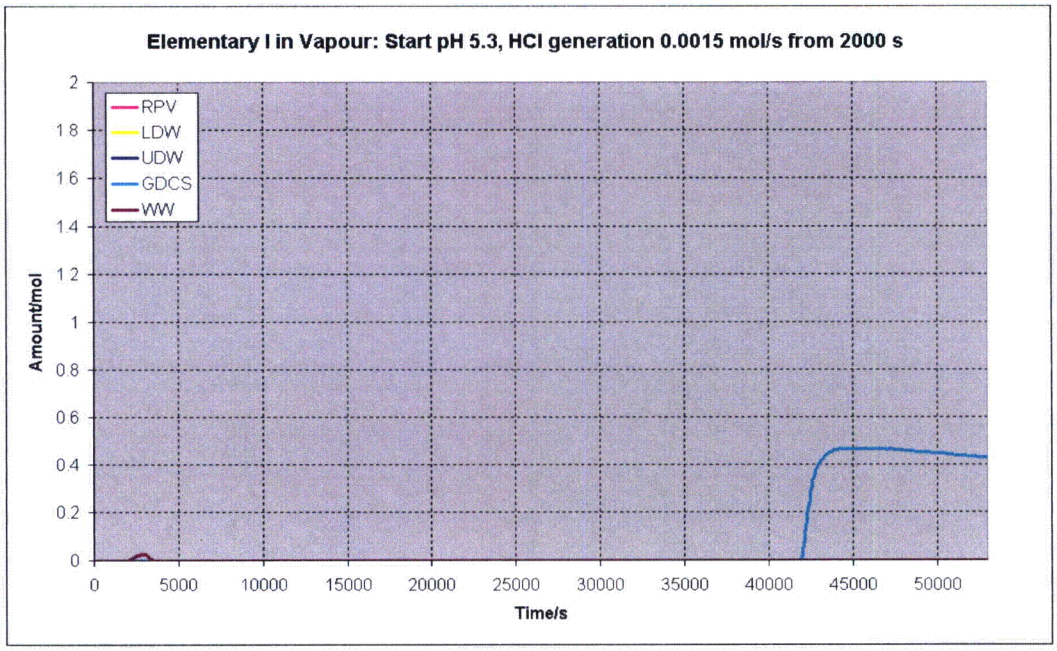

Figure 23. *Elementary I in vapor: start pH 5.3 and HCl generation 0.0015 mol/s.*

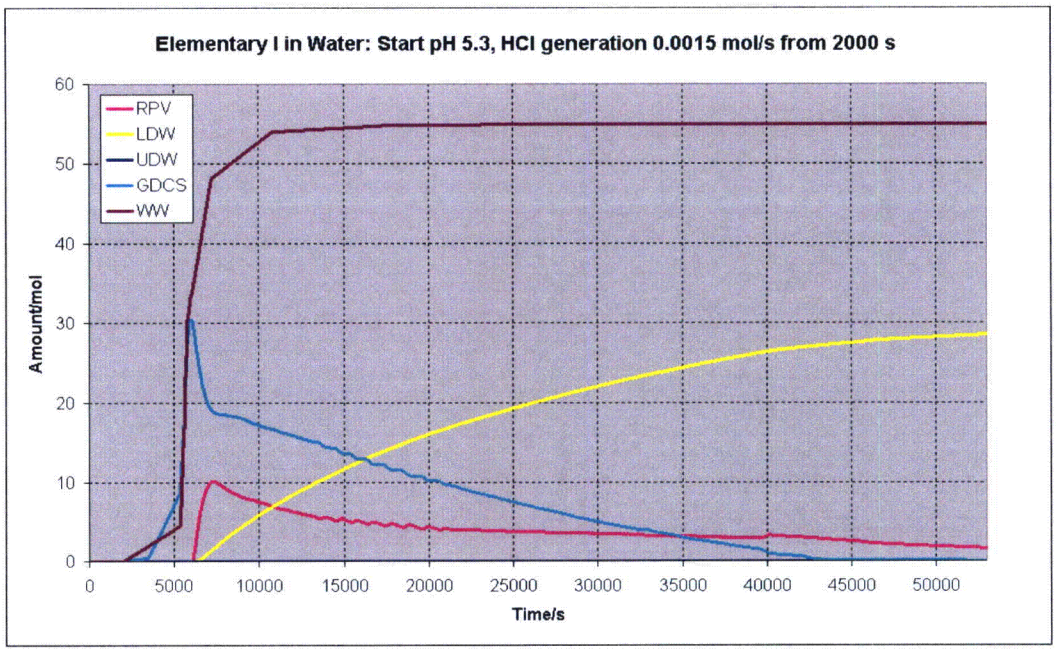

Figure 24. *Elementary I in waters. Start pH 5.3 and HCl generation 0.0015 mol/s.*

7.9.3 pH Case C Results

In the pH case C only HCl was considered and added to UDW. The HCl release rate was estimated with the dose rates of DCD Tier 2, Ch. 3 scaled to correspond time t=2000 s. Figures 25-28 show results from pH calculation with ChemSheet where start pH was set as 5.3 and HCl generation was set as 0.0060 mol/s from 2000 s. The pH in GDCS becomes acidic around 29000 s. The pH in RPV becomes acidic around 40 000 s. The pH in other containers stays alkaline.

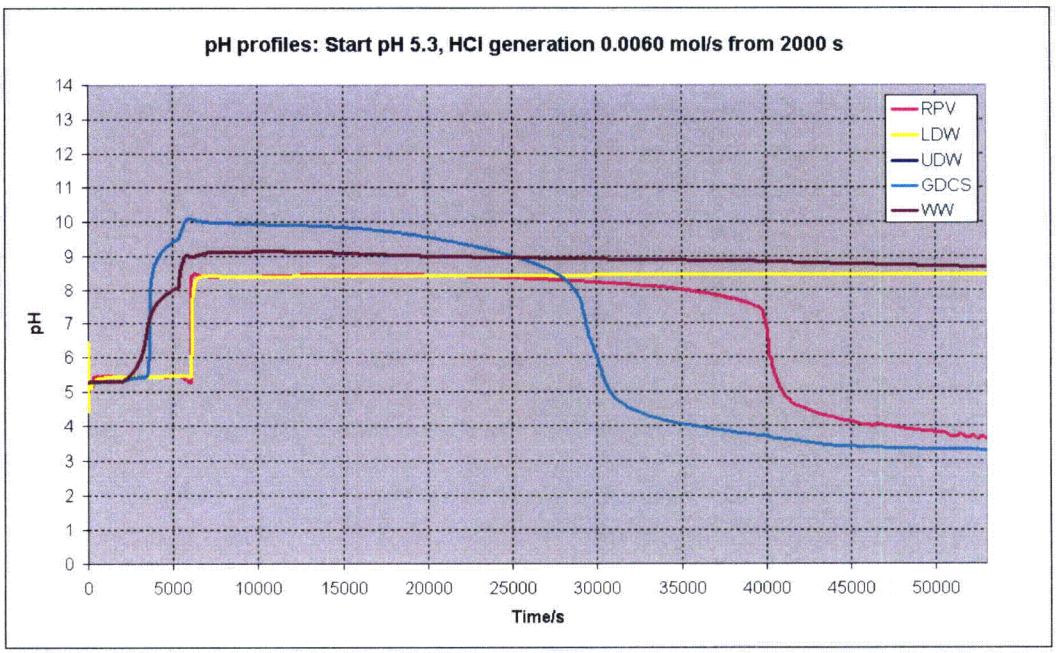

Figure 25. *pH profiles: start pH 5.3 and HCl generation 0.0060 mol/s.*

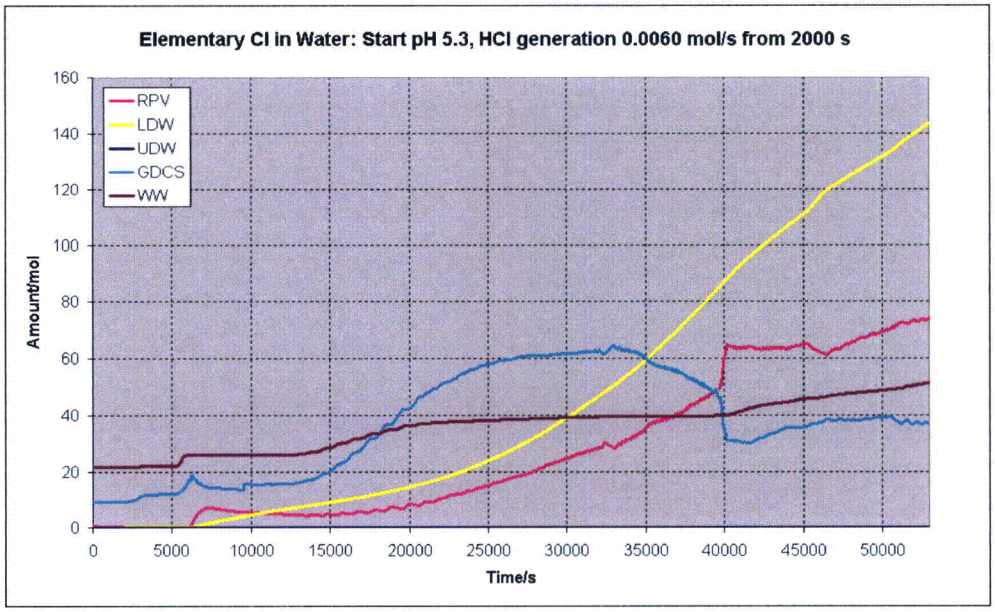

Figure 26. *Elementary Cl in water: start pH 5.3 and HCl generation 0.0060 mol/s.*

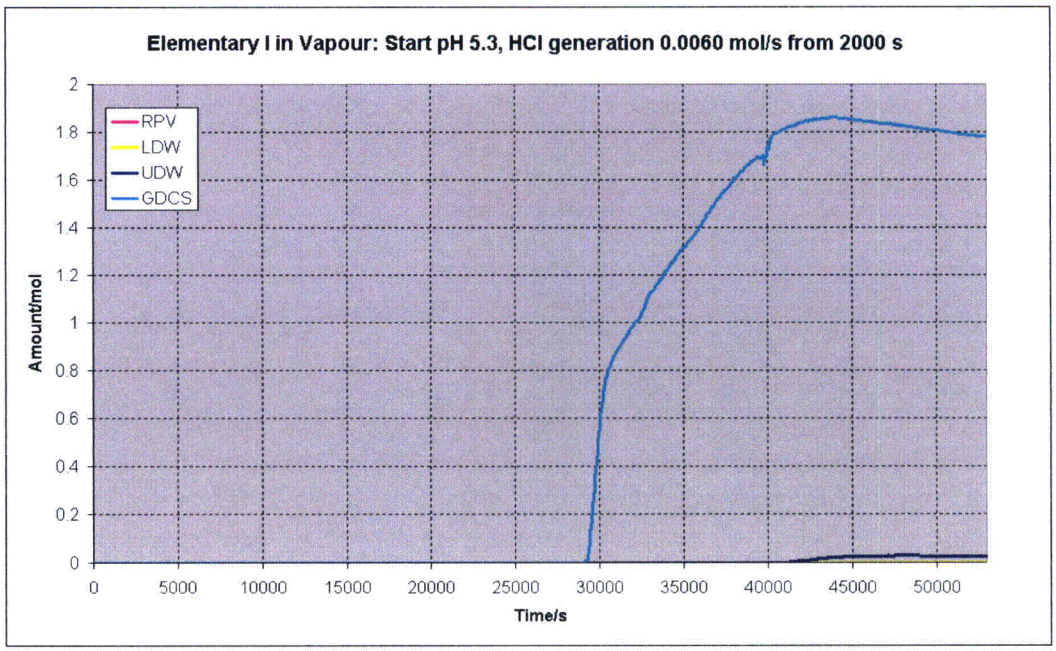

Figure 27. *Elementary Cl in vapor: start pH 5.3 and HCl generation 0.0060 mol/s.*

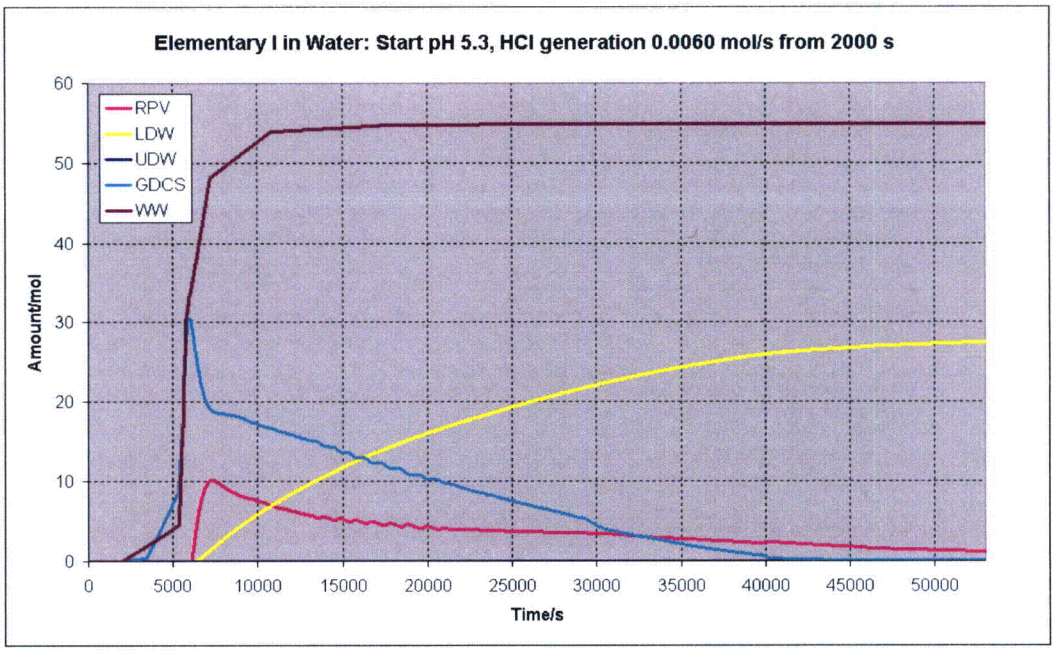

Figure 28. *Elementary I in water: start pH 5.3 and HCl generation 0.0060 mol/s.*

7.9.4 pH Case D Results

In the pH case D the HCl release was calculated by scaling the DCD Tier 2, Ch. 3 dose rate by a rough accounting for the decay of activity along time. Figures 29-32 show results from pH calculation with ChemSheet where start pH was set as 5.3 and HCl generation was set as 0.0038 mol/s from 2000 s. The pH in GDCS becomes acidic around 34 000 s. The pH in RPV becomes acidic around 46 500 s. The pH in other containers stays alkaline.

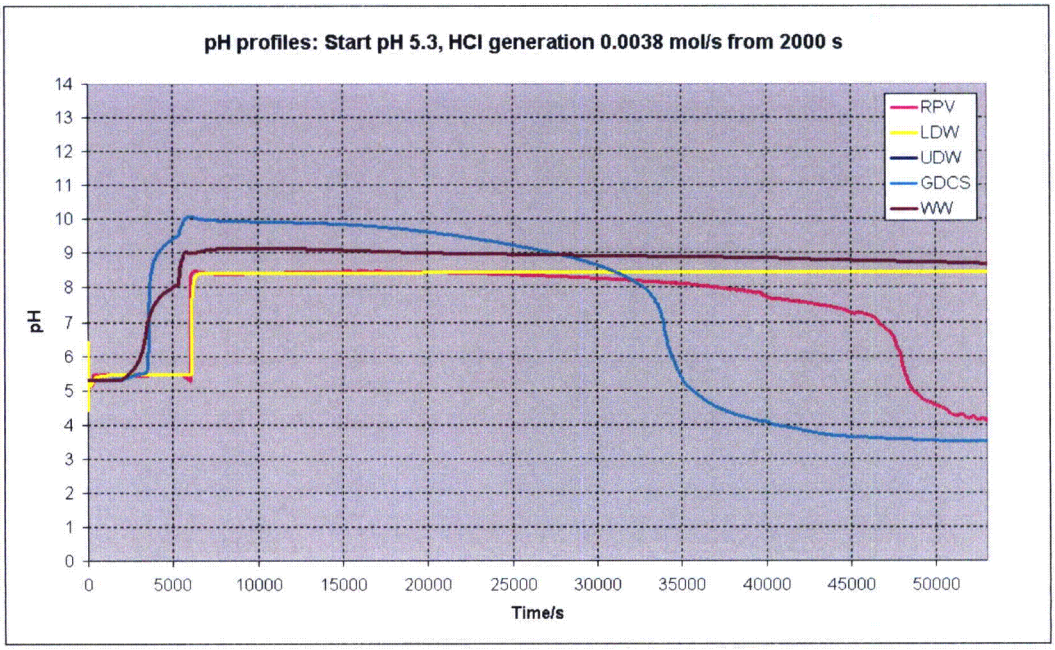

Figure 29. *pH profiles: start pH 5.3 and HCl generation 0.0038 mol/s.*

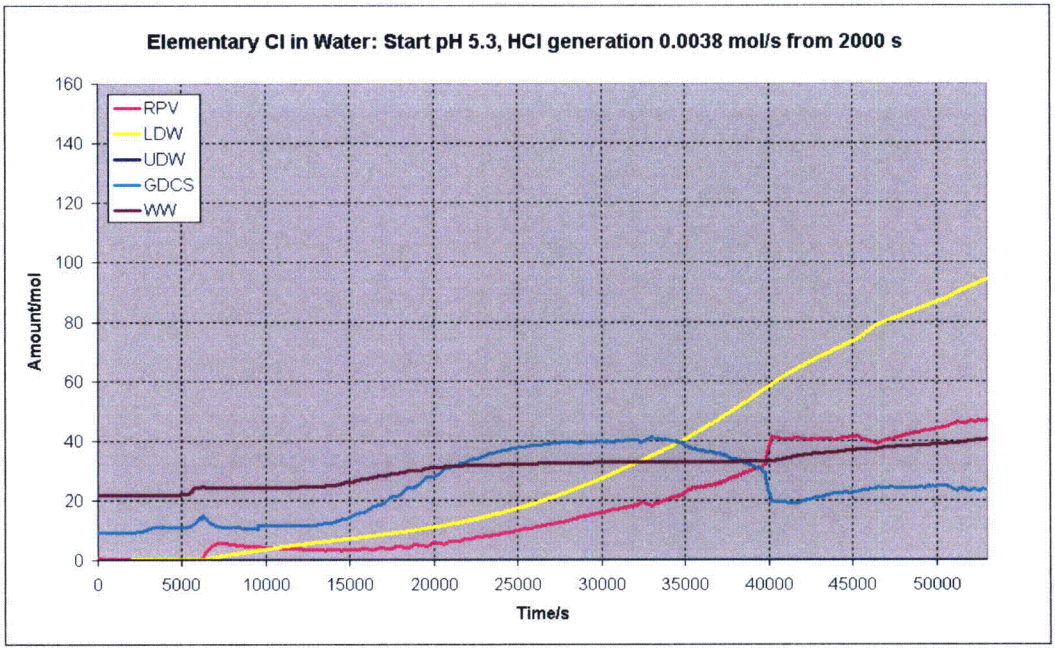

Figure 30. *Elementary Cl in water: start pH 5.3 and HCl generation 0.0038 mol/s.*

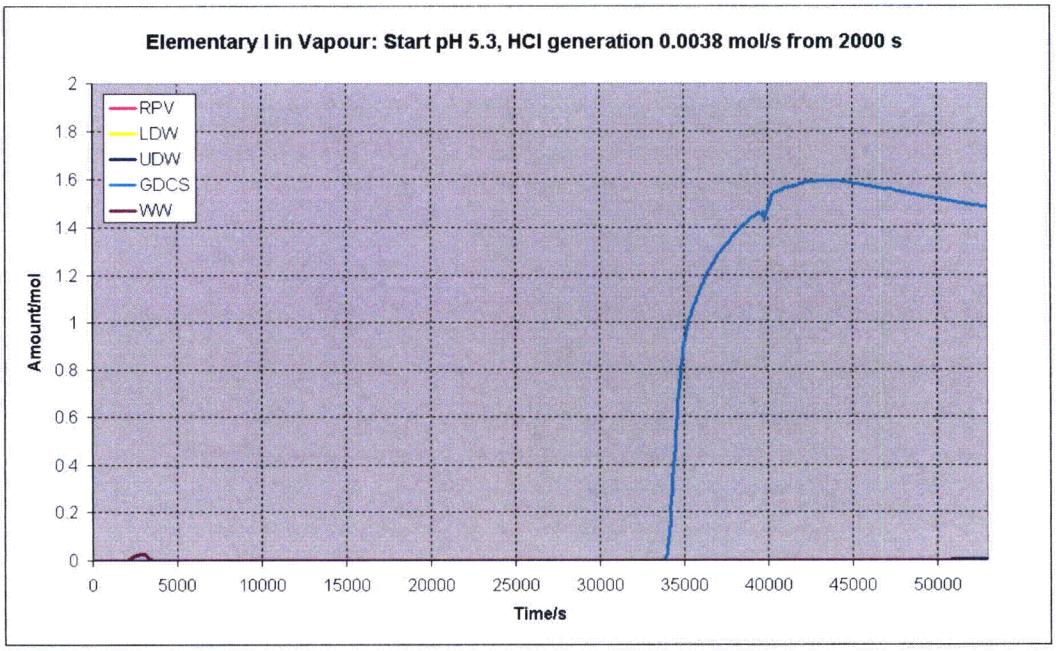

Figure 31. *Elementary I in vapor: start pH 5.3 and HCl generation 0.0038 mol/s.*

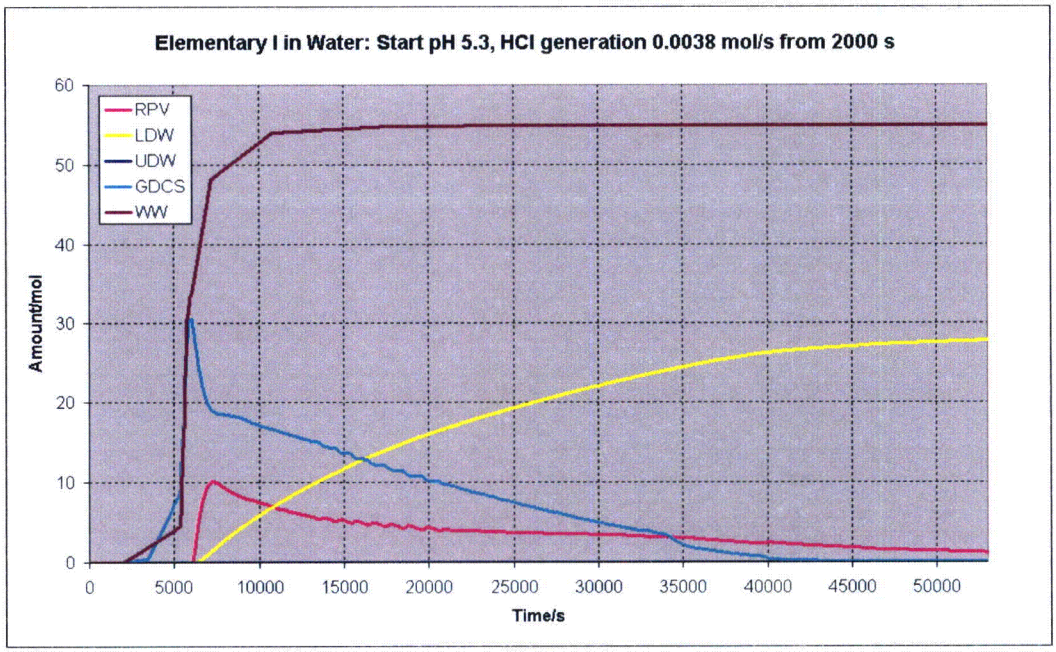

Figure 32. *Elementary I in water: start pH 5.3 and HCl generation 0.0038 mol/s.*

7.9.5 pH Case E

The pH-case E is a sensitivity run of the pH case C, showing the effect of the start pH of the pools being neutral instead of being at pH 5.3.

Figures 33-36 show results from pH calculation with ChemSheet where start pH was neutral and HCl generation was set as 0.0060 mol/s from 2000 s. The pH in GDCS becomes acidic around 29 000 s. The pH in RPV becomes acidic around 40 000 s. The pH in other containers stays alkaline. These results are practically same than the results where the start pH was set as 5.3.

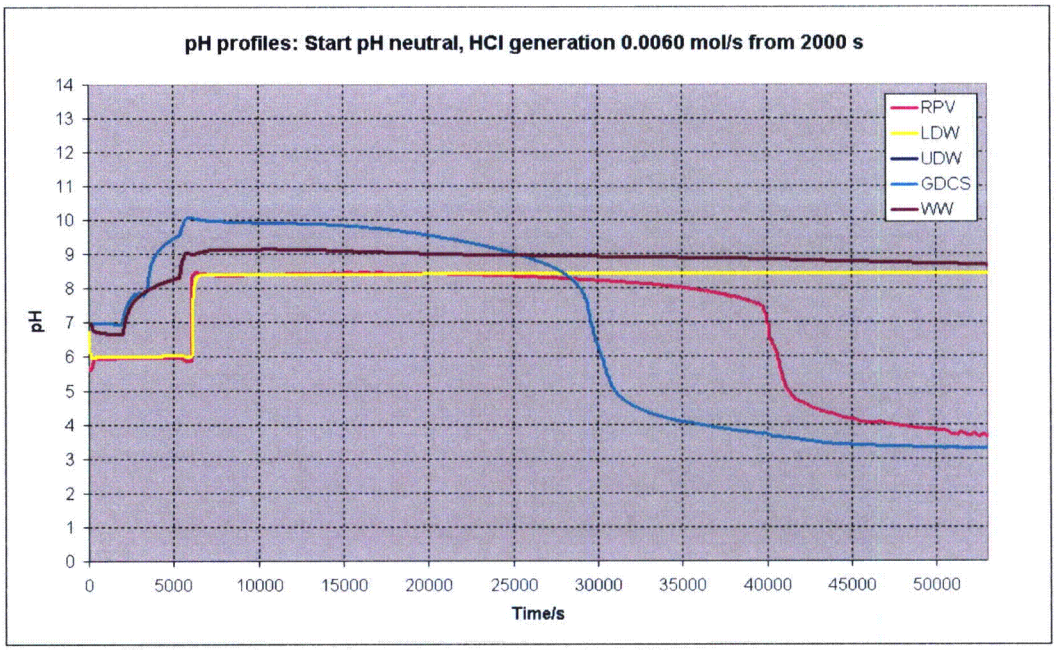

Figure 33. *pH profiles: start pH neutral and HCl generation 0.0060 mol/s.*

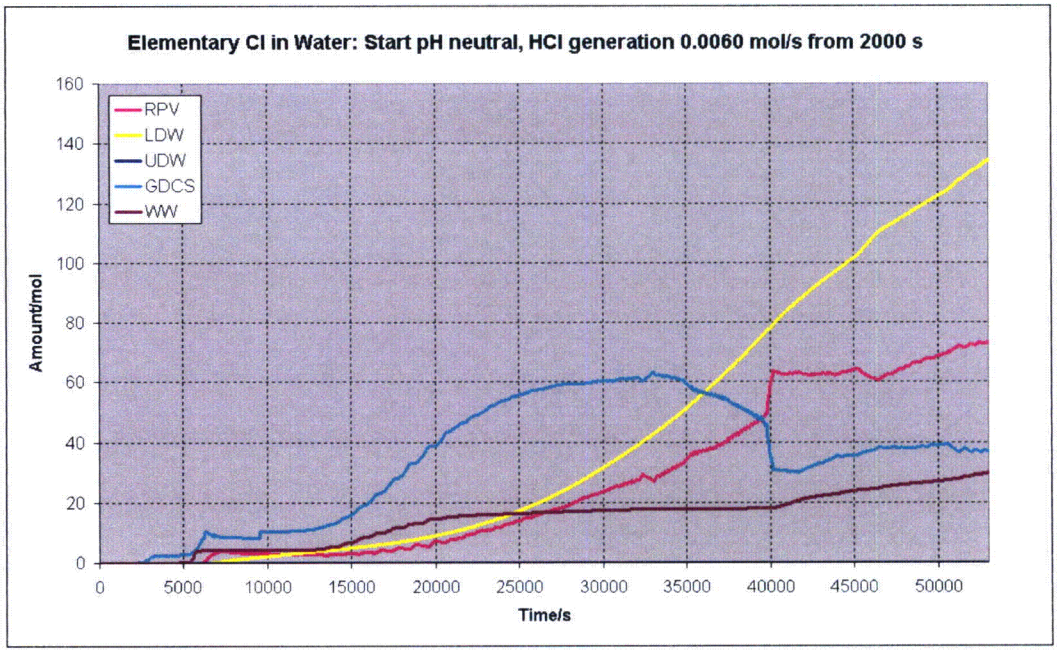

Figure 34. *Elementary Cl in water: start pH neutral and HCl generation 0.0060 mol/s.*

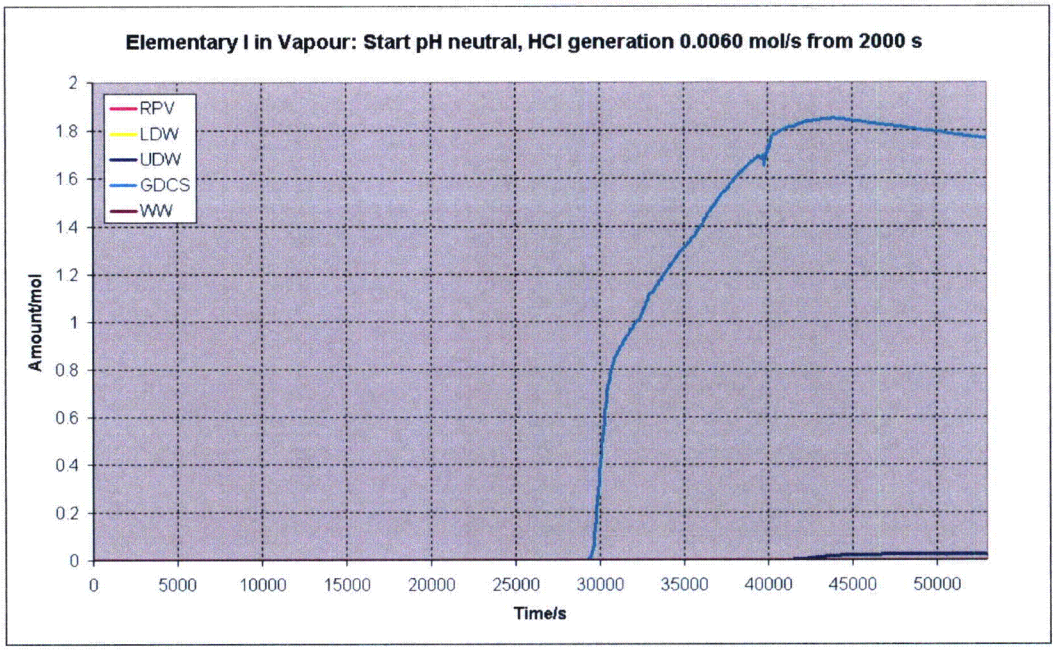

Figure 35. *Elementary I in vapor: start pH neutral and HCl generation 0.0060 mol/s.*

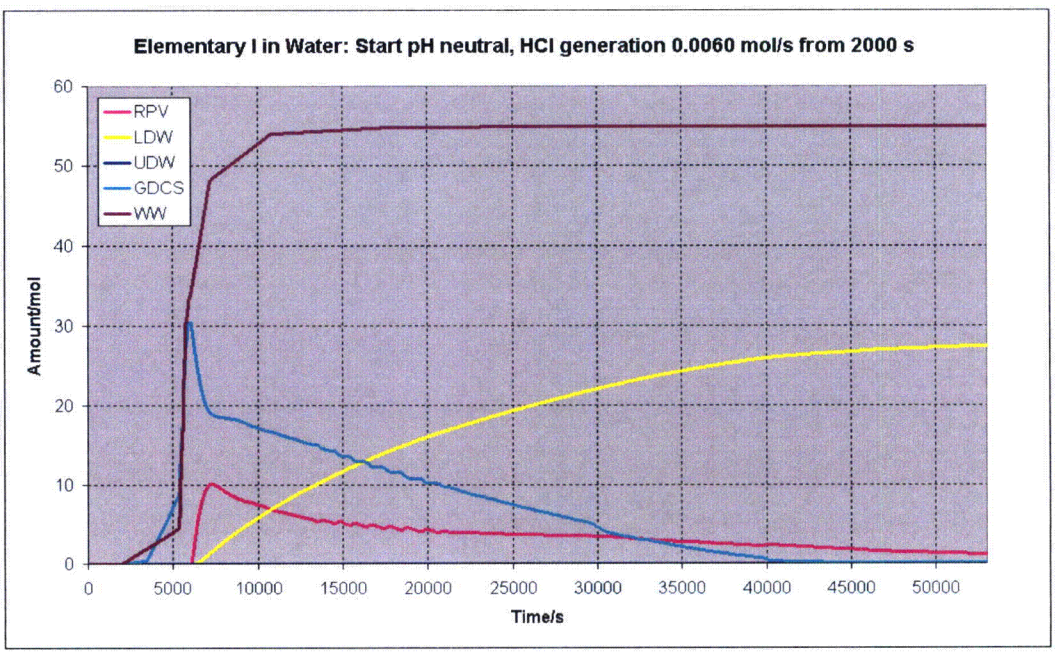

Figure 36. *Elementary I in water: start pH neutral and HCl generation 0.0060 mol/s.*

7.9.6 pH Case F

The pH-case F is a sensitivity run of the pH-case A showing the effect of all HCl added to the Upper Drywell.

Figures 37-40 show results from pH calculation with ChemSheet where start pH was set as 5.3 and total HCl generation was 430 mol (100 v-% in UDW) and total HNO_3 generation was 5.2 mol (100 v-% in GDCS). These amounts correspond to the total formations of HCl and HNO_3 between 2000 s to 53 000 s. The pH in GDCS becomes acidic around 23000 s. The pH in RPV becomes acidic around 37 000 s. The pH in other containers stays alkaline. The effect of HNO_3 on pH is negligible (if compared to HCl).

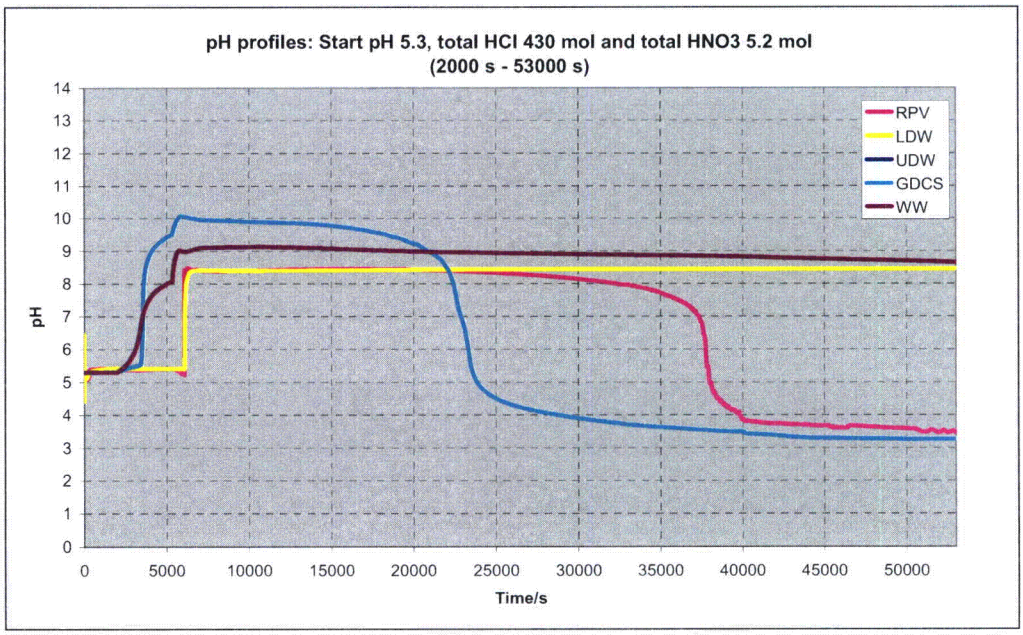

Figure 37. *pH profiles: start pH 5.3 and total HCl 430 mol and total HNO_3 5.2 mol. HCl formation in UDW and HNO_3 formation in GDCS.*

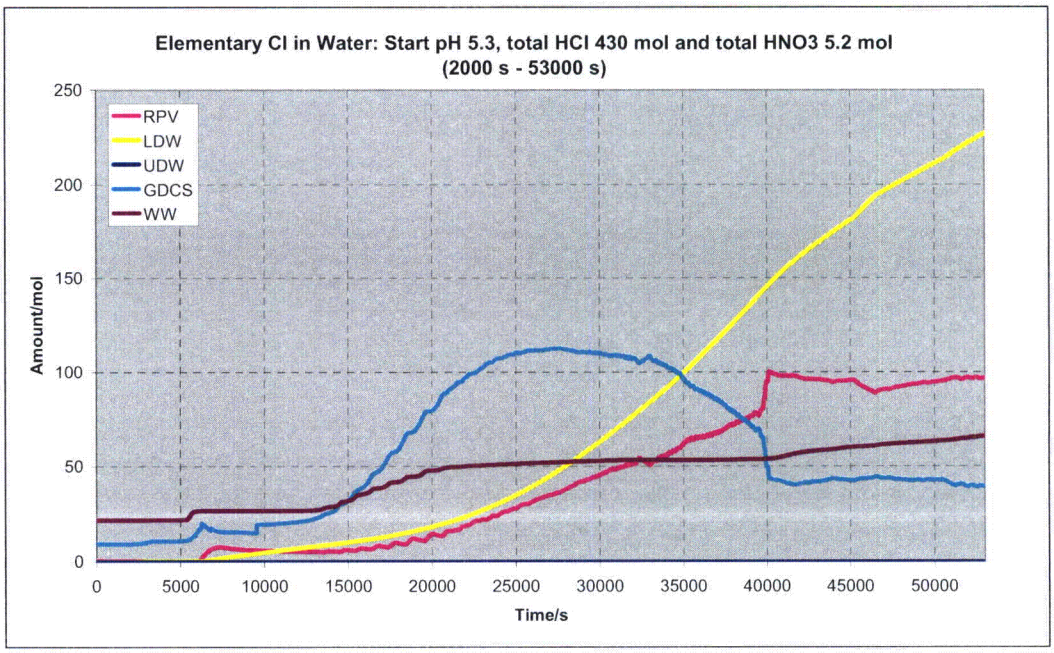

Figure 38. *Elementary Cl in water: start pH 5.3 and total HCl 430 mol and total HNO_3 5.2 mol. HCl formation in UDW and HNO_3 formation in GDCS.*

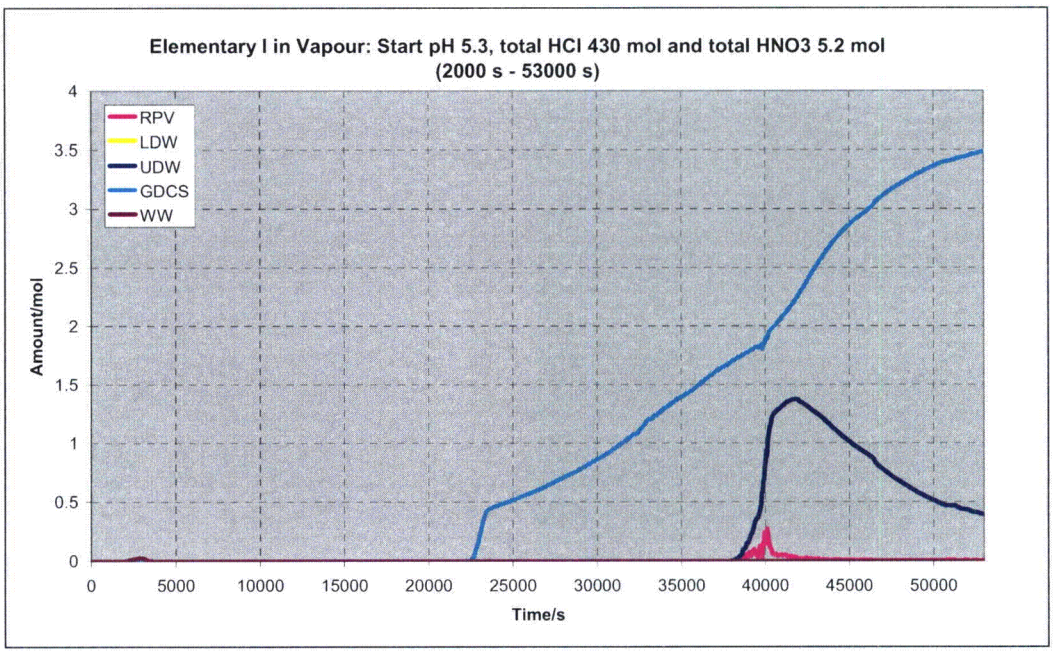

Figure 39. *Elementary I in vapor: start pH 5.3 and total HCl 430 mol and total HNO_3 5.2 mol. HCl formation in UDW and HNO_3 formation in GDCS.*

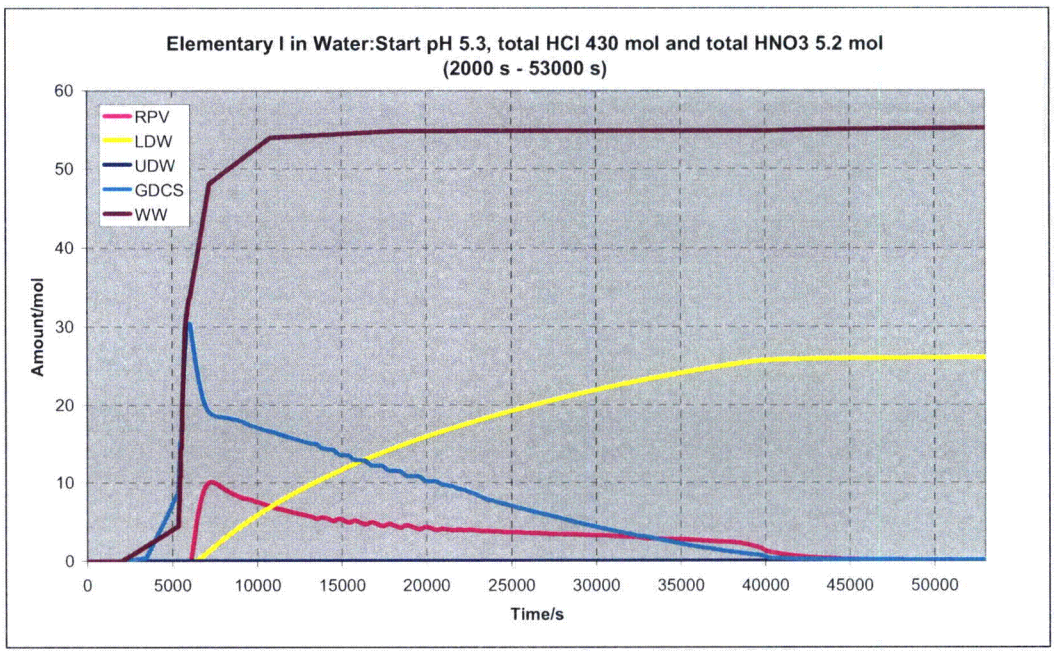

Figure 40. *Elementary I in water: start pH 5.3 and total HCl 430 mol and total HNO_3 5.2 mol. HCl formation in UDW and HNO_3 formation in GDCS.*

8 Analysis of a source term from the containment in Scenario 1 (Bottom Drain Line Break with ADS)

The hypothetical accident scenario begins with a failure of reactor pressure vessel (RPV) bottom drain line ($A=2.165 \cdot 10^{-3}$ m^2). The reactor is scrammed at time 0 s. All Isolation Condenser Drain Lines are assumed to be blocked thus failing to provide any coolant injection to the RPV. GDCS pool injection is assumed to be unavailable until 7400 s (variation 1) or till 6083 s (variation 2) from the accident beginning. This timing specification of reflooding was used in this run to allow high oxidation in the core but to prevent Pressure vessel failure. During the reflooding the GDCS injection lines are fully open. Equalization line is opened simultaneously with the GDCS injection. All 6 PCCS units are operating through out the accident progression.

The following key event summary is for information of the overall time events in the scenario.

Table 33. *Key event summary of the BDL Break scenario.*

Event	Timing (s)	
Reactor scram	0	
Level L2 signal	2	
Level L1 signal	8	
SRV #1 open	19	
SRV #2 open	64	
DPV valve # 1 open	108	
DPV valve # 2 open	154	
Level TAF (core uncovered)	327	
Oxidation starts	1486	
FP gap release, core rings 1, 2 and 3	1983	
FP gap release, core ring 4	1985	
FP gap release, core ring 5	2003	
Core fully uncovered	2125	
Core support plate failure by yielding, ring 1	5372	
Core support plate failure by yielding, ring 2	5389	
Core support plate failure by yielding, ring 4	5585	
GDCS injection line open	7400	6083
Equalization line opened	7400	6083
Core fully recovered	8220	6900
GDCS pool empty	-	-
In-vessel H_2 production (kg)	369	376
End of calculation	23867	56943

8.1 Reactor coolant system behavior

The reactor core is uncovered at 327 s (=5.5 min) from the beginning of accident due to of coolant through BDL break (Fig. 41). No core makeup is available till 7400 s (=2 hr). The core is fully uncovered at 2125 s (=35 min). The core in uncovered for 1.7 hr before start of reflooding. Core is fully recovered at about 8220 s (=2.3 hr).

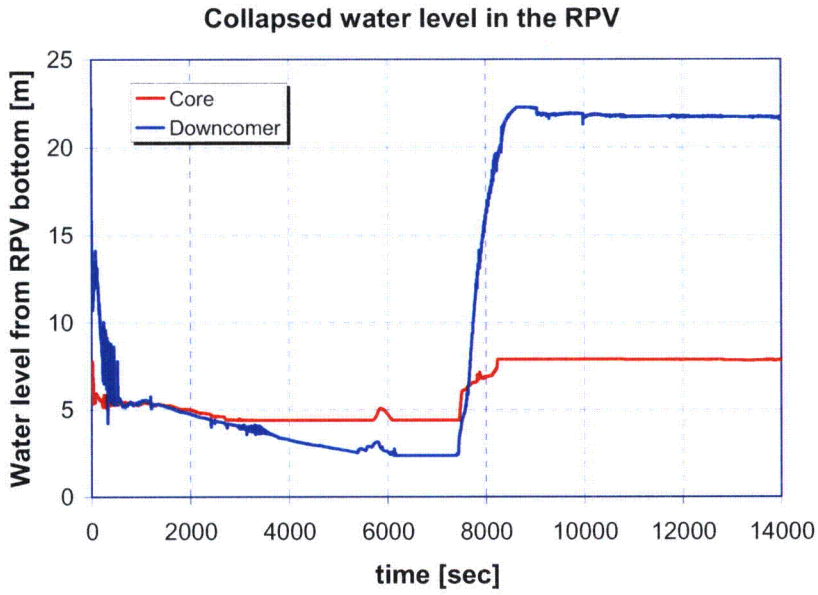

Figure 41. *Collapsed water level in the core and the downcomer. Bottom Drain Line Break ($A=2.165 \cdot 10^{-3}$ m^2) case with ADS and reflooding by GDCS injection at 7400 s.*

The temperature of cladding in core ring 1 (Fig. 42) begins to increase after full uncovery of the core. The temperatures in the upper parts of the core reach Zr melting temperatures. Molten Zr, however, is set to be held up by ZrO_2 layer till the ZrO_2 temperature reaches 2400 K. Following the start of GDCS injection oxidation increases in the core and causes a rapid temperature escalation in the upper half of the core and causes relocation of molten Zr downwards. Material relocation is seen in Fig. 42 as rapid decrease of temperature to zero. As the surrounding Zr disappears in the uppermost node also the fuel pellets relocate downwards as particle debris.

The total mass of ZrO_2 in the core is depicted in Figure 43. [[

]]

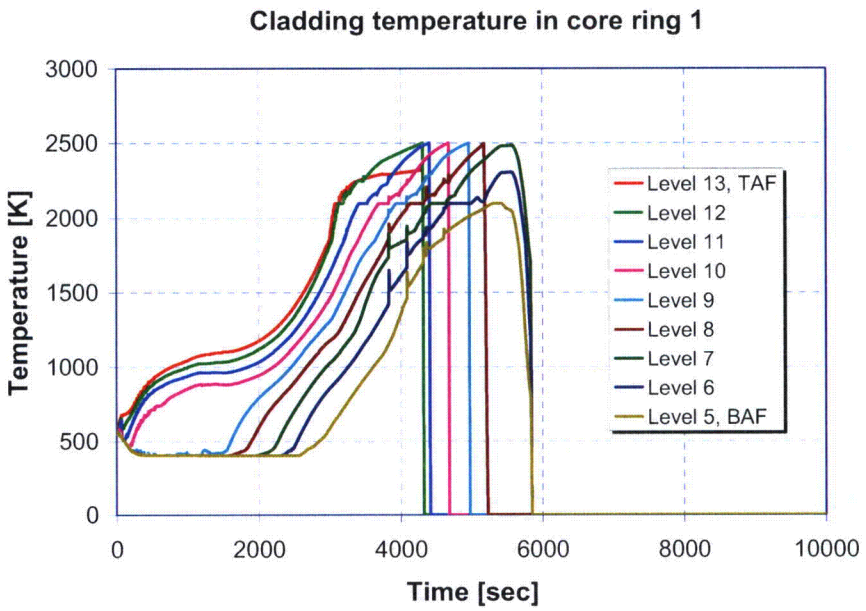

Figure 42. *Cladding temperature in core ring 1. Bottom Drain Line Break ($A=2.165 \cdot 10^{-3}$ m^2) case with ADS and reflooding by GDCS injection at 7400 s.*

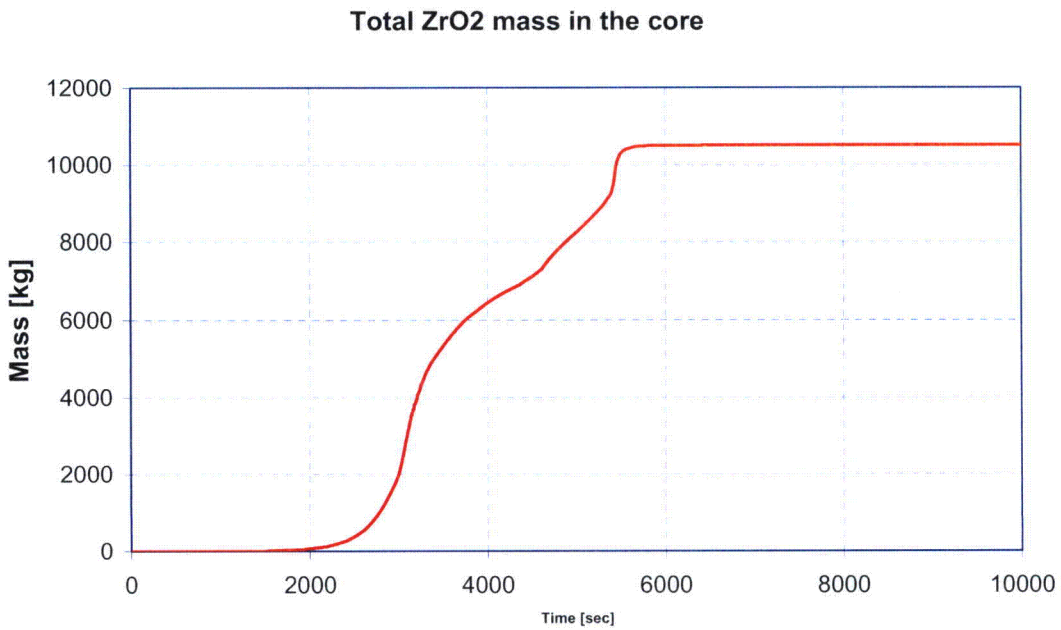

Figure 43. *Total mass of ZrO_2 in the core. Bottom Drain Line Break ($A=2.165 \cdot 10^{-3}$ m^2) case with ADS and reflooding by GDCS injection at 7400 s.*

The total hydrogen mass generated in the core is 369 kg (Fig 44).

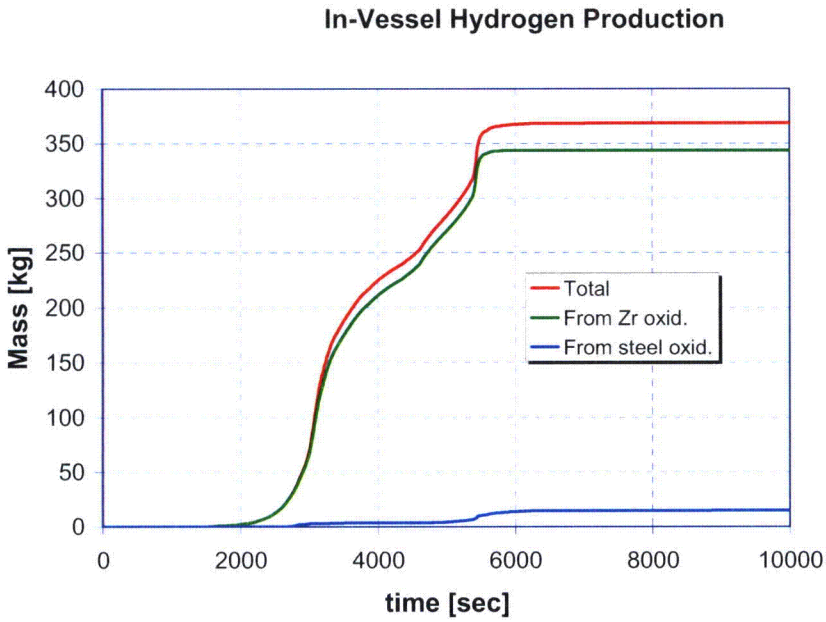

Figure 44. *Cumulative hydrogen release from the core materials. Bottom Drain Line Break ($A=2.165 \cdot 10^{-3}$ m^2) case with ADS and reflooding by GDCS injection at 7400 s.*

The cumulative coolant injection to the RCS and break flow out of the RCS are presented in the Figs. 45 and 46, respectively. Reflooding is able to cool the core and prevent the pressure vessel failure.

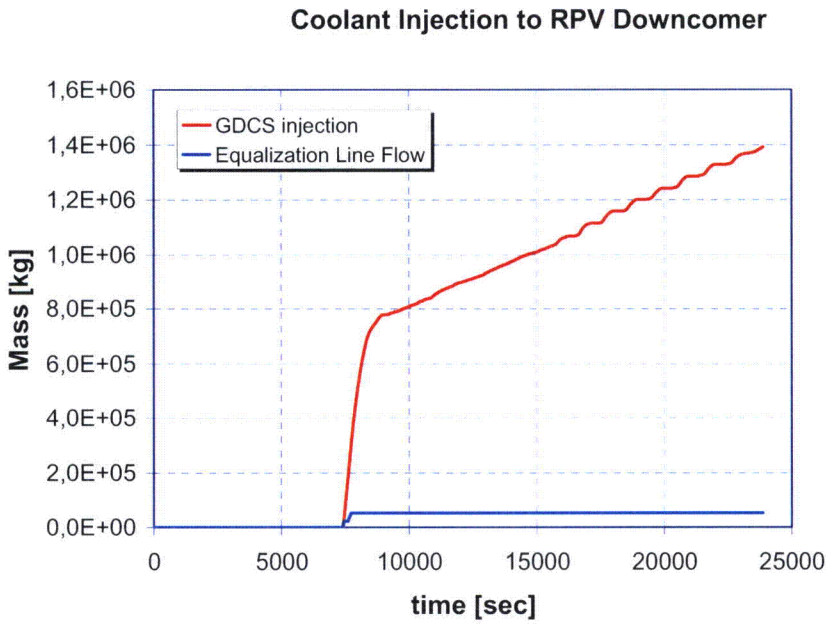

Figure 45. *Cumulative coolant injection to the RPV from different water sources. Bottom Drain Line Break ($A=2.165 \cdot 10^{-3}$ m^2) case with ADS and reflooding by GDCS injection at 7400 s.*

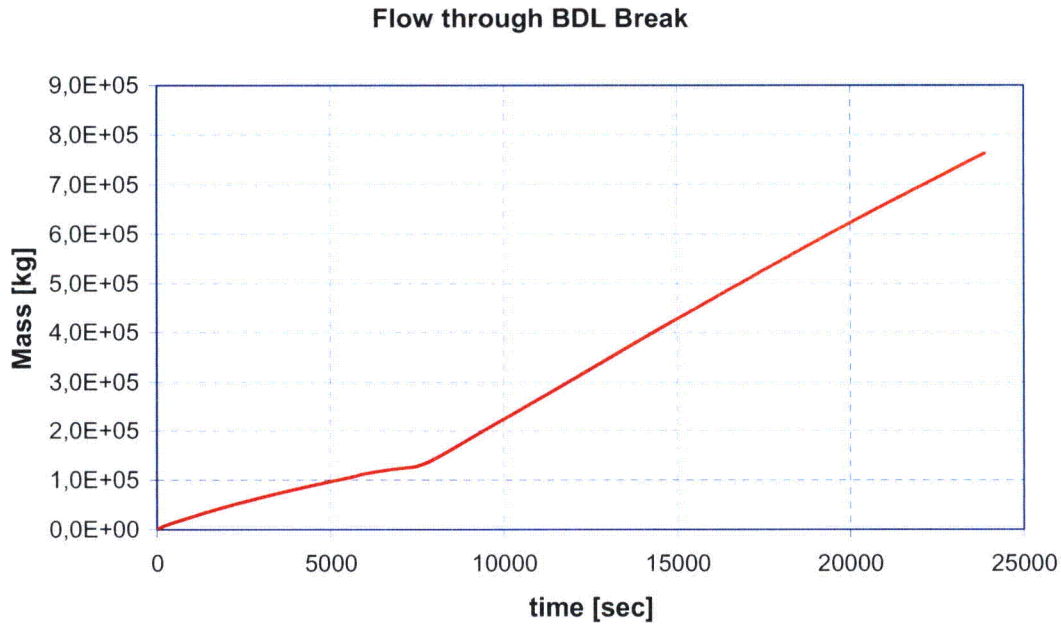

Figure 46. *Cumulative coolant break flow. Bottom Drain Line Break ($A=2.165 \cdot 10^{-3}$ m^2) case with ADS and reflooding by GDCS injection at 7400 s.*

The pressure in the RCS is presented in Fig 47. The initial pressure in the RPV is 7.2 MPa. Following the opening of Depressurization Valves the pressure decreases to about 0.2 MPa.

Core melt relocations to the lower head at about 5800 s increases steam production and RCS pressure to about 0.4 MPa.

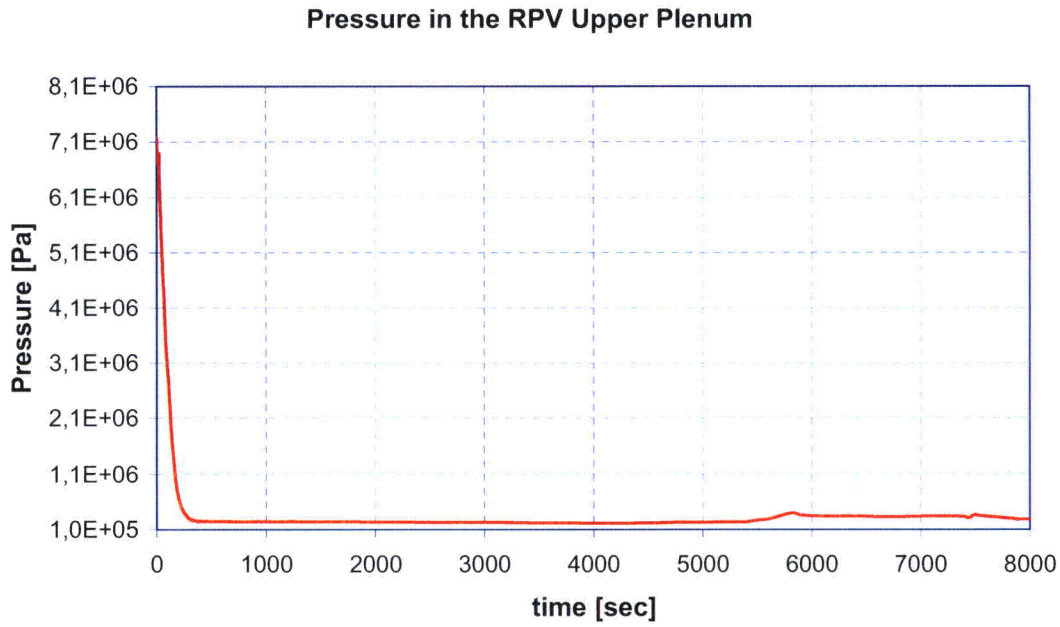

Figure 47. *Pressure in the RPV. Bottom Drain Line Break ($A=2.165 \cdot 10^{-3}$ m^2) case with ADS and reflooding by GDCS injection at 4100 s.*

8.2 Containment behavior

The pressure in the containment increases due to blowdown through the DPV valves and the Bottom Drain Line Break to about 0.23 MPa (Figs. 48a and b). The start of reflooding from GDCS pool at 6083 s or at 7400 s increase the pressure in the containment rapidly peaking at 0.34 MPa. The drywell pressure decreases after start of reflooding due to decrease in steaming rate from the lower head melt pool when cold water is injected to the RPV. At about 15 000 s the pressure starts to increase again by continuous steam release from the RPV through Depressurization Valves. The partial pressure of steam in the Upper Drywell increases reaching 0.4 MPa at the end of the calculation in case of reflooding at 6083 s (Fig. 49). After 20 000 s the Upper Drywell is practically all steam. Hydrogen is released from the RPV to the upper drywell and further vented via PCCS Vent Line to the Wetwell pool. The partial pressure of non-condensables and steam increases in the Wetwell being about 0.34 MPa at the end of calculation (Fig. 50).

The gas temperature in the drywell peak at about 1700 K due to hot hydrogen and steam discharge from the RPV during reflooding (Fig. 51).

The water mass in GDCS is shown in Fig. 52. The inventory is nearly depleted at 40 000 s (=11 hrs).

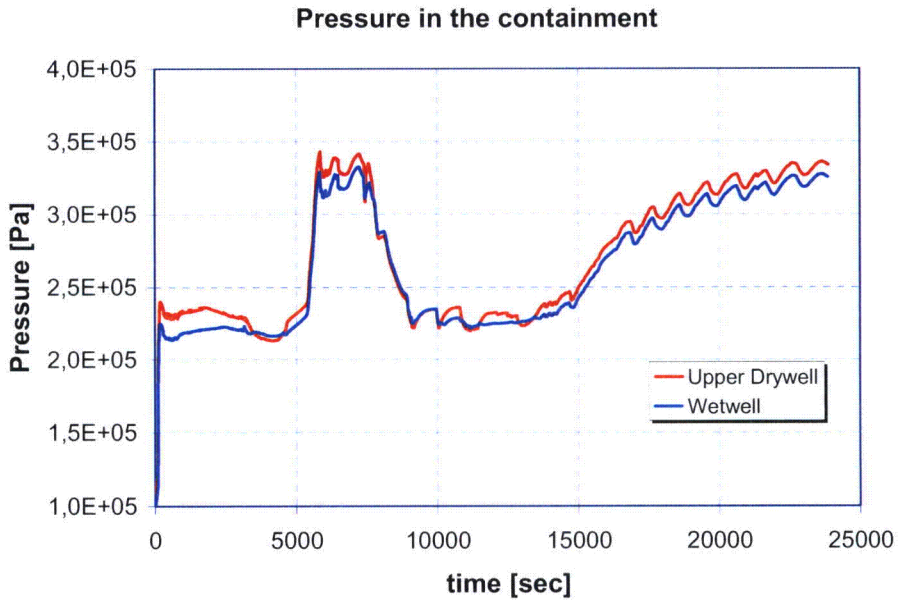

Figure 48a. *Pressure in the containment. Bottom Drain Line Break ($A=2.165 \cdot 10^{-3}$ m^2) case with ADS and reflooding by GDCS injection at 7400 s.*

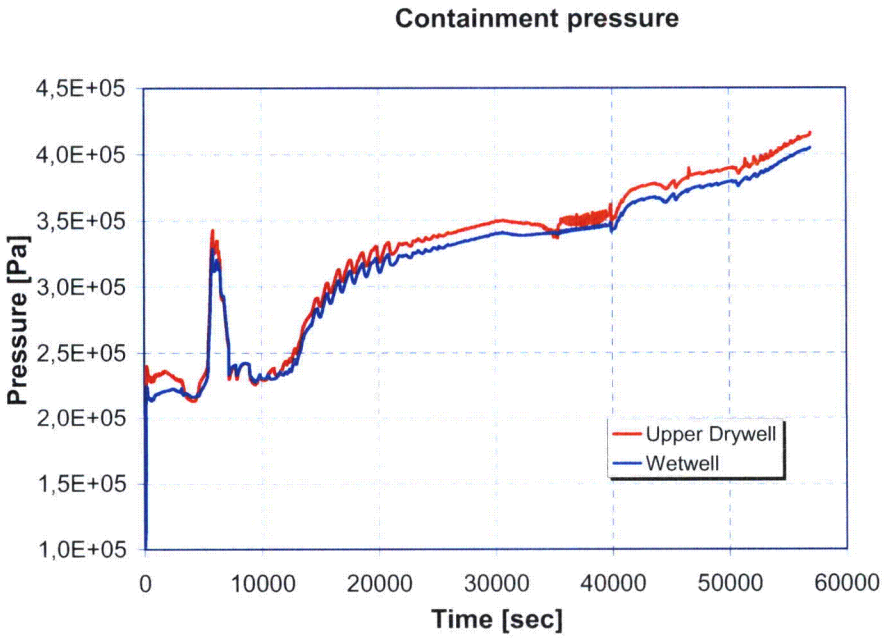

Figure 48b. *Pressure in the containment. Bottom Drain Line Break ($A=2.165 \cdot 10^{-3}$ m^2) case with ADS and reflooding by GDCS injection at 6083 s.*

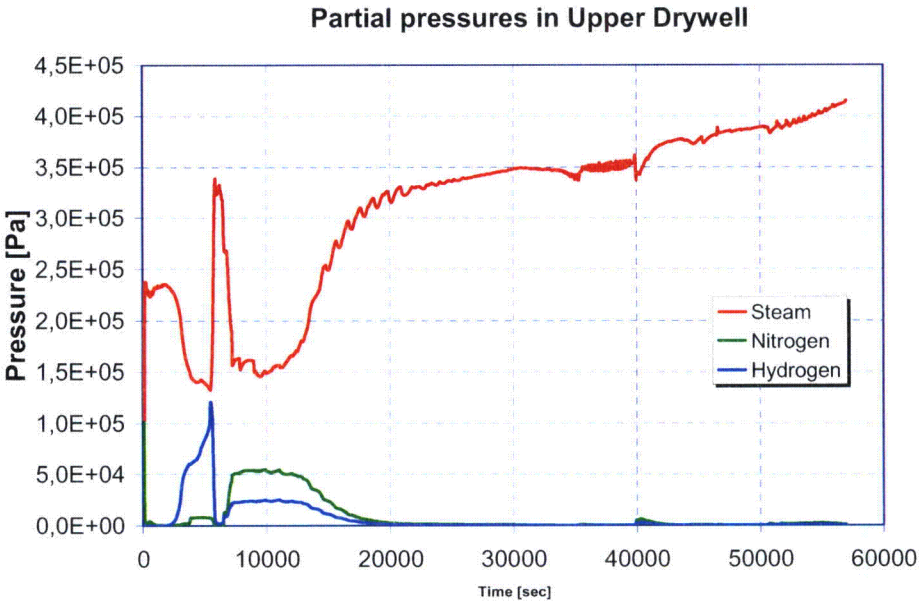

Figure 49. *Partial pressures of steam, nitrogen and hydrogen in the upper drywell. Bottom Drain Line Break ($A=2.165 \cdot 10^{-3}$ m^2) case with ADS and reflooding by GDCS injection at 6083 s.*

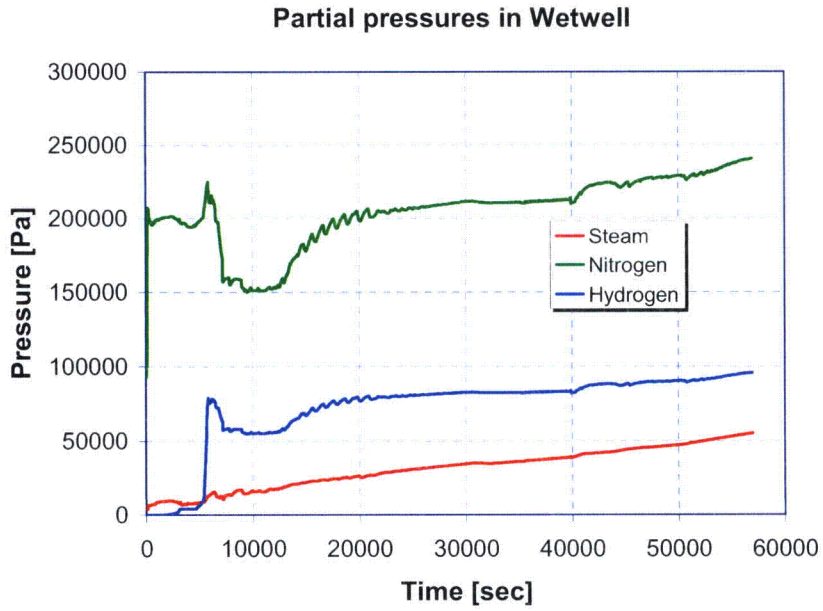

Figure 50. *Partial pressures of steam, nitrogen and hydrogen in the Wetwell. Bottom Drain Line Break ($A=2.165 \cdot 10^{-3}$ m^2) case with ADS and reflooding by GDCS injection at 6083 s.*

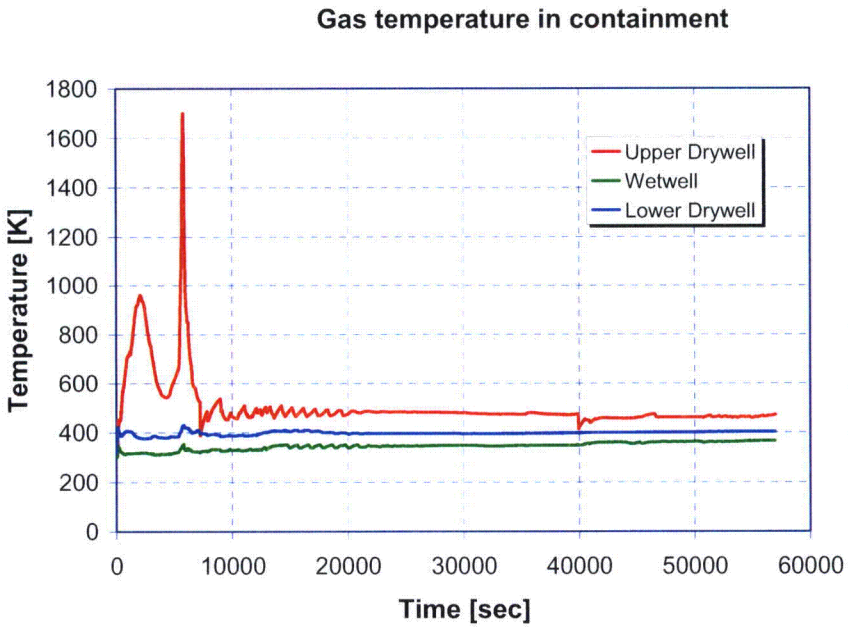

Figure 51. *Atmosphere temperature in the containment. Bottom Drain Line Break ($A=2.165 \cdot 10^{-3}$ m^2) case with ADS and reflooding by GDCS injection at 6083 s.*

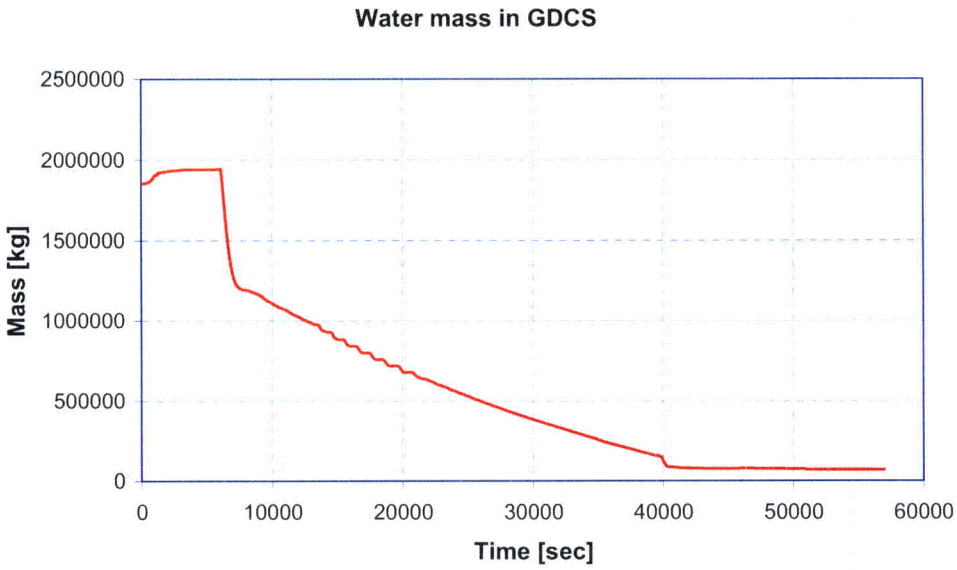

Figure 52. *Water mass in the GDCS pool. Bottom Drain Line Break ($A=2.165 \cdot 10^{-3}$ m^2) case with ADS and reflooding by GDCS injection at 6083 s.*

Figure 53 illustrates the water pool temperatures in the GDCS pool. The temperature of GDCS pool increases due to condensate flow from the GDCS wall structure.

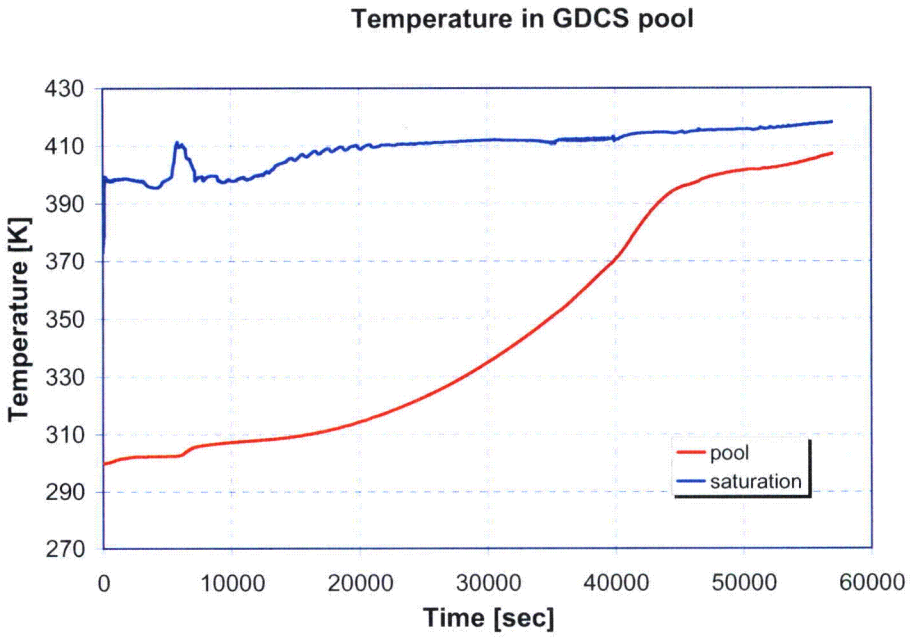

Figure 53. *GDCS pool temperatures. Bottom Drain Line Break ($A=2.165 \cdot 10^{-3}$ m^2) case with ADS and reflooding by GDCS injection at 4100 s.*

The Suppression Pool temperature increases at the top of the pool but remains below saturation (Fig. 54). The temperature stratification in the suppression pool is modeled by dividing the pool volume into four vertically adjacent control volumes. The temperature difference between the top and the bottom of the pool is about 60 K at the end of calculation. However, this result should be considered as a rough estimate, since MELCOR code does not properly model fluid dynamics for mixing.

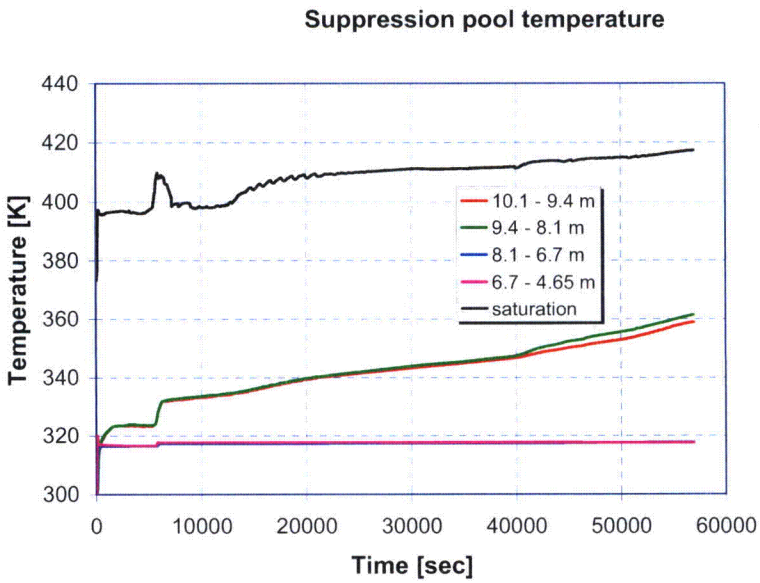

Figure 54. *Suppression pool temperature. Bottom Drain Line Break ($A=2.165 \cdot 10^{-3}$ m^2) case with ADS and reflooding by GDCS injection at 6083 s.*

The nominal containment leakage is modeled as a single flow path from the upper drywell with the assumption the leakage rate is 0.5 % of the containment gas volume (=13 580 m3) per day at 310 kPa (g). The respective average velocity is obtained from Bernoulli's equation

$$A \cdot v = A \cdot \sqrt{\frac{2 \cdot \Delta p}{\rho}} = 0.005 \cdot 13580 / 86400 \quad \mathrm{m^3/s}, \tag{71}$$

where $\Delta p = 310$ kPa, $\rho_{steam}=6.12$ kg/m^3. This yields A= $2.469 \cdot 10^{-6}$ m^2.

The cumulative atmosphere flow rate through the containment leakage is presented in Fig. 55.

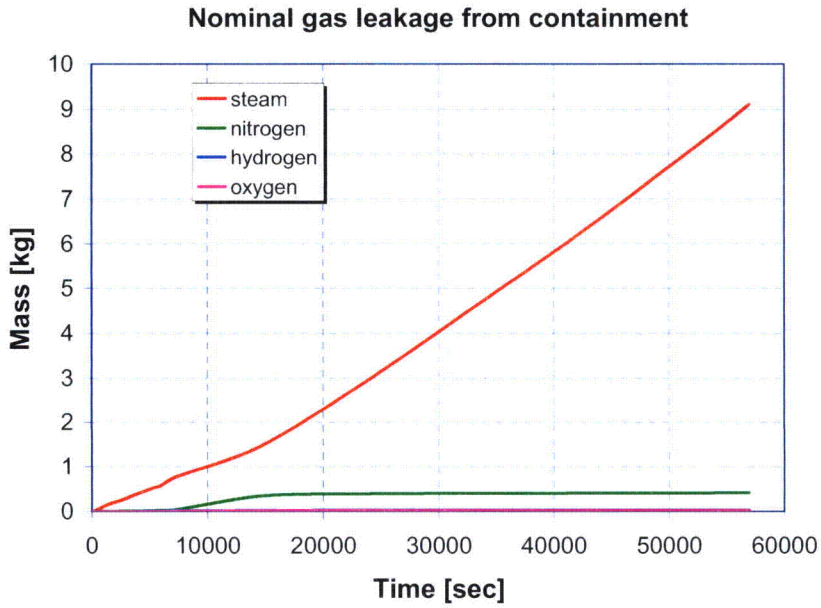

Figure 55. *Water level in the Lower Drywell. Bottom Drain Line Break ($A=2.165 \cdot 10^{-3}$ m^2) case with ADS and reflooding by GDCS injection at 6083 s.*

The cumulative water and non-condensable gas flow rates through the PCCS condensers are shown in Figs. 56, 57 and 58. A total of 400 metric tons of steam enters the PCCS with most of it condensed in the PCCS, only 45 metric tons of steam is vented to the Suppression Pool. About 60 metric tons of water flows from the Suppression Pool into the PCCS Vent Line and back through the Drain Line after reflooding. The horizontal vents a cleared for a short time period after initiation of reflooding (Fig. 59) increasing the pressure in the Wetwell above that of the PCCS water box. This causes the reverse water flow in the Vent Line. A sparger at the end of Vent Line may cause a higher flow friction for reverse flow, thus reducing it, but the loss coefficients in the applied MELCOR model were equal for both forward and reverse flows.

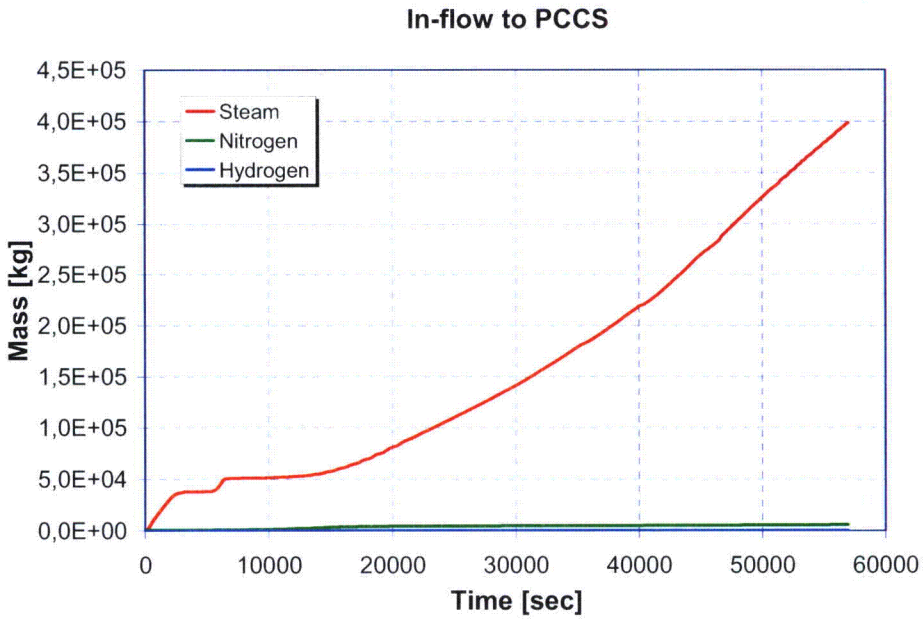

Figure 56. *Cumulative mass inflow to PCCS units). Bottom Drain Line Break ($A=2.165 \cdot 10^{-3}$ m^2) case with ADS and reflooding by GDCS injection at 6083 s.*

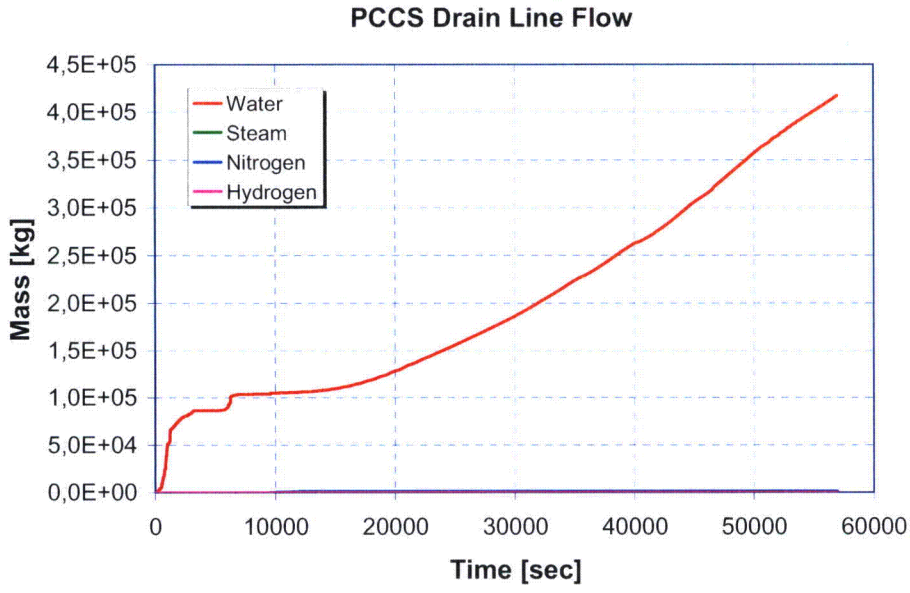

Figure 57. *Cumulative mass flow through the PCCS Drain Lines. Bottom Drain Line Break ($A=2.165 \cdot 10^{-3}$ m^2) case with ADS and reflooding by GDCS injection at 6083 s.*

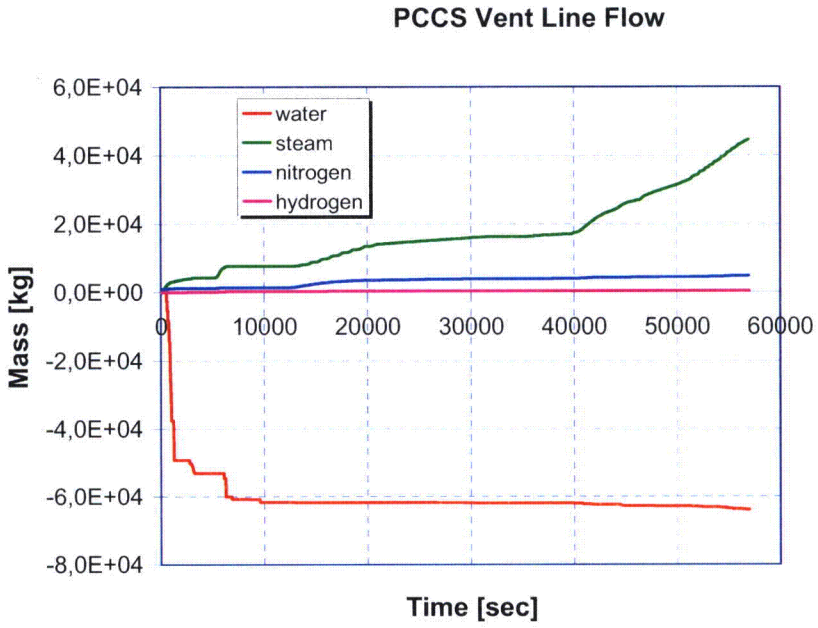

Figure 58. *Cumulative mass flow through PCCS Vent Line. Bottom Drain Line Break ($A=2.165 \cdot 10^{-3}$ m^2) case with ADS and reflooding by GDCS injection at 6083 s.*

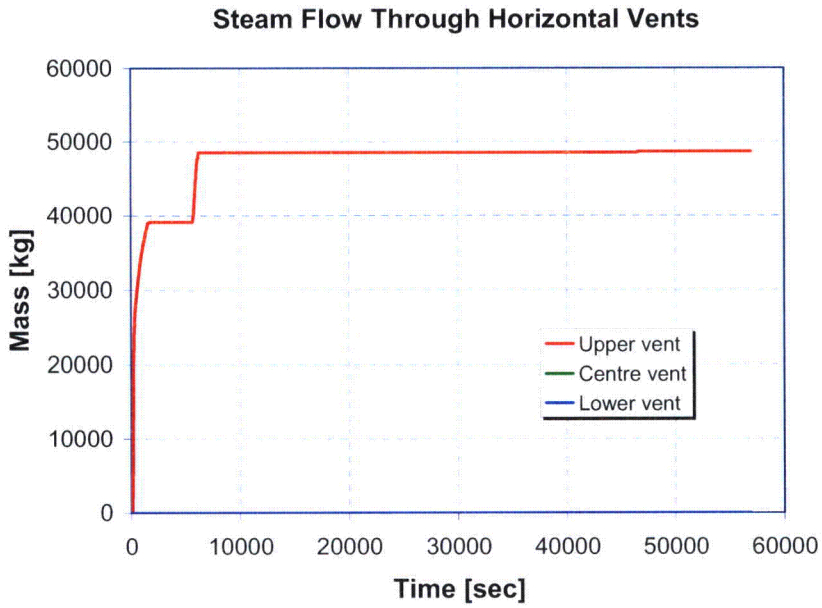

Figure 59. *Cumulative steam flow through Horizontal Vents. Bottom Drain Line Break ($A=2.165 \cdot 10^{-3}$ m^2) case with ADS and reflooding by GDCS injection at 6083 s.*

8.3 Fission product behavior

The release fractions of fission products from the fuel were calculated using the CORSOR-M option in MELCOR. In general the release fractions remained lower than presented in [8] because of relatively early reflooding. Table 34 gathers the calculated release fractions at time steps at 1 h, 6083 s and 2 h. These are compared to the release fractions presented in NUREG-1465 [8].

Table 34. *Release fractions of fission products from the fuel.*

Fission product class	Calculated release fractions from the fuel			Early in-vessel Release for BWRs in [8]
	3600 s	**6083 s**	**7200 s**	
Noble gases	0.131	0.818	0.82	0.95
Cs	0.136	0.754	0.808	0.25
Sr+Ba	$3.62 \cdot 10^{-5}$	$4.93 \cdot 10^{-3}$	$5.30 \cdot 10^{-3}$	0.02
I_2	0	0	0	
Te	$2.97 \cdot 10^{-3}$	0.684	0.722	0.05
Ru	$1.34 \cdot 10^{-9}$	$2.18 \cdot 10^{-6}$	$3.01 \cdot 10^{-6}$	$2.5 \cdot 10^{-3}$
Mo	$1.27 \cdot 10^{-3}$	$3.24 \cdot 10^{-2}$	$3.30 \cdot 10^{-2}$	$2.5 \cdot 10^{-3}$
Ce	$7.79 \cdot 10^{-11}$	$9.77 \cdot 10^{-7}$	$1.27 \cdot 10^{-6}$	$5.0 \cdot 10^{-4}$
La	$1.08 \cdot 10^{-7}$	$1.03 \cdot 10^{-4}$	$1.39 \cdot 10^{-4}$	$2 \cdot 10^{-4}$
U	$1.24 \cdot 10^{-7}$	$1.05 \cdot 10^{-4}$	$1.63 \cdot 10^{-4}$	
Cd	$6.22 \cdot 10^{-4}$	$3.19 \cdot 10^{-2}$	$3.15 \cdot 10^{-2}$	
CsI	0.125	0.818	0.818	0.35

The calculated release fractions from the core are lower for noble gases but higher for cesium, iodine and tellurium and than presented in NUREG-1465.

Fig. 60 shows the history of the fission product release fractions of the classes with highest releases.

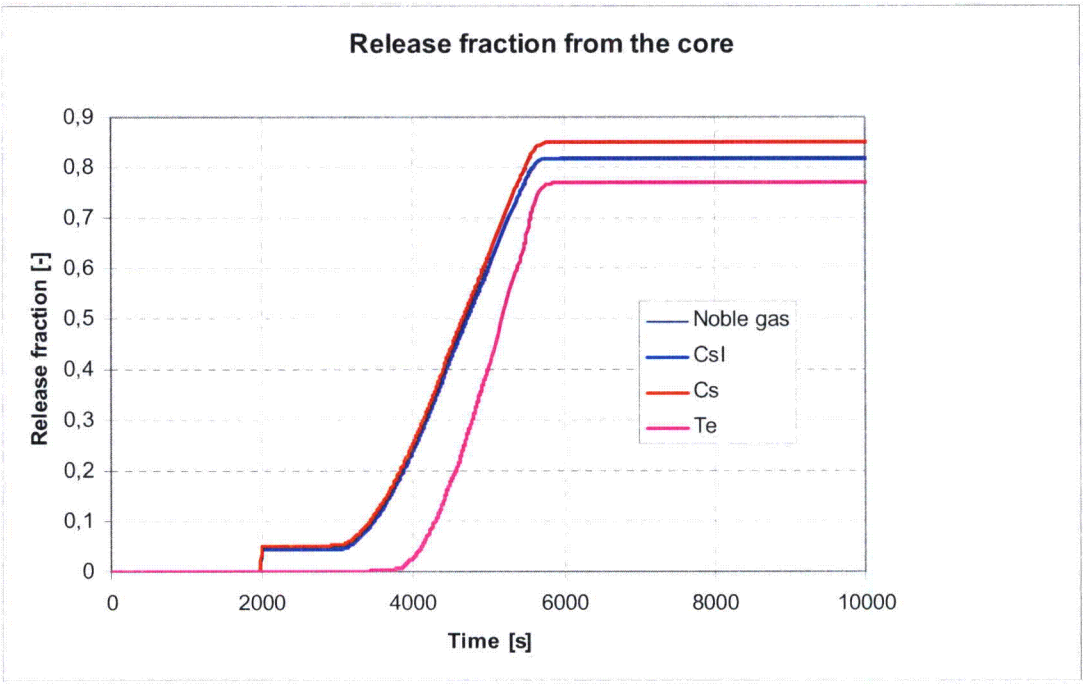

Figure 60. *Release fractions of noble gases, Cs, CsI and Te from the fuel. Bottom Drain Line Break ($A=2.165 \cdot 10^{-3}$ m^2) case with ADS and reflooding by GDCS injection at 6083 s.*

The fission product release from the containment is low (Fig. 61). For noble gases, CsOH and CsI the release fractions of the initial whole core inventory to reactor building are $4.67 \cdot 10^{-5}$, $1.18 \cdot 10^{-5}$ and $^{1.29} \cdot 10^{-5}$, respectively.

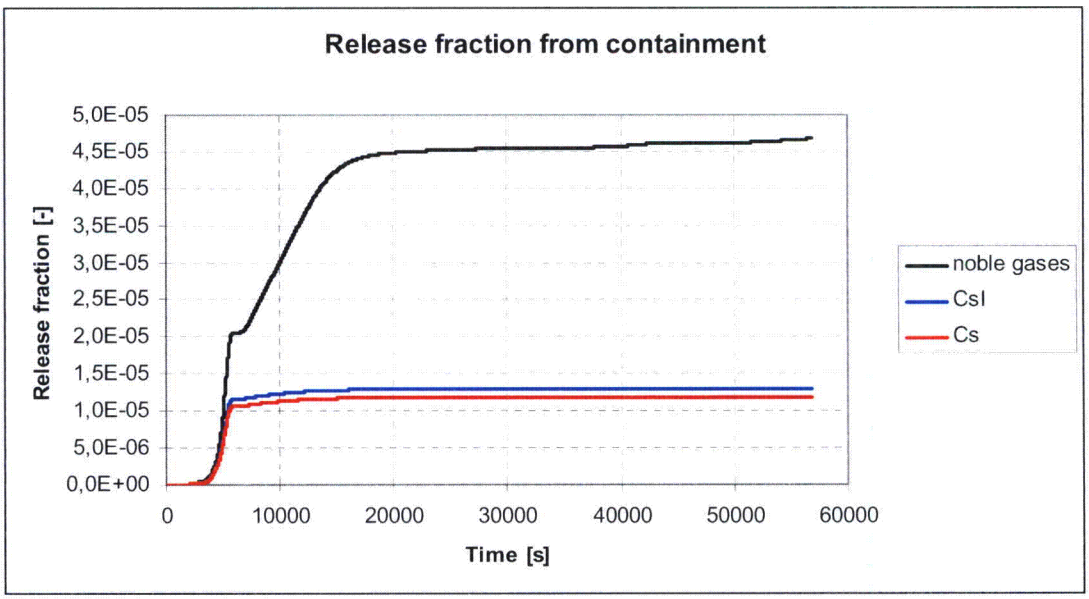

Figure 61. *Fraction of initial core inventory of noble gases, CsI and Cs that is released from the containment through nominal leakage path. Bottom Drain Line Break ($A=2.165 \cdot 10^{-3}$ m^2) case with ADS and reflooding by GDCS injection at 6083 s.*

The total airborne CsI aerosol mass in the containment has a maximum value first in the upper drywell due to discharge of the DPV valves (Fig. 62). The airborne mass degrades rapidly after start of reflooding and scrubbing to suppression pool via horizontal vents. After recooling of the core the CsI aerosols are removed from the Drywell atmosphere by gravitational settling and condensation in the PCCS. The airborne mass in the Wetwell reduces slowly after about 12 500 s. This due to a fact that the Wetwell atmosphere is dry and the particles are not able to grow by steam condensation on the particles. Also the mass concentration is rather low limiting the growth by agglomeration.

The total CsI aerosol concentration in the containment water pools is presented in Fig. 63. Suppression pool retains most of the CsI aerosols. The aerosol mass in the GDCS pool increases after start of the core heat up due to fission product removal with the condensate flow from the PCCS. After start of GDCS injection the CsI concentration decreases along with the coolant injection to the RPV downcomer. The total CsI mass in the RPV is shown in Fig. 64. A maximum of 2.9 kg of CsI is in the RPV water during the simulation.

The deposition of CsI aerosols on Upper Drywell structures is presented in Fig. 65.

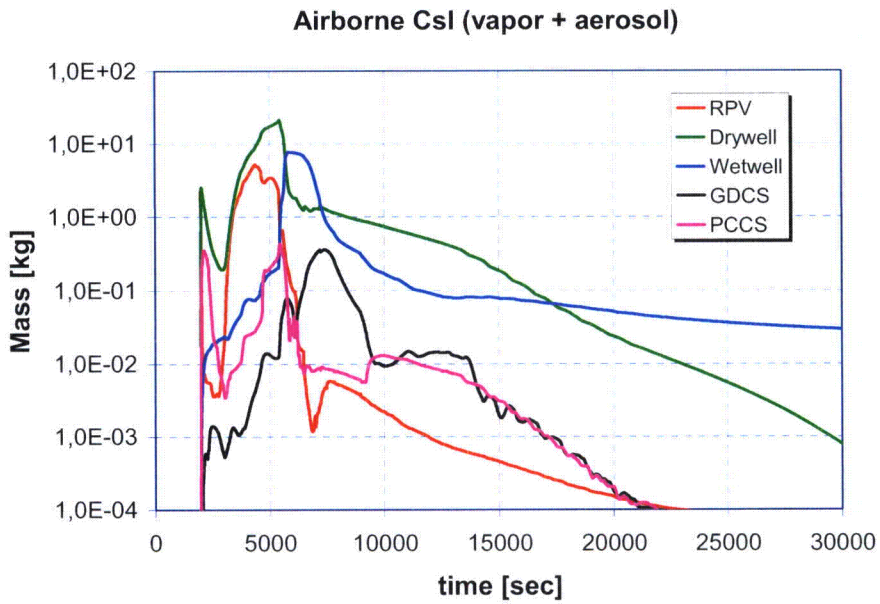

Figure 62. *Total airborne CsI aerosol mass in the containment. Bottom Drain Line Break ($A=2.165 \cdot 10^{-3}$ m^2) case with ADS and reflooding by GDCS injection at 6083 s.*

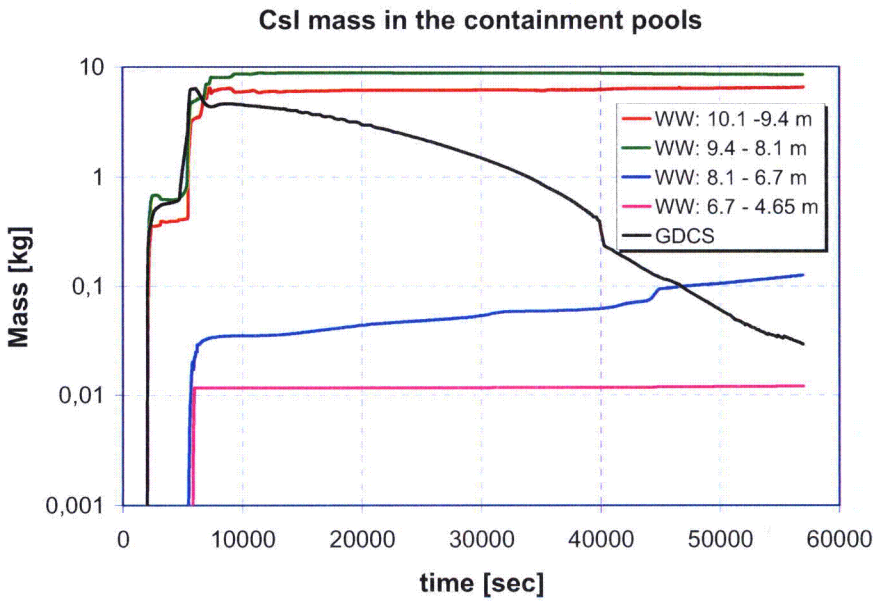

Figure 63. *Total CsI aerosol mass in the Suppression Pool and the GDCS Pool. Bottom Drain Line Break ($A=2.165 \cdot 10^{-3}$ m^2) case with ADS and reflooding by GDCS injection at 6083 s.*

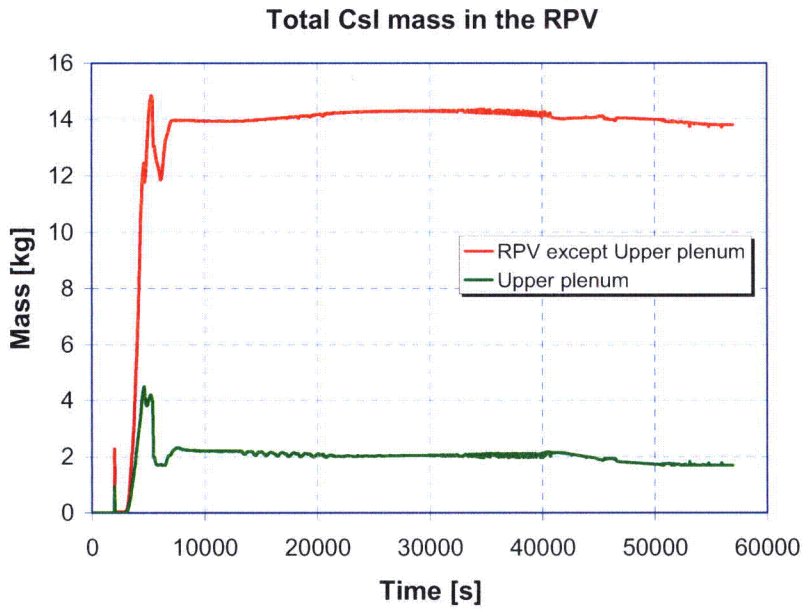

Figure 64. *Total CsI mass in the RPV Upper Plenum and the rest of the RPV. Bottom Drain Line Break ($A=2.165 \cdot 10^{-3}$ m^2) case with ADS and reflooding by GDCS injection at 6083 s.*

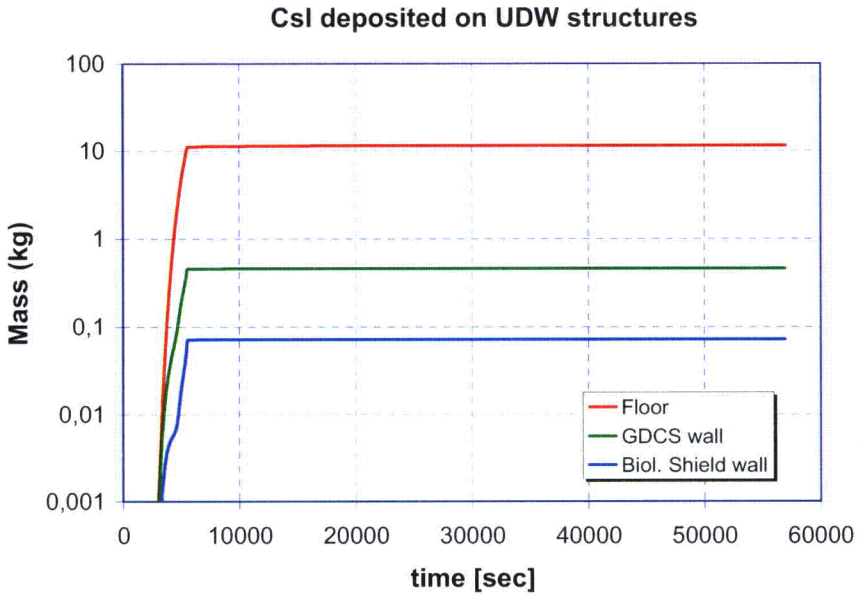

Figure 65. *Total deposited CsI aerosol mass on Upper Drywell structures. Bottom Drain Line Break ($A=2.165 \cdot 10^{-3}$ m^2) case with ADS and reflooding by GDCS injection at 6083 s.*

The total airborne CsI mass released from the RPV through the SRVs, DPVs and the BDL Break to the containment is illustrated in Fig. 66.

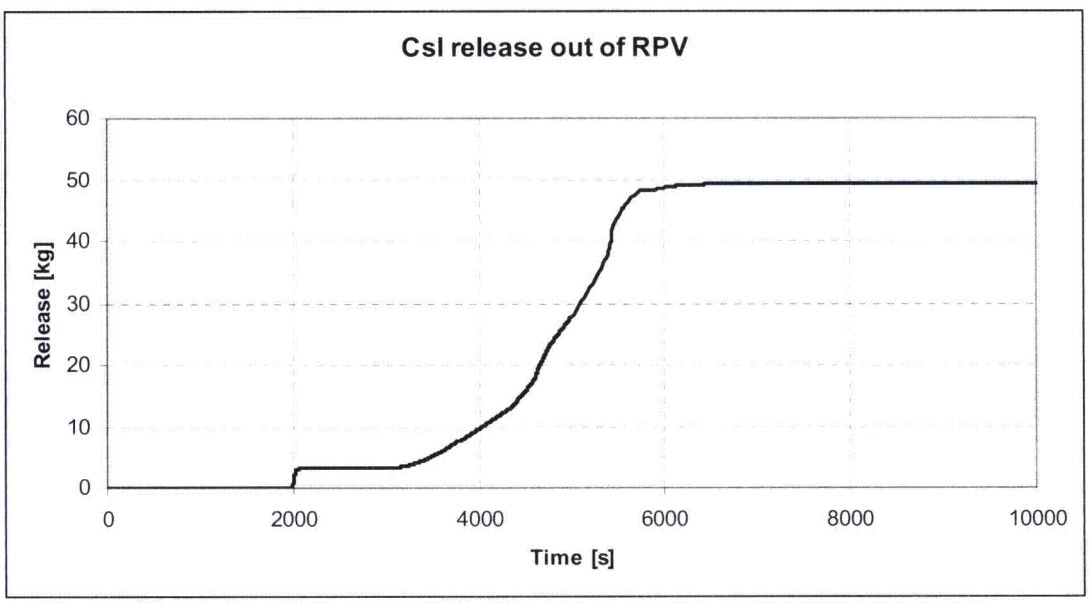

Figure 66. *Release of airborne CsI from the RPV to the containment. . Bottom Drain Line Break ($A=2.165 \cdot 10^{-3}$ m^2) case with ADS and reflooding by GDCS injection at 6083 s.*

The decontamination factor for PCCS obtained by dividing the airborne CsI aerosol entering the PCCS by the airborne mass of CsI exiting the PCCS through the PCCS Drain Line and Vent Line flow junctions is shown in Fig. 67. The decontamination factor is about 17 prior to

reflooding and about 4.4 after the start of reflooding. These numbers correspond to 94 % and 75 % deposition, respectively.

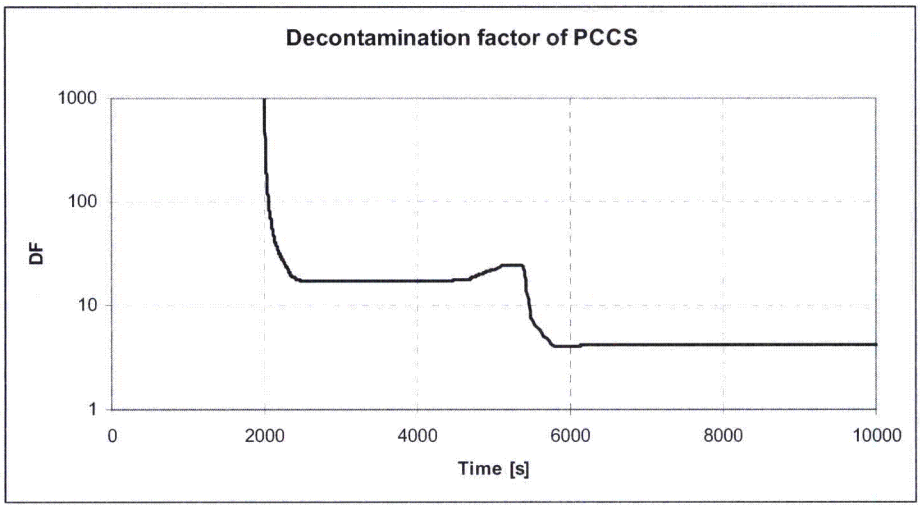

Figure 67. *Estimate of time-averaged decontamination factor in the PCCS calculated as airborne CsI mass that has entered the PCCS divided by airborne mass that has exited the PCCS (through Drain Line and Vent Line). Bottom Drain Line Break ($A=2.165 \cdot 10^{-3}$ m^2) case with ADS and reflooding by GDCS injection at 6083 s.*

Figure 68 shows another way to estimate decontamination factor through the PCCS. The DF is calculated as in flowing mass over a plot file time step divided by outgoing mass over a plot file time step. During time interval 9700 - 13000 s the DF is 2.0 - 3.1, which is close to the estimate with the detailed retention model.

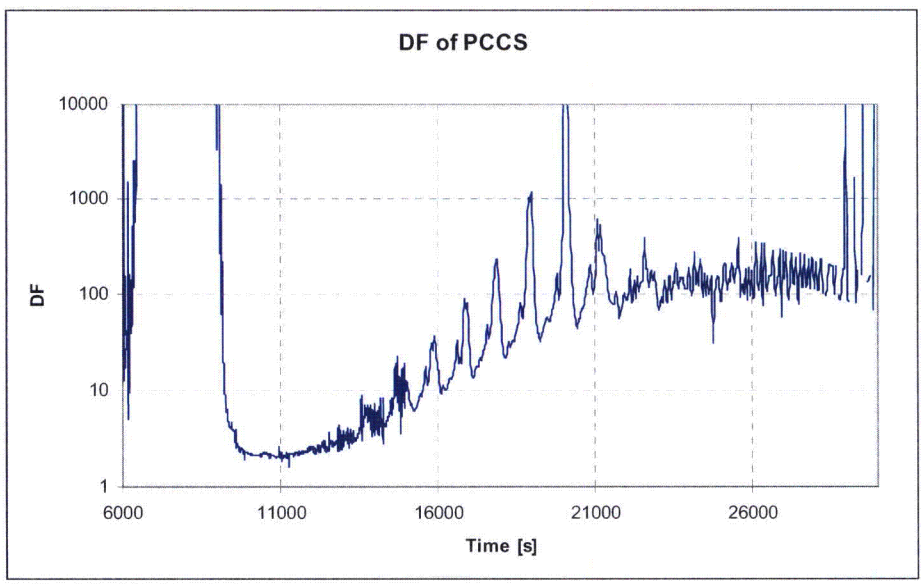

Figure 68. *Decontamination factor of PCCS calculated as in-flowing mass over a plot file time step divided by outgoing mass over a plot file time step. Bottom Drain Line Break ($A=2.165 \cdot 10^{-3}$ m^2) case with ADS and reflooding by GDCS injection at 6083 s.*

The CsI decontamination factor for the whole containment can be defined as the ratio of total CsI released from the RPV divided by the total airborne mass of CsI in the containment. The value for containment decontamination factor ranges from 1.4 to 3467 (Fig. 69).

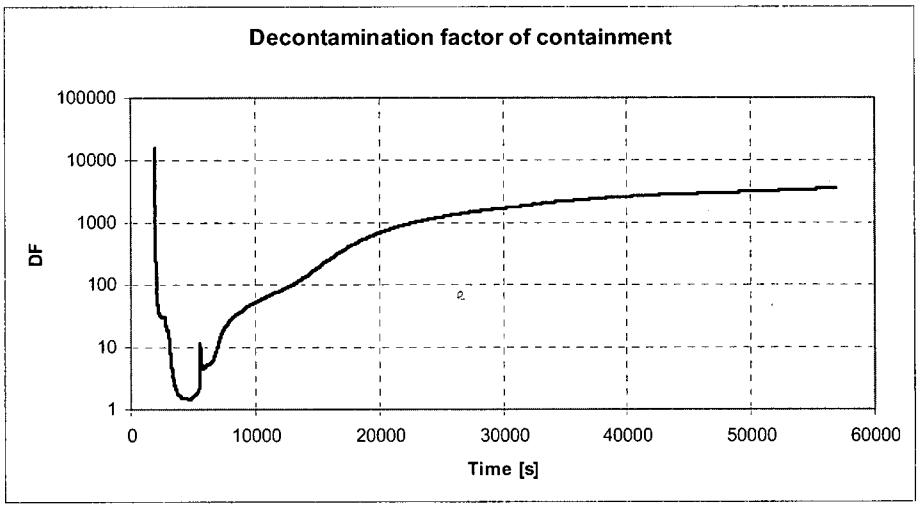

Figure 69. *The decontamination factor of CsI aerosols for the containment calculated as total CsI mass released from the RPV to containment divided by total airborne aerosol mass in the containment atmosphere. Bottom Drain Line Break ($A=2.165 \cdot 10^{-3}$ m^2) case with ADS and reflooding by GDCS injection at 6083 s.*

The mass balance of CsI in the reactor coolant system and in the containment is reported in Table 35. The numbers in Table 35 are hand-calculated from the original CsI mass data in obtained from the Tabular Output for different printout intervals of the MELCOR run.

Table 35. *Fractional distribution of CsI mass at different time steps (1, 2, 3, 4, 5, 6, 7, 8, 12 and 15.8 h). Fractions are determined as: Mass in a specified location/total mass released from the core.*

Time= 1	Total	Airborne	In the pool	Deposited on structures
RPV	2,63E-01	1,81E-01	4,78E-04	8,10E-02
RPV Upper Plenum	1,14E-01	1,07E-01	0,00E+00	7,46E-03
ICS	1,09E-03	8,94E-04	6,04E-05	4,15E-05
Drywell (upper+middle+lower)	3,97E-01	2,92E-01	1,54E-03	1,04E-01
Wetwell	1,18E-01	4,34E-03	1,14E-01	3,74E-06
GDCS	9,83E-02	1,12E-04	9,82E-02	8,29E-08
Annulus	6,87E-03	6,43E-03	1,05E-04	3,38E-04
PCCS	1,28E-03	1,01E-03	3,22E-06	2,67E-04
Reactor Building	3,88E-06	3,88E-06	0,00E+00	9,24E-14
Total	9,99E-01	5,92E-01	2,14E-01	1,93E-01

Time= 2 h	Total	Airborne	In the pool	Deposited on structures
RPV	2,24E-01	4,57E-05	4,13E-02	1,82E-01
RPV Upper Plenum	3,57E-02	4,33E-04	8,05E-03	2,72E-02
ICS	1,52E-04	1,16E-05	1,25E-04	5,54E-01
Drywell (upper+middle+lower)	3,31E-01	2,13E-02	2,05E-02	2,89E-01
Wetwell	2,48E-01	2,71E-02	2,21E-01	4,52E-04
GDCS	8,96E-02	5,58E-03	8,40E-02	1,20E-05
Annulus	1,56E-02	1,95E-03	1,12E-04	1,35E-02
PCCS	1,73E-04	1,37E-04	2,53E-07	3,65E-05
Reactor Building	1,44E-05	1,44E-05	0,00E+00	3,77E-13
Total	9,44E-01	5,65E-02	3,75E-01	5,12E-01

Time= 3 h	Total	Airborne	In the pool	Deposited on structures
RPV	2,23E-01	2,36E-05	4,09E-02	1,82E-01
RPV Upper Plenum	3,53E-02	2,40E-05	8,12E-03	2,72E-02
ICS	3,62E-04	1,28E-06	3,44E-04	1,60E-05
Drywell (upper+middle+lower)	3,38E-01	1,00E-02	3,66E-02	2,92E-01
Wetwell	2,47E-01	2,09E-03	2,45E-01	2,13E-05
GDCS	8,33E-02	2,13E-04	8,30E-02	1,15E-05
Annulus	1,55E-02	1,05E-03	1,94E-04	1,42E-02
PCCS	2,33E-04	1,87E-04	1,14E-07	4,49E-05
Reactor Building	1,53E-05	1,53E-05	8,61E-07	9,79E-13
Total	9,44E-01	1,37E-02	4,15E-01	5,16E-01

Time= 4 h	Total	Airborne	In the pool	Deposited on structures
RPV	2,24E-01	8,26E-06	4,14E-02	1,82E-01
RPV Upper Plenum	3,33E-02	5,53E-08	6,07E-03	2,72E-02
ICS	3,62E-04	2,05E-07	3,45E-04	1,60E-05
Drywell (upper+middle+lower)	3,47E-01	3,85E-03	5,01E-02	2,93E-01
Wetwell	2,49E-01	1,29E-03	2,48E-01	7,81E-06
GDCS	7,49E-02	5,35E-05	7,48E-02	1,15E-05
Annulus	1,54E-02	5,39E-04	2,30E-04	1,46E-02
PCCS	8,95E-05	6,65E-05	1,57E-07	2,28E-05
Reactor Building	1,57E-05	1,57E-05	0,00E+00	1,60E-12
Total	9,44E-01	5,83E-03	4,21E-01	5,17E-01

Time= 5 h	Total	Airborne	In the pool	Deposited on structures
RPV	2,26E-01	3,49E-06	4,34E-02	1,82E-01
RPV Upper Plenum	3,40E-02	1,39E-08	6,82E-03	2,72E-02
ICS	3,62E-04	1,36E-08	3,45E-04	1,60E-05
Drywell (upper+middle+lower)	3,56E-01	8,24E-04	6,21E-02	2,93E-01
Wetwell	2,50E-01	9,86E-04	2,50E-01	6,50E-06
GDCS	6,18E-02	8,67E-06	6,28E-02	1,05E-05
Annulus	1,52E-02	2,13E-04	2,53E-04	1,48E-02
PCCS	1,18E-05	8,58E-06	2,09E-08	3,14E-06
Reactor Building	1,58E-05	1,58E-05	0,00E+00	2,24E-12
Total	9,43E-01	2,06E-03	4,25E-01	5,17E-01

Time= 6 h	Total	Airborne	In the pool	Deposited on structures
RPV	2,28E-01	1,84E-06	4,56E-02	1,82E-01
RPV Upper Plenum	3,24E-02	5,55E-09	5,26E-03	2,72E-02
ICS	3,62E-04	1,68E-10	3,46E-04	1,60E-05
Drywell (upper+middle+lower)	3,66E-01	2,35E-04	7,27E-02	2,93E-01
Wetwell	2,51E-01	7,13E-04	2,50E-01	4,17E-06
GDCS	5,10E-02	1,66E-06	5,10E-02	5,08E-08
Annulus	1,52E-02	2,79E-05	2,70E-04	1,49E-02
PCCS	2,32E-06	1,80E-06	1,07E-08	5,11E-07
Reactor Building	1,58E-05	1,58E-05	0,00E+00	2,87E-12
Total	9,43E-01	9,97E-04	4,25E-01	5,17E-01

Time= 7 h	Total	Airborne	In the pool	Deposited on structures
RPV	2,29E-01	1,32E-06	0,0464	0,182
RPV Upper Plenum	3,25E-02	3,25E-09	0,005319	0,027179
ICS	3,62E-04	4,83E-11	0,000346	1,6E-05
Drywell (upper+middle+lower)	3,76E-01	8,25E-05	0,082641	0,292949
Wetwell	2,51E-01	0,000574	0,250019	3,65E-06
GDCS	4,03E-02	7,83E-07	0,040274	9,86E-10
Annulus	1,52E-02	6,41E-06	0,000272	0,014952
PCCS	8,30E-07	6,5E-07	1,65E-09	1,79E-07
Reactor Building	1,58E-05	1,58E-05	0	3,51E-12
Total	9,44E-01	6,82E-04	4,25E-01	0,517

Time= 8 h	Total	Airborne	In the pool	Deposited on structures
RPV	2,29E-01	1,08E-06	0,0467	0,182
RPV Upper Plenum	3,28E-02	2,92E-09	0,00561	2,72E-02
ICS	3,62E-04	4,57E-11	0,000346	1,60E-05
Drywell (upper+middle+lower)	3,85E-01	2,19E-05	0,0921	2,93E-01
Wetwell	2,51E-01	0,000492	0,250	3,18E-06
GDCS	3,03E-02	4,04E-07	0,03033	9,84E-10
Annulus	1,52E-02	2,63E-06	0,000272	1,50E-02
PCCS	3,71E-07	2,94E-07	1,11E-09	7,56E-08
Reactor Building	1,58E-05	1,58E-05	0	4,14E-12
Total	9,43E-01	0,000535	0,426	5,17E-01

Time= 12 h	Total	Airborne	In the pool	Deposited on structures
RPV	2,25E-01	2,30E-07	0,0445	1,81E-01
RPV Upper Plenum	3,28E-02	3,19E-09	0,005621	2,72E-02
ICS	3,59E-04	3,08E-11	0,000343	1,60E-05
Drywell (upper+middle+lower)	4,08E-01	1,18E-06	0,115449	2,93E-01
Wetwell	2,51E-01	0,000286	0,250903	2,35E-06
GDCS	2,79E-03	1,35E-06	0,002785	1,37E-08
Annulus	2,29E-02	4,02E-07	0,007992	1,49E-02
PCCS	1,33E-08	1E-08	9,59E-11	3,14E-09
Reactor Building	1,58E-05	1,58E-05	0	6,69E-12
Total	9,43E-01	0,000305	0,428	5,16E-01

Time= 15.8 h	Total	Airborne	In the pool	Deposited on structures
RPV	2,21E-01	2,36E-09	4,06E-02	1,81E-01
RPV Upper Plenum	2,72E-02	8,54E-09	0,00E+00	2,72E-02
ICS	3,52E-04	2,03E-10	3,36E-04	1,60E-05
Drywell (upper+middle+lower)	4,17E-01	4,38E-07	1,26E-01	2,91E-01
Wetwell	2,51E-01	2,27E-04	2,51E-01	1,80E-06
GDCS	5,26E-04	5,97E-07	5,26E-04	5,20E-09
Annulus	2,59E-02	5,40E-07	1,10E-02	1,49E-02
PCCS	6,13E-09	4,71E-09	5,34E-11	1,36E-09
Reactor Building	1,58E-05	1,58E-05	0,00E+00	9,11E-12
Total	9,44E-01	2,44E-04	4,29E-01	5,14E-01

9 Summary

For assessment of Fission product retention in a PCCS a separate 1-D model to calculate particle deposition in tube flow was developed. The model was validated against 1-tube heat exchanger experiments conducted previously at VTT. The model can calculate heat transfer as well as particle deposition by diffusiophoresis and thermophoresis reasonably accurately. Diffusiophoresis and thermophoresis were expected to be the main deposition mechanisms also in the case of PCCS.

Based both on experimental and modeling results, it can be said that deposition by diffusiophoresis could remove as much as 50% of particles from the gas flow. However, aerosol did not accumulate to the heat exchanger. In all experiments condensed water rinsed deposited particles from the tube walls even though particle mass concentration was increased up to 6 g/m^3 (NTP). If steam mass flow rate through the PCCS is 10 kg/s, such concentration would correspond approximately to 75 g/s mass flow rate of particles. Based on experiments conducted at VTT the assumption that deposited particles are entirely rinsed from PCCS by the condensed water is well justified.

Particle deposition in a PCC tube was calculated with the developed 1-D model using a wide range of values for steam mass flow rate, gas temperature, pressure, and steam volume fraction and particle size. In the modeling work it was assumed that pool would be boiling around the tubes and steam would be saturated in PCC. The results showed that more than 90% of particles could be deposited in PCC, if the steam mass flow rate would be low. In turbulent flow the maximum deposition could be observed to be about 40%.

The aerosol retention models of MELCOR 1.8.6 have been tested by comparing them to heat exchanger experiments conducted at VTT. The result was that MELCOR generally underestimates heat transfer and steam condensation rates in the heat exchanger tubes. This is probably the reason why also the aerosol retention is underestimated. In addition, the MELCOR results were compared to the 1-D aerosol deposition model. The 1-D model gives better results for the experiments that involve steam condensation, but MELCOR is better at predicting the aerosol retention in the dry experiments.

The fission product release from the core was for noble gases about 82 %, for Cs 75 % and CsI 82 % of the whole core inventory. The modeled single-hole leakage for containment nominal leakage resulted in release fractions of noble gases, CsOH and CsI to the reactor building to be $5.71 \cdot 10^{-5}$, $1.65 \cdot 10^{-5}$ and $1.68 \cdot 10^{-5}$ of the core release, respectively. At 15.8 h into the accident 13 % of the CsI released from the core was in the Lower Drywell pool, 25 % in the Suppression Pool and 4 % in the water inside the Reactor Pressure Vessel (RPV). A total of 51 % of released CsI was deposited on structures.

When approximating the decontamination factor of CsI aerosol in the PCCS from MELCOR results by dividing the airborne mass entering the PCCS by the airborne mass exiting the PCCS one obtains a decontamination factor varying between 4.4 and 17 during the bulk of the accident time.

The CsI decontamination factor for the whole containment can be defined as the ratio of total CsI released from the RPV divided by the total airborne mass of CsI in the containment. The value for containment decontamination factor ranges from 1.4 to 3467 on the basis of MELCOR calculation.

The pH of the containment pools was calculated with ChemSheet code with the history of mass flow rates and pool masses obtained from MELCOR results and given as boundary conditions to ChemSheet. The formation of HCl due to radiolytical release of Cl from the cable insulations and the formation of HNO_3 was estimated as a function of dose rate with the method presented in NUREG/CR-5950. The sensitivity of pH to HCl release rate was examined by varying the HCl release rate. The drainage of CsOH with the PCCS condensate flow through the PCCS Drain Line keeps the water in GDCS alkaline in the beginning of the accident as CsOH is highly soluble to water and a strong base. But as the amount of airborne CsOH in the Upper Drywell reduces and GDCS water mass decreases due to injection to the RPV the pH in GDCS is also decreases due to acidic flow from Upper Drywell/PCCS containing soluble HCl. The time range when pH in the GDCS turns to acidic depends on the formation rate of HCl. In the Base Case the GDCS shifts from basic to acidic at 12.5 h. In the base case all other pools are alkaline.

In performed sensitivity runs with the HCl formation rate of 0.0015 mol/s the shift from alkaline to acidic in GDCS takes place around 11 h and the pH after 15 h is already 3.95. With the HCl release rate of 0.0060 mol/s the shift from basic to acidic takes place at about 8 h with the pH being 3.31 at 15 h. With the highest estimated HCl formation rate the initial pH (being neutral or 5.3) had little effect. Also with the HCl formation rate of 0.0060 mol/s the water in reactor vessel becomes acidic at around 11 h and with 0.0038 mol/s around 13 h. This is due to high flow rate of acidic water from GDCS.

In all cases the pH in LDW stays alkaline after buffer solution injection is started (at 6080 s) and the pH in WW becomes alkaline due to sufficient amount of CsOH.

10 References

1. ESBWR Design Control Document, Tier 1 and 2, Rev 1.

2. Soffer, L., Burson, S.B., Ferrell, C.M., Lee, R.Y., Ridgely, J.N., Accident Source Terms for Light-Water Nuclear Power Plants, NUREG-1465. 1995.

3. Incropera, F.P., DeWitt, D.P., Fundamentals of Heat and Mass Transfer, fifth ed., John Wiley & Sons, New York, 2002.

4. Waldmann, L., Schmitt, K.H., Thermophoresis and diffusiophoresis of particles in a heated boundary layer, In: Davies, C.N. (Ed.), Aerosol Science, Academic Press, London, 1966.

5. Talbot, L., Cheng, R.K., Schefer, R.W., Willis, D.R., Thermophoresis of particles in a heated boundary layer, J. Fluid Mech. 101, (1980) 737-758.

6. Hinds, W.C., Aerosol Technology, second ed., Wiley-Interscience, 1999.

7. Papavergos, P.G., Hedley, A.B., Particle deposition behaviour from turbulent flows, Chem. Eng. Res. Des. 62 (1984) 275-295.

8. Gnieliski, V., New equations for heat and mass transfer in turbulent pipe and channel flow, International Chemical Engineering Vol. 16, No. 2, April 1976.

9. Fuller, E.N., Schettler, P.D., Giddings, J.C., A new method for prediction of binary gas-phase diffusion coefficients, Ind. Eng. Chem. 58 (1966) 19-27.

10. Churchill, S. V., Chu, H. H. S., Correlating equations for laminar and turbulent free convection from a horizontal cylinder, Int. Journal of Heat and Mass Transfer 18 (1975) 1049-1053.

11. Rohsenow, W.M., A method of correlating heat transfer data for surface boiling liquids, Trans. ASME 74 (1952) 969-976.

13. Auvinen, A., Enqvist, Y.: Status report on aerosol removal model for PCC, VTT research report VTT-R-07050-06, 16.8.2006.

14. Auvinen, A., Jokiniemi, J., Renvall, T.: Kokeet aerosolien depositiomekanismien tutkimiseksi – Aerosol deposition studies, VTT Project report PRO6/T30/02, 20.12.2002.

15. Sevón, T., Validation of MELCOR 1.8.6 Aerosol Retention Models for ESBWR PCCS, VTT research report VTT-R-07651-06, 28.8.2006.

16. E.C. Beahm, R. A. Lorenz, C. E. Weber, Iodine Evolution and pH Control, NUREC/CR-5950 , ORNL/TM-12242

18. DRF-A13-00282.

19. General Electric ESBWR Design Control Document Tier 2, Chapter 3, Radiation Environment Conditions Inside Containment Vessel for Accident Conditions, Appendix 3H-11, 26A6642AN, Revision 1 January 2006

20. B. Pershagen, Light Water Reactor Safety, Pergamon Press, Oxford, England, 1989.

21. D.D. Thayer, D.H. Houston, N.A. Lurie, Updated Best- Estimate LOCA radiation Signature, NUREC/CR- 2367, August 1981.

22. ESBWR Design Control Document, Tier 2, Chapter 9, Auxiliary Systems, Table 9.3-3

23. E-mail from Chris Pratt to Ilona Lindholm, 6.10.2006

11 Appendix A Measured and estimated mass size distributions in 1-tube heat exchanger experiments.

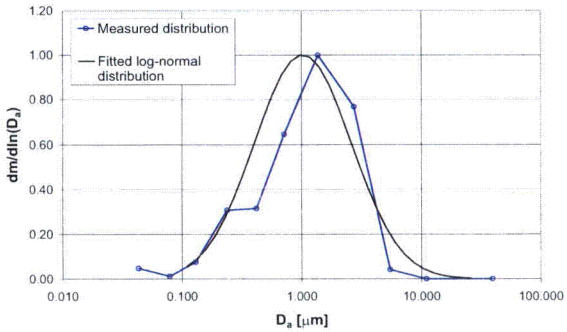

Fig. A.1. Ag particles AMMD = 1.02 µm, σ_g = 2.54, Exp. 1.1 (inlet).

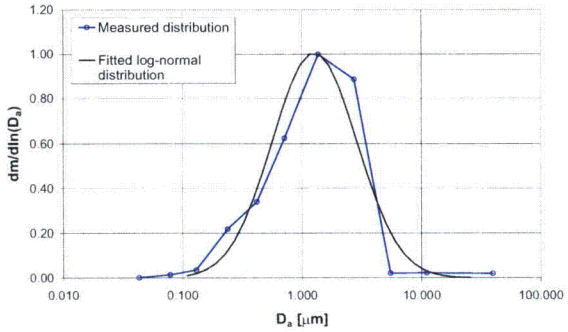

Fig. A.2. Ag particles AMMD = 1.28 µm, σ_g = 2.26, Exp. 1.1. (outlet).

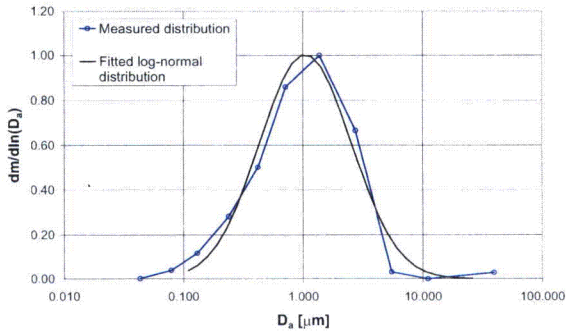

Fig. A.3. Ag particles AMMD = 1.05 µm, σ_g = 2.42, Exp. 1.1 (inlet).

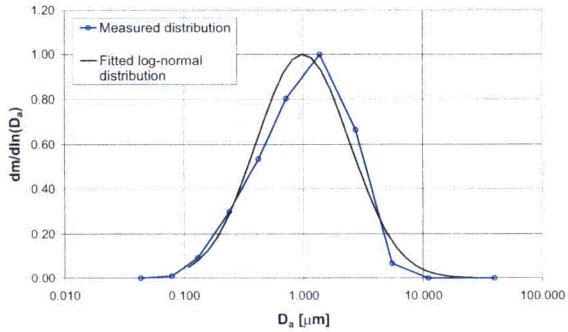

Fig. A.4. Ag particles AMMD = 1.00 µm, σ_g = 2.47, Exp. 1.1. (outlet).

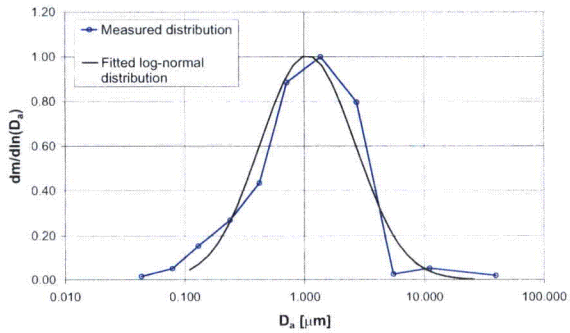

Fig. A.5. Ag particles AMMD = 1.07 µm, σ_g = 2.49, Exp. 1.2 (inlet).

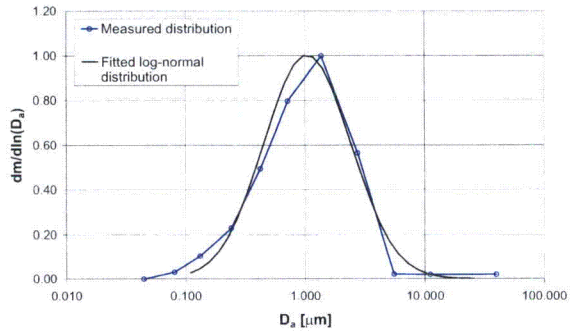

Fig. A.6.. Ag particles AMMD = 1.05 µm, σ_g = 2.31, Exp. 1.2 (outlet).

Appendix A

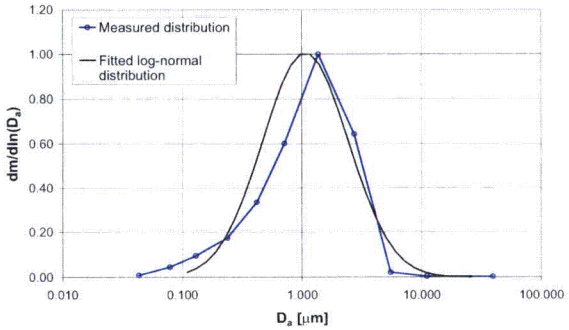

Fig. A.7. Ag particles AMMD = 1.07 µm, σ_g = 2.29, Exp. 1.2 (inlet).

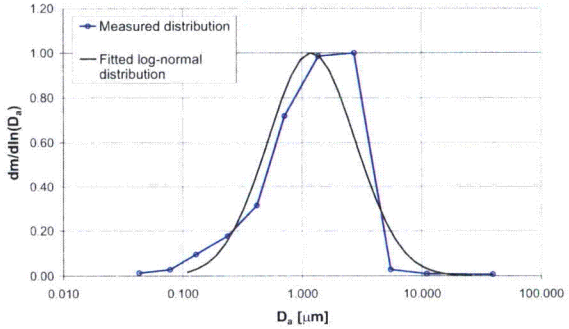

Fig. A.8.. Ag particles AMMD = 1.20 µm, σ_g = 2.32, Exp. 1.2 (outlet).

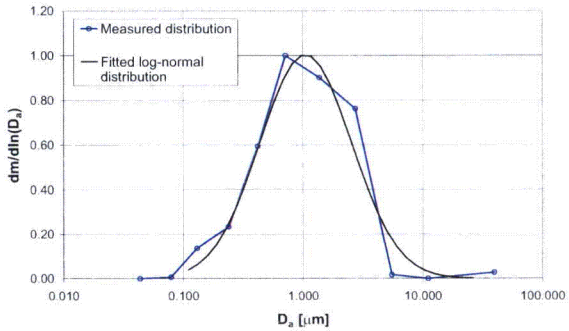

Fig. A.9. Ag particles AMMD = 1.05 µm, σ_g = 2.43, Exp. 1.3 (inlet).

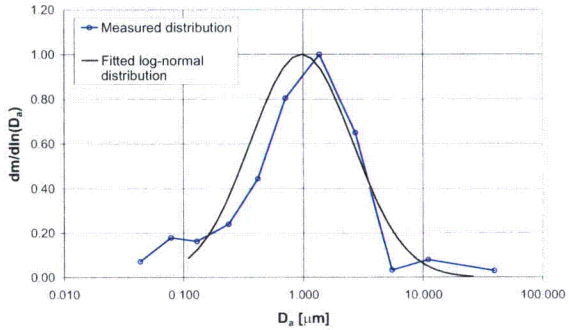

Fig. A.10.. Ag particles AMMD = 0.97 µm, σ_g = 2.68, Exp. 1.3 (outlet).

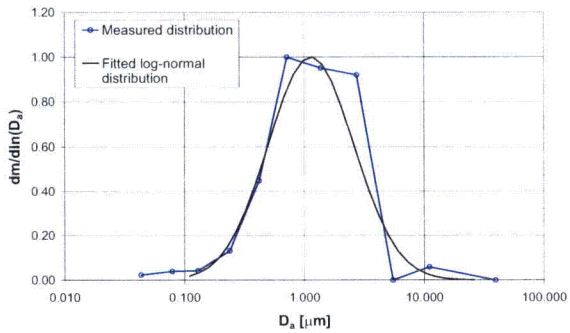

Fig. A.11. Ag particles AMMD = 1.14 µm, σ_g = 2.29, Exp. 1.3 (inlet).

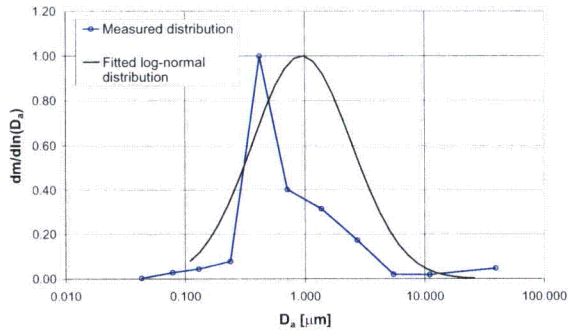

Fig. A.12.. Ag particles AMMD = 0.95 µm, σ_g = 2.61, Exp. 1.3 (outlet).

Appendix A

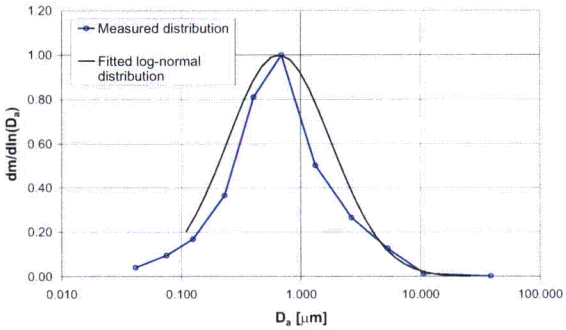

Fig. A.13. NaCl particles AMMD = 0.66 µm, σ_g = 2.73, Exp. 2.1 (inlet).

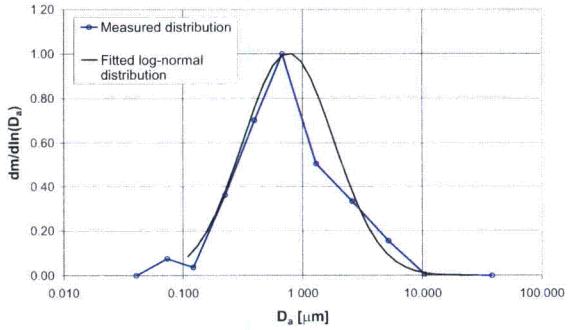

Fig. A.14.. NaCl particles AMMD = 0.76 µm, σ_g = 2.40, Exp. 2.1 (inlet).

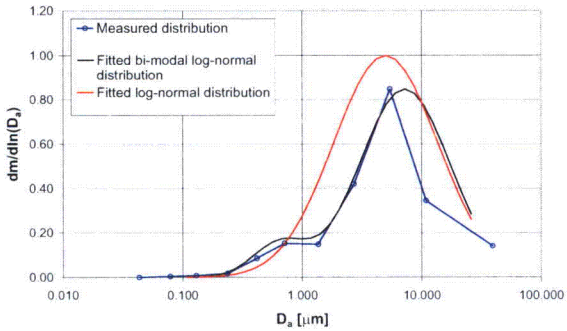

Fig. A.15. Cu particles
AMMD1 = 7.23 µm, σ_{g1} = 2.04, 85%
AMMD2 = 0.65 µm, σ_{g2} = 1.64, 15%
Exp. 2.2 (inlet).

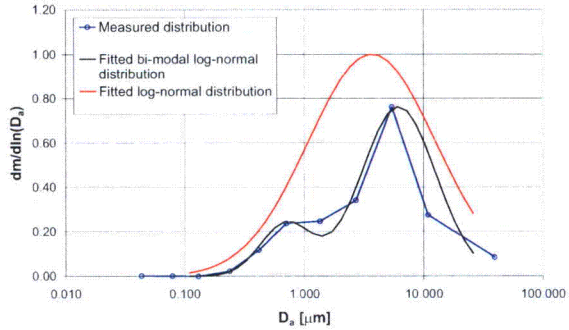

Fig. A.16.. Cu particles
AMMD1 = 6.17 µm, σ_{g1} = 2.04, 76%
AMMD2 = 0.71 µm, σ_{g2} = 1.64, 24%
Exp. 2.2 (inlet).

12 Appendix B: ChemApp

12.1 Introduction

ChemApp is derived from the renowned ChemSage family of thermochemical calculation programs, which are widely used in universities, corporate and government laboratories.
It offers new possibilities and perspectives for the use of thermochemical calculations across a wide spectrum of applications by providing an easily programmable interface to complex equilibrium calculation techniques.
ChemApp consists of a library of subroutines for data handling and phase equilibrium calculation purposes. It is available as an object code library for a variety of platforms and can be added as a module to virtually any existing or new software, major application areas are CFD (computational fluid dynamics) and process simulation programs.

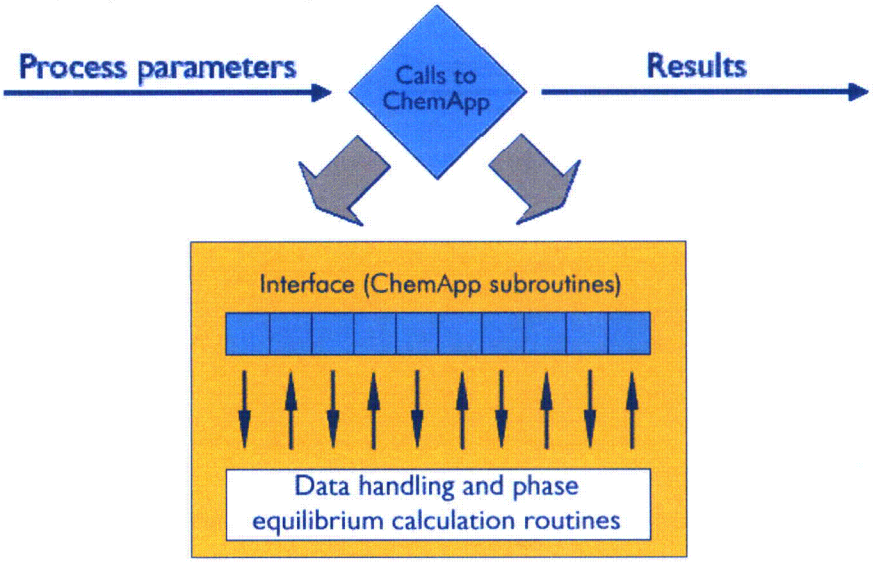

Figure 12-1. Schematic representation showing the integration of ChemApp into a process modeling or simulation program.

ChemApp provides the powerful calculation capabilities of ChemSage in the form of a programmer's library. It consists of a rich set of subroutines which provides all the necessary tools for the calculation of complex multicomponent, multiphase chemical equilibria and the determination of the associated energy balances.
ChemApp uses the 'engine' and data handling capabilities of the renowned ChemSage thermochemical application program. You find the same speed and reliability of convergence of calculations. You can use the same thermochemical data combined with the same comprehensive library of models for non ideal solution phases. ChemApp is modular, which makes it easy to integrate into third party applications and also facilitates the incorporation of future improvements and extensions.

12.2 Thermochemical data

The same comprehensive library of models for non-ideal solution phases available in ChemSage is also built into ChemApp. Thus, the wide range of existing thermochemical data

for ChemSage is available for ChemApp too. ChemApp also uses the same thermochemical data-file format as ChemSage.

Table 13-1. Solution models available in ChemApp

Model	Application area
Redlich-Kister-Muggianu Kaufman-Kohler Four-suffix Margules Kohler-Toop Hoch-Arpshofen	for general use with substitutional or associated solution phases
Compound energy formalism Species chemical potential/bond energy formalism	solid alloys
Ionic two sublattice model	ionic liquids
Equivalent fraction sublattice model	molten salts
Gaye-Kapoor-Frohberg cell model	ionic oxidic mixtures
Blander-Pelton modified quasichemical model	ionic oxidic mixtures with non-oxidic solutes
Wagner	metallic dilute solutions
Pitzer	concentrated aqueous solutions
Virial equation	non-ideal gas phases

12.3 Programming steps

Only three stages of simple programming are necessary to proceed from initialization of ChemApp to collection of results

1. Initialize the interface, read a thermodynamic data-file, and adjust the chemical system.

2. Set initial conditions for the equilibrium calculation.

3. Perform the calculation and collect results.

In the simplest cases, each programming step requires calling only one or two of the ChemApp interface routines. For more complicated applications, the number of routines called in each step increases; however, the demands on programming capabilities are never particularly difficult.

12.3.1 Initializing the interface and reading a thermodynamic data-file

This first step of each program entails initializing the interface, reading a thermodynamic data-file into the program, and changing default units, if necessary.
A further series of programming subroutines enable the chemical system to be adjusted to match the requirements of the calculation

- identification of phases, phase constituents, and system components

- delete or activate phases and/or constituents from a calculation

The latter group of routines provides a very useful set of tools, since they allow the suppression of otherwise stable phases in order to calculate metastable conditions. Also, by elimination of phases and/or constituents which are known not to be stable under the chosen conditions, considerable increase in computation speed can be gained.

12.3.2 Setting the initial conditions for the equilibrium calculations

ChemApp offers considerable flexibility for defining initial conditions for a chemical equilibrium calculation. Two different methods are available that will cover most cases experienced in practice.

- By defining the global conditions of the system.

  Using this method, it is merely needed to set single conditions for pressure and temperature, and enter incoming species to define the composition of the system. For example, if the thermodynamic equilibrium for the system SiO2-CaO is to be calculated, using a ChemSage - compatible data-file that contains the elements Ca, Si, and O, it is only required to define the temperature and pressure of the system, and the total amounts of SiO2 and CaO present. Instead of temperature and pressure, other variables of state can be chosen too.

- By defining streams.

  A stream is considered as a medium for transferring non-reacted matter to a reaction zone. It has constant temperature and pressure, and contains one or more phases of given composition. Hence, when using this method, the conditions for the three variables - composition, temperature and pressure - need to be defined for one or more input streams. For instance, one stream entering a reaction zone can consist of O2 (g), preheated to a temperature of 1500K, while the other consists of CO (g) at room temperature.
  This method must be used for calculation of the extensive properties of reactions; for example, those involving the heat balance or the adiabatic temperature of a combustion process. It is also convenient to use it for reactor calculations, where it is known what is entering the system and it is desired to calculate results at various stages during and at the end of the process.

12.3.3 Performing the calculation and collecting results

Only one subroutine needs to be called to execute phase equilibrium calculations defined by pressure, temperature, and input composition.
Like ChemSage, ChemApp is also able to perform extensive property target calculations (defined by an extensive property change) and phase target calculations (defined be the search for a particular phase). If, in the previous step, such a target calculation has been defined, the necessary additional information is supplied upon calling the equilibrium calculation routine.
Results from a phase equilibrium calculation are retrieved by using only a single subroutine.
For the following variables results can be obtained

- Total pressure, total volume, temperature
- Equilibrium amount of phases, phase constituents, and system components
- Chemical potential and activity
- Heat capacity, enthalpy, entropy, and Gibbs energy of the equilibrium state
- Mass or mole fraction of a system component or phase constituent

ChemApp can also calculate the thermodynamic properties, Cp, H, S, and G, of a phase and its constituents.
For full online documentation of ChemApp-interface see:
http://gttserv.lth.rwth-aachen.de/~cg/Software/ChemApp/IndexFrame.htm

13 Appendix C: ChemSheet

13.1 Introduction

ChemSheet combines the flexibility and practicality of spreadsheet applications with the thermodynamic and simulation capabilities of Gibbs Energy minimization. Its applications are appropriate for metallurgical, chemical and process industries as well as for geochemists and environmentalists. Also there is a special appeal to those in universities and chemical education.
ChemSheet allows rigorous chemical and thermodynamic calculations to be computed within the familiar environment of Microsoft Excel spreadsheet. Even though ChemSheet uses complex numerical procedures with extensive thermodynamic data linked with appropriate reaction kinetics, it produces the results on a simple Excel spreadsheet and thus makes the simulation accessible to the general user.
ChemSheet applies the ChemApp thermodynamic programming library, which handles repetitive complex equilibrium calculations for a diverse range of chemical and thermodynamic applications. ChemApp can be used to calculate both the composition and the thermodynamic properties of a multi-phase, multi-component system at given conditions. With ChemApp, versatile one-dimensional phase-mapping and target calculations can also be done.
The applications range from analysis of laboratory and environmental data to practical process simulation and design. In ChemSheet each process chemistry model can be formatted to practical worksheet from which calculations are made.

13.2 Definition of Terms

A thermodynamic system consists of a number of phases, where some may have a composition expressed as amounts of a number of phase constituents, and others can have an invariant composition. Phases are divided into three groups:

1. The gaseous phase.
2. Condensed mixtures (liquid and solid state).
3. Condensed stoichiometric phases (liquid and solid state).

Phases and phase constituents always have thermochemical properties (activities, chemical potentials, enthalpies, volumes, etc.). Phase constituents have compositions expressed as amounts (i.e. stoichiometric coefficients) of a number of components. A component is a system-wide entity, which is stressed by calling it a system component. Usually components are elements, but it is also possible for them to be stoichiometric combinations of elements. For example, in an oxide system based on calcia and silica, CaO and SiO2 may be used, as well as Ca, Si, and O

13.3 Nomenclature Used in ChemSheet

Names of components, constituents of a phase, phases and streams are case sensitive and can consist of a string of letters up to 24 characters in length. For example, 'CO' and 'Co' are two different phase constituents. Some names are reserved because they have some special meaning in ChemSheet:

13.4 Using ChemSheet

Several concepts are introduced which are important to know about when beginning to use ChemSheet. They include the description of the two ways initial conditions can be defined (global conditions and streams

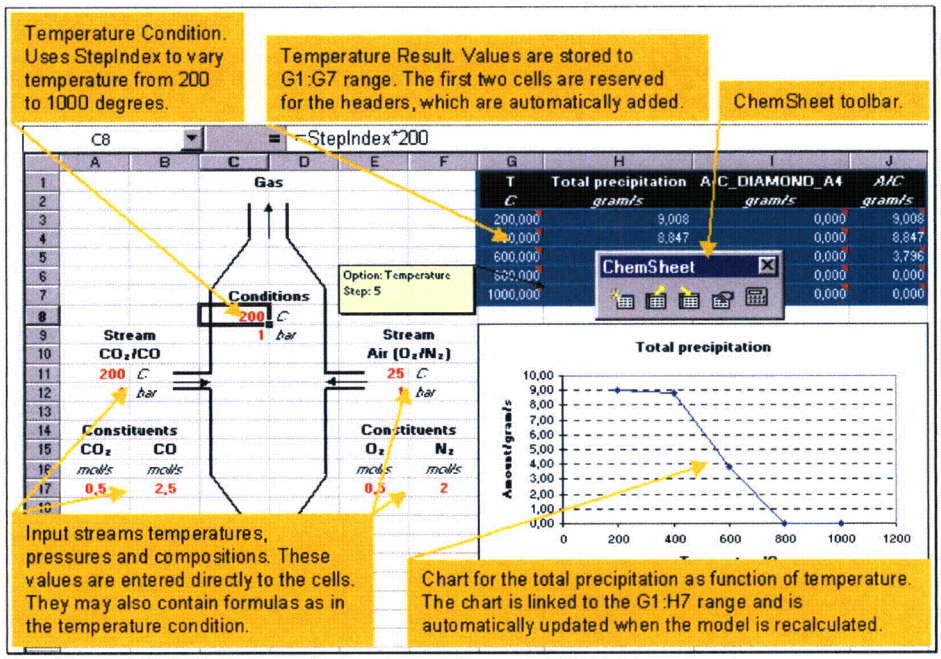

Figure 13-2. Example ChemSheet Application.

Here is a picture with some comments added of a more advanced ChemSheet application using Streams. It contains many features of Excel that can be used with ChemSheet.
In this application all the necessary input values are entered to worksheet cells, so they can be quickly changed without opening the ChemSheet dialog box.
The cells are linked to the ChemSheet model using cell references and the values of cells are evaluated for each calculation step. After changing one or more values in the linked cells the model needs only to be recalculated by clicking the Calculate ChemSheet Model command in ChemSheet toolbar and the result values and charts linked with them are automatically updated.
ChemSheet dialog can be opened by clicking New ChemSheet Model or Edit ChemSheet Model commands in ChemSheet toolbar. In ChemSheet dialog you can define all the necessary input values for one or more equilibrium calculations and also the results you wish to retrieve and store to Excel worksheets.

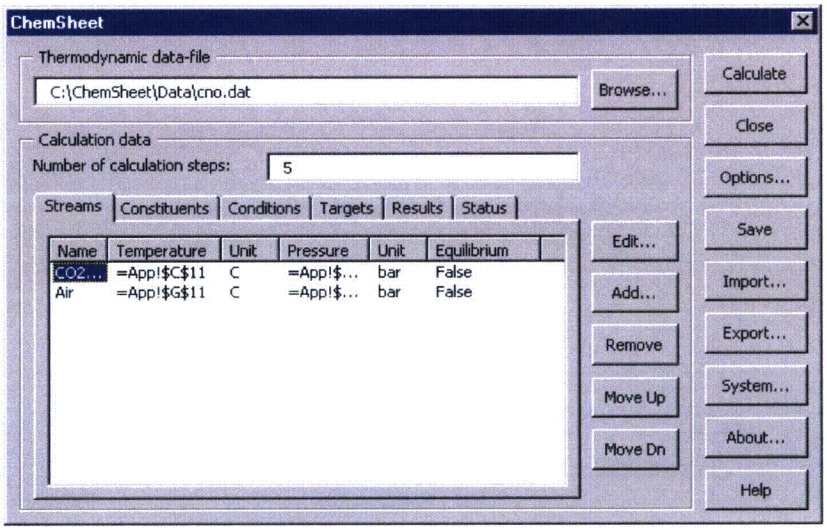

Figure 13-3. ChemSheet dialog.

13.5 Using Initial Conditions

ChemSheet offers you considerable flexibility for defining initial conditions for a chemical equilibrium calculation. Two different methods are available that will cover most cases experienced in practice:

1. Using Global Conditions of the System

2. Using Streams

Below is a schematic picture of an equilibrium calculation when using Global Conditions.

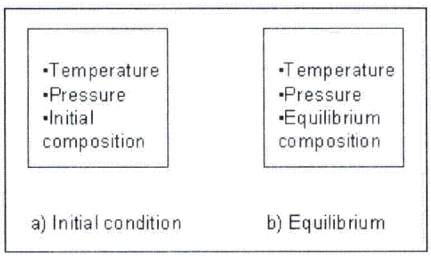

Figure 13-4. Global conditions.

You merely need to set single values for temperature and pressure, and enter amounts of incoming species to define the composition of the system at its initial stage.
This input method is used if the amounts of the incoming species are merely given to define the overall composition of the system.

Below is a schematic picture of equilibrium calculation when using Streams.

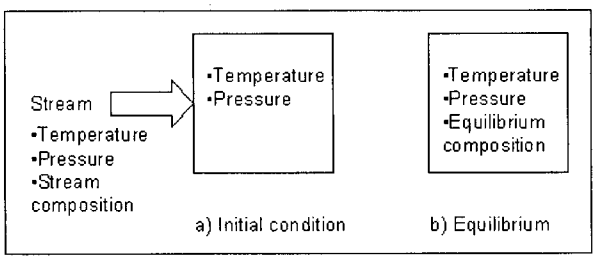

Figure 13-5. Streams.

You set three variables – temperature, pressure and composition – for one or more input streams and set single values for temperature and pressure of the system.
This input method is used if the reaction between the input streams is to be calculated, especially in the respect to the change of the extensive properties: heat capacity, enthalpy, entropy, Gibbs energy, or volume.

You have also an option to make target calculations, if some of the variables used above are unknown but some other variables are known, e.g. the heat balance (enthalpy of the equilibrium condition minus enthalpy of the initial condition) or the presence of a phase at equilibrium.

13.6 Using Global Conditions of the System

Using this method, you merely need to set single values for pressure and temperature, and enter incoming species to define the initial composition of the system. For example, if you wish to calculate the thermodynamic equilibrium for the system SiO2-CaO, using a thermodynamic data-file that among others contains the elements Ca, Si, and O, he would only need to define the temperature and pressure of the system, and the total amounts of SiO2 and CaO present. You can also enter incoming amounts as components, i.e. total number of elements Ca, Si, O present. As a result of the calculation you will be given the amounts of the stable phases in the system, and if a phase is a mixture phase, also the equilibrium composition of the phase.

13.6.1 Selecting Global Conditions

1. Choose the Edit command in the ChemSheet menu or press the Edit ChemSheet model button in the ChemSheet toolbar. If you don't have the ChemSheet toolbar visible, select it with the Toolbars command in View menu. The ChemSheet dialog box appears.

2. Click the Options. The Options dialog box appears.

3. Click the Global conditions in Initial Conditions.

Note – Global Conditions is the default value when you start a new ChemSheet model. If you change the Initial condition all the Calculation data will be reset. So you should change the Initial condition first and only then start defining the Calculation data.

13.6.2 Adding a New Condition

The procedure to define conditions is the same regardless of the method you have chosen to define the initial conditions in the Options dialog box – only incoming species are defined

differently. When you are using Streams, the incoming species are defined as stream constituents. To add a new Condition:

1. Choose the New command in the ChemSheet menu or press the New ChemSheet Model button in the ChemSheet toolbar. If you don't have the ChemSheet toolbar visible, select it with the Toolbars command in View menu. The ChemSheet dialog box appears.

2. Click Conditions tab in the Calculation data.

3. Click Add to add a new Condition. The Condition dialog box appears.

4. Select the state variable and necessary options for it and give its value. If some controls are outlined with grey color, then their values are not needed for the selected set of options.

5. Click Ok.

If you add other conditions than temperature, pressure, or incoming amount, then you have to add a target variable.

13.7 Using Streams

A stream is a means for transferring non-reacted matter to a reaction zone. It has constant temperature and pressure, and contains one or more phases of fixed composition. When using this method, user sets the three variables – temperature, pressure and composition for each input stream and set single conditions for temperature and pressure of the system. For example, one stream entering a reaction zone may comprise O2 (g) pre-heated to a temperature of 1500 K, and the other may consist of CO (g) at room temperature.
The Streams method must be used for calculation of the changes of extensive properties of reactions; for example, those involving the heat balance of a combustion process. It is also convenient to use it for reactor calculations, where you know what is entering the system and you wish to calculate results at various stages during and at the end of the process.
When setting the incoming amounts for a stream, only phases and phase constituents can be used for this purpose. If one wants to enter the incoming amounts for a stream in terms of the system components (i.e. usually the elements), but the phase constituents of that phase are not elements, one has to perform an intermediate calculation using another ChemSheet model that uses Global conditions.

Other conditions, especially temperature and pressure of the system, are defined just as when using Global Conditions.

13.7.1 Selecting Streams

1. Choose the Edit command in the ChemSheet menu or press the Edit ChemSheet model button in the ChemSheet toolbar. If you don't have the ChemSheet toolbar visible, select it with the Toolbars command in the View menu. The ChemSheet dialog box appears.

2. Click Options. The Options dialog box appears.

3. Click Streams in Initial Conditions.

Note – Global conditions is the default value when you start a new ChemSheet model. If you change the Initial Condition all the Calculation data will be reset. So you should change the Initial Condition first and only then start adding the Calculation data.

13.7.2 Adding a New Stream

To add a new Stream:

1. Choose the New command in the ChemSheet menu or press the New ChemSheet Model button in the ChemSheet toolbar. If you don't have the ChemSheet toolbar visible, select it with the Toolbars command in View menu. The ChemSheet dialog box appears.
2. Click Streams tab in Calculation data.
3. Click Add to add a new Stream. The Stream dialog box appears.
4. Give the stream name, the temperature and its unit and the pressure and its unit.
5. Click Ok.

13.7.3 Adding a New Stream Constituent

To add a new Constituent to a previously defined Stream:

1. Choose the New command in the ChemSheet menu or press the New ChemSheet Model button in the ChemSheet toolbar. If you don't have the ChemSheet toolbar visible, select it with the Toolbars command in View menu. The ChemSheet dialog box appears.
2. Click Constituents tab in Calculation data.
3. Click Add to add a new constituent. The Constituent dialog box appears.
4. Select the stream, the phase and the phase constituent and give its value.
5. Click Ok.

13.8 Getting Results

In ChemSheet getting results comprises two things: selection of the state variable and the range of worksheet cells used to store the values of that state variable for each calculation steps. The range can be a reference to a cell or range of cells or can refer to multiple areas. An area is a range of contiguous cells or a single cell. The values are stored to the areas from left to right and top to bottom. So the value for the first calculation step is stored to the first cell in the first area (upper left corner of the area) and the value for the last step is stored to last cell in the last area (lower right corner of the area).
Note – If you have selected Headers for a Result, then the first two cells in the first area are reserved to them.

Here is an example where three results have been defined:

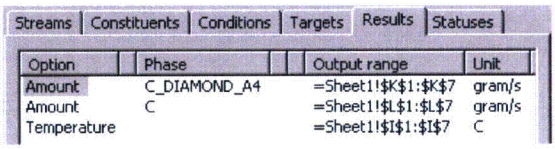

Figure 13-6. Results in ChemSheet dialog.

If the Headers and Comments options are selected then the results are stored as follows:

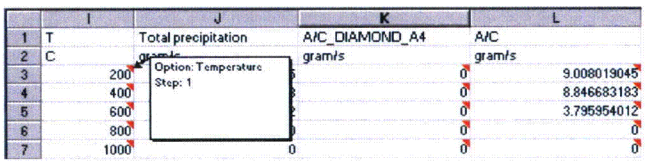

Figure 13-7. Results in worksheet.

The first cells in each range contain the ID of the Option (state variable) and the second cells contain the Unit of the state variable.

13.8.1 Adding a New Result

To add a new Result:

1. Choose the New command in the ChemSheet menu or press the New ChemSheet Model button in the ChemSheet toolbar. If you don't have the ChemSheet toolbar visible, select it with the Toolbars command in View menu. The ChemSheet Dialog box appears.

2. Click Results tab in Calculation data.

3. Click Add to add a new Result to the list. The Result dialog box appears.

4. Select the result variable and the necessary options for it and give the range where to store the values for each calculation step. If some controls are outline with grey color, then their values are not needed for the selected set of options.

5. Click Ok.

13.9 Using Formulas

You can use formulas in any value field in ChemSheet. When you normally do any calculation you change some value between the successive calculation steps and see how that affects the new equilibrium.

The names *StepIndex*, *StepCount*, *MapIndex*, and *MapIndex2* are defined when you start a new ChemSheet model or open a workbook that contains a ChemSheet model. The value of *StepCount* is the same as the Number of Steps that is given in ChemSheet dialog box. The value of *StepIndex* varies from one to the number of steps so that you can always use it in your formulas to refer to the index number of the current calculation step. Their values are updated at the start of each calculation step before the results for that step are written. After

all the calculation has ended its value is restored as one. Here is an example where the equilibrium temperature is changed using the *StepIndex*:

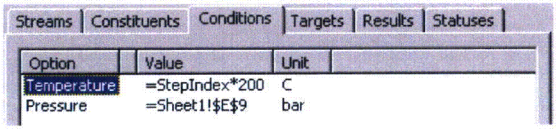

Figure 3-8. Using formulas.

So initially its value is 200 C and then it increases by 200 at each successive calculation step. The value of the equilibrium pressure is defined as a cell reference. Its actual value is the same as the value of the cell **E9** in worksheet Sheet1. The value of cell is evaluated in each calculation step so it too can contain a formula that uses StepIndex.
The previous formula is a very simple one. If you want to calculate at temperatures that are not incremented by a constant value you can enter the temperature values to a range in a worksheet and use the Index function. For example you can enter the following values to range **A1:A5**:

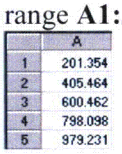

Figure 13-9. Random temperatures.

and then set the formula for temperature as follows:

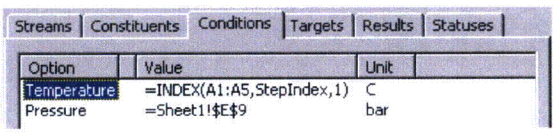

Figure 13-10. Using INDEX-worksheet function.

You can use any of the worksheet functions that are available. For the list of functions select the Functions command in Insert menu in Excel.
You can also use you own functions if you know how to program with Visual Basic

13.9.1 Using Units of State Variables

ChemSheet supports several units for each quantity. The quantities are:

- Pressure
- Volume
- Temperature
- Energy
- Amount
- Time

Time is only available when you have chosen to use Streams as Initial Conditions. Time is added to all the units when it is applicable: amount means amount of flow (e.g. mol/s),

enthalpy means enthalpy of flow (e.g. J/s), and so on. This way you can use different time scales when giving initial conditions (as it may be the case with the real world application that you are simulating) and need not to do the unit conversion yourself.
For all variables there are lists of example units. If the unit combination you want to use is not present in a list, just type it to the text box. The numerator and the denominator are divided with the slash character and other quantity units with the dash character. Blanks are ignored. For example these are both the same unit for entropy flow:
J/K-s
$J / s - K$

But this is not valid unit for entropy flow:

J/K/s

Note – If you use streams and are not interested in time scales, just give all the time units as seconds (or with any time unit as long as you make sure that you use the same time unit everywhere).

13.10 Available units for Quantities

Table13-2. Available units.

Quantity	ID	Unit	Comment
Pressure	P	bar	P/bar
		atm	P/atm = P/bar/1.01325
		Pa	P/Pa = P/bar/0.00001
		kPa	P/kPa = P/bar/0.01
		psi	P/psi = P/bar/0.06894757
		torr	P/torr = P/bar/1.01325/760
Volume	V	dm3	V/dm3
		cm3	V/cm3 = V/dm3/0.001
		m3	V/m3 = V/dm3/1000
		ft3	V/ft3 = V/dm3/28.316846592
		in3	V/in3 = V/dm3/0.016387064
Temperature	K	K	T/K
		C	T/C = (T/K - 273.15)
		F	T/F = 1.8 * (T/K - 273.15) + 32

Energy	E	J	E/J
		cal	E/cal = E/J/4.184
		Btu	E/Btu = E/J/1055.06
		kWh	E/kWh = E/J/3,600,000
Amount	A	mol	M/mol
		gram	M/gram
		kg	M/kg = M/gram/1,000
		tonne	M/tonne = M/gram/1,000,000
		pound	M/pound = M/gram/453.59237
Time	t	s	t/s
		min	t/min = t/s/1/60
		h	t/h = t/s/1/3600
		d	/d = t/s/1/86400

13.11 Thermodynamic Data

There are three different kinds of data-files that can be used with ChemSheet:

1. Ascii files (*.DAT)
2. Binary files (*.BIN)
3. Transparent files (*.CST

Ascii files can be made with ChemSage and HSC programs and they can be freely edited by hand. When making data-files with HSC program you must convert the generated ChemSage 3.0 data-file to 4.0 format with ChemFile program that is included in ChemSheet package.
Binary files are stored in a way that doesn't permit the end user to extract or change thermochemical data from the data-file. This is mainly done in cases where the license agreement with the supplier of the data doesn't permit the distribution in plain text format. In these cases the distribution of the data-file in non-ASCII form is the only way to make it available to the users of our software. Due to the nature of FORTRAN standard for writing binary data to files, or rather, the lack thereof, binary data-files are usually not portable across platforms

Transparent files are more portable than binary files. Transparent data-files, like binary data-files, are stored in a way that doesn't permit the end user to extract or change thermochemical data from the data-file. This is mainly done in cases where the license agreement with the supplier of the data doesn't permit the distribution in plain text format. In these cases the

distribution of the data-file in non-ASCII form is the only way to make it available to the users of our software. Transparent files can be made with FactSage program.
A comprehensive list of readily available standard data-files that are adequate for many applications can be obtained from GTT-Technologies. Customized data-files can also be prepared to meet a user's specific requirements. ChemSage data-files are mostly in the form of an ASCII text-file and can easily be updated and refined, if necessary.

A significant feature of the ChemApp thermodynamic programming library used with ChemSheet is that it incorporates a comprehensive library of excess Gibbs energy models for various types of non-ideal solution phases. Additional 'customer-specified' models can be added upon request from GTT-Technologies.

13.12 Sodium pentaborate

These reference values are from Eagle-Picher (http://www.eaglepicher.com/EaglePicherInternet) report on enriched sodium pentaborate products for BWR operators:
http://www.eaglepicher.com/NR/rdonlyres/1183A34B-F387-4D85-A79A-C4C5F1FB806C/0/w_c_03.pdf

Table 13-3. Physical properties of sodium pentaborate

Form	White Crystals
Enrichment	To 99% at 1% ^{10}boron
Formula	$Na_2O*5B_2O_3*10H_2O$
Specific gravity	1.71 g/cm^3
Boron Content	17.21% at ^{10}boron

Table 13-4. Solubility in water (natural isotopic composition)

Temperature/C	% anhydrous salt by composition
0	6.28
10	8.10
20	10.55
30	12.20
40	17.40
50	21.80
60	26.90
70	32.25
80	37.84
90	43.80
100	50.30

13.13 Sodium diborate (common name Borax)

Borax ($Na_2O{\cdot}2B_2O_3{\cdot}10H_2O$) is the most common of sodium borate based buffer solutions. In this project it is used as a reference solution to validate the thermodynamic model as measured titration curves for it were found in the literature[2].

Table 13-5. 100 mL of 0.025 M Borax buffer solution titrated with 0.1 M HCl[2]

HCl mL	pH
4.0	9.1
9.2	9.0
14.2	8.9
19.2	8.8
23.2	8.7
27.0	8.6
30.4	8.5
33.2	8.4
35.4	8.3
37.6	8.2
39.4	8.1
41.0	8.0

Table 13-6. 100 mL of 0.025 M Borax buffer solution titrated with 0.1 M NaOH[2]

NaOH mL	pH
1.8	9.2
7.2	9.3
12.4	9.4
17.6	9.5
22.2	9.6
26.2	9.7
30.0	9.8
33.4	9.9
36.6	10.0
39.0	10.1
41.0	10.2
42.6	10.3

13.14 Thermodynamic System

The thermodynamic system used in pH calculation is shown below.

[2] Robinson, R. A., and Stokes, R. H., Electrolyte solutions, the measurement and interpretation of conductance, chemical potential, and diffusion in solutions of simple electrolytes, 2nd ed., rev. London, Butterworths, 1968

Table 13-7. Thermodynamic system.

Phase	Constituent	Components					
		B	**Na**	**H**	**O**	**Cl**	**e**
Gas	H_2O			2	1		
	HCl			1		1	
Water	H_2O			2	1		
	H+			1			-1
	OH-			1	1		1
	$B(OH)_3$	1		3	3		
	$B(OH)_4$-	1			2		1
	Cl-					1	1
	Na+		1				-1
NaCl	NaCl		1			1	
NaOH	NaOH		1	1	1		
$Na_2O{\cdot}2B_2O_3{\cdot}10H_2O$	$Na_2O{\cdot}2B_2O_3{\cdot}10H_2O$	4	2	20	17		
$Na_2O{\cdot}5B_2O_3{\cdot}10H_2O$	$Na_2O{\cdot}5B_2O_3{\cdot}10H_2O$	10	2	20	26		

Thermodynamic system consists of ideal gas phase (Gas), aqueous phase (Water) and for condensed salts, NaCl, NaOH, sodium diborate (Borax) and sodium pentaborate. Aqueous phase is modeled using Pitzer formalism.

13.15 Calculation Results

Initial calculations were made with ChemSheet software using the thermodynamic system in Table 13-7. At this stage no calculation is made with any real or estimated process values. These calculations are used to verify the thermodynamic system and its applicability to pH calculations with sodium pentaborate and HCl systems in general.

First two reference calculations were made where results were compared against measured pH values with 0.025 M Borax buffer solution (Figs. 3 and 4).

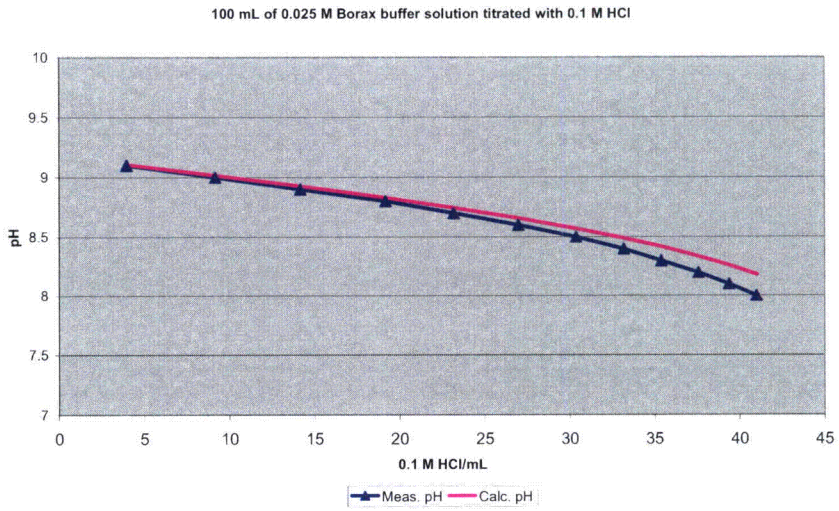

Figure 13-11. Comparison of calculated and measured pH in a case of Borax buffer solution titrated with 0.1 M HCl.

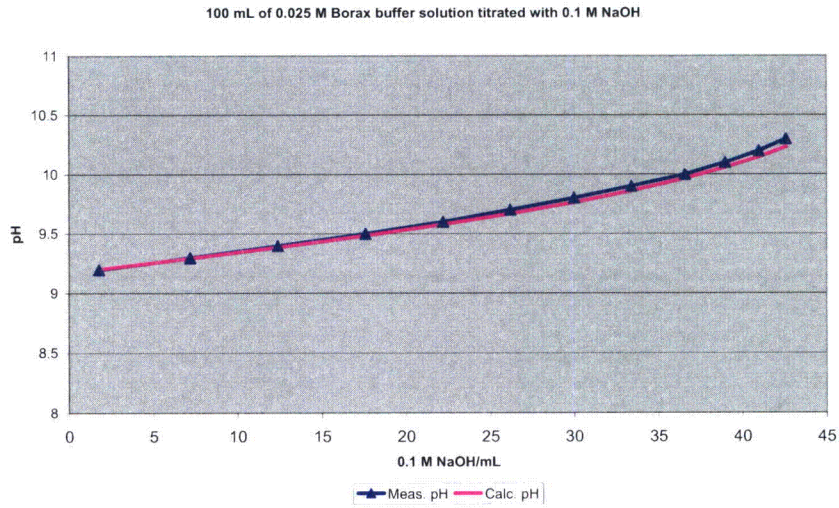

Figure 13-12. Comparison of calculated and measured pH in a case of Borax buffer solution titrated with 0.1 M NaOH.

With low acid and base concentrations calculated and measured values are almost equal but especially with higher acid (HCl) concentration there is a clear difference but the result is still adequate.

Next calculation was made with sodium pentaborate solution where natural boron concentration is 1600 ppm (according to standby liquid control system specifications).

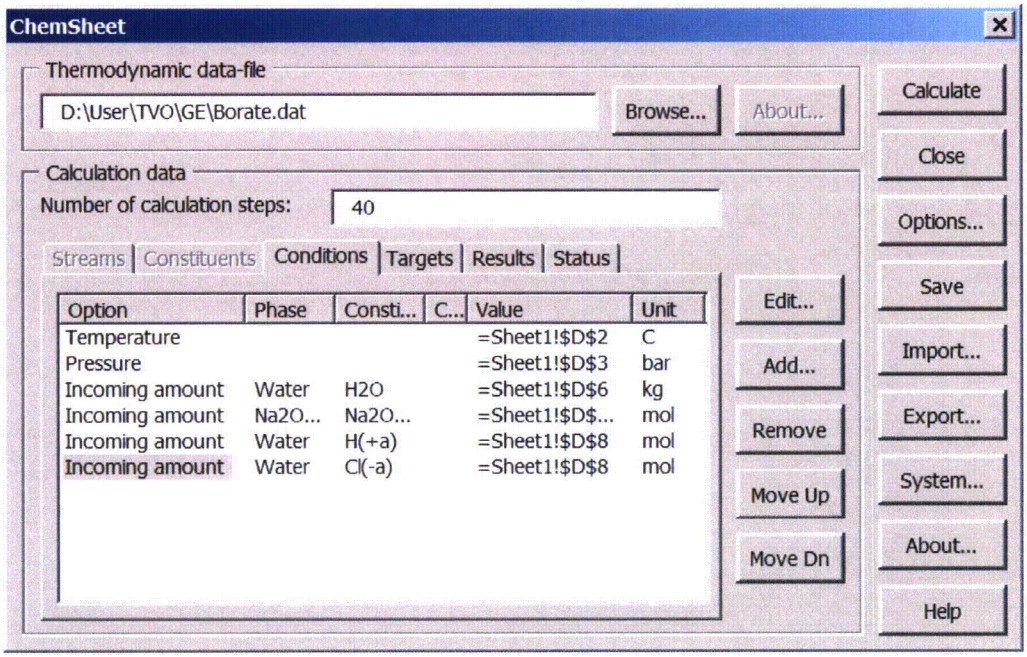

Figure 13-13. ChemSheet dialog showing the initial conditions of pH calculation. Actual values were given in Excel worksheet cells.

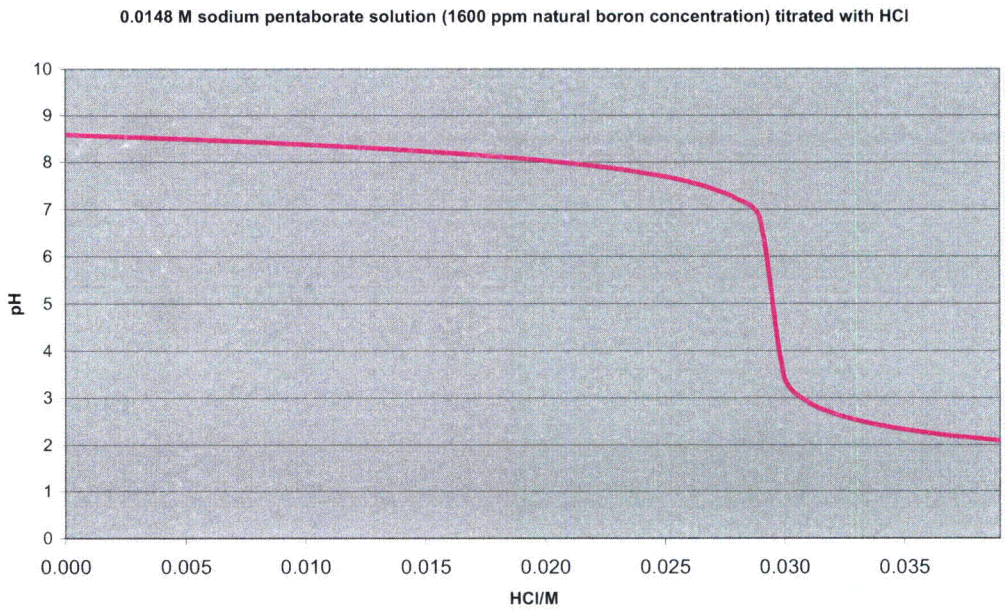

Figure 13-14. Calculation of pH in case of 0.0148 M sodium pentaborate titrated with HCl.

It can be seen that pH changes to acidic when HCl concentration is greater than 0.029 mol/kg_{H2O}. This result is not verified yet (it is only based on calculation).

Similar titration curve was found for sodium diborate (Borax) at http://www.borax.com/detergents/pheffect.html.

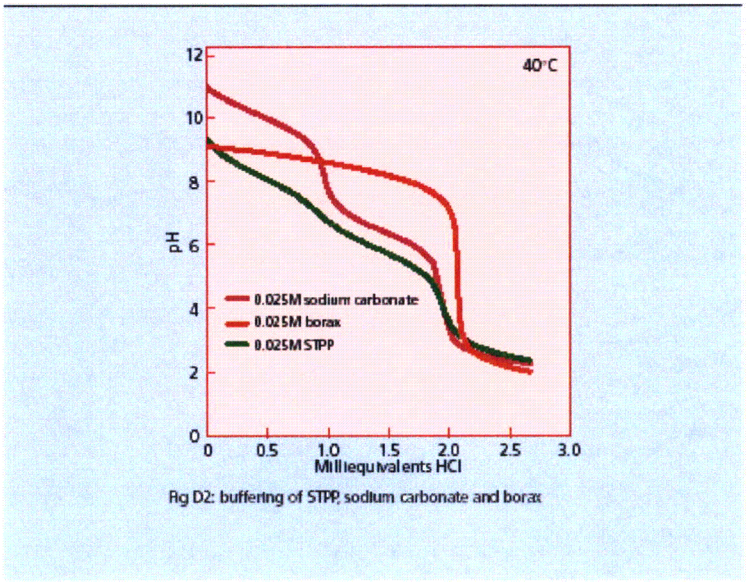

Figure 13-15. Titration curve for 0.025 M Borax buffer solution found at http://www.borax.com/detergents/pheffect.html.

The same titration curve was also calculated with ChemSheet.

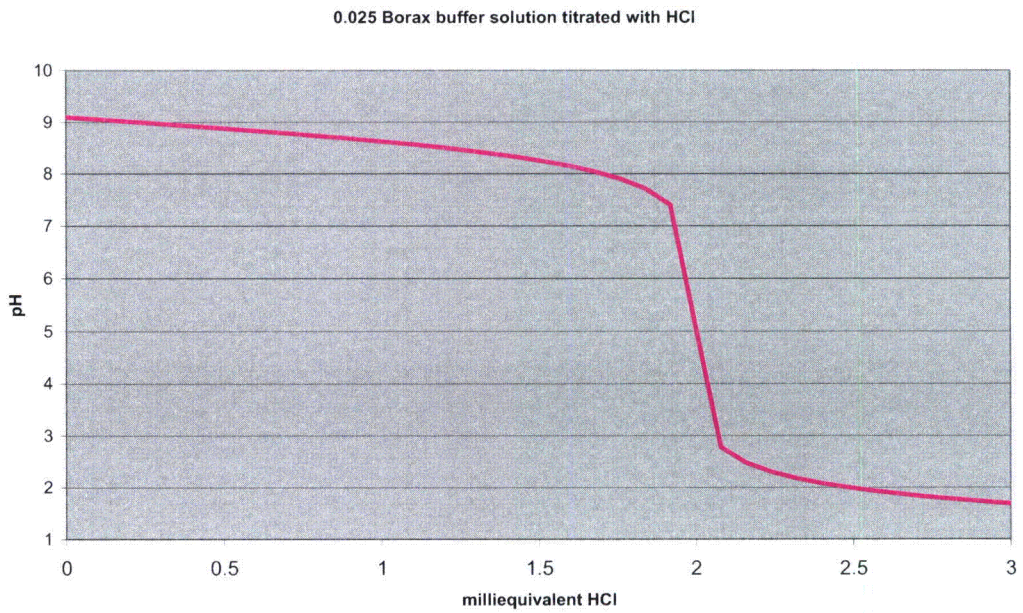

Figure 13-16. Titration curve at 40 C for 0.025 M Borax buffer solution calculated with ChemSheet.

It can be seen that the calculated titration curve is quite similar.

It can be concluded that the used thermodynamic data is applicable to pH calculations at temperature range between 25-50 degrees Celsius and at moderate pressure (1-5 atm). Probably it can be used at temperatures even close to boiling point of water (depending on the absolute pressure).

In the next stage a ChemSheet pH model will be made where process data is taken from MELCOR simulation.

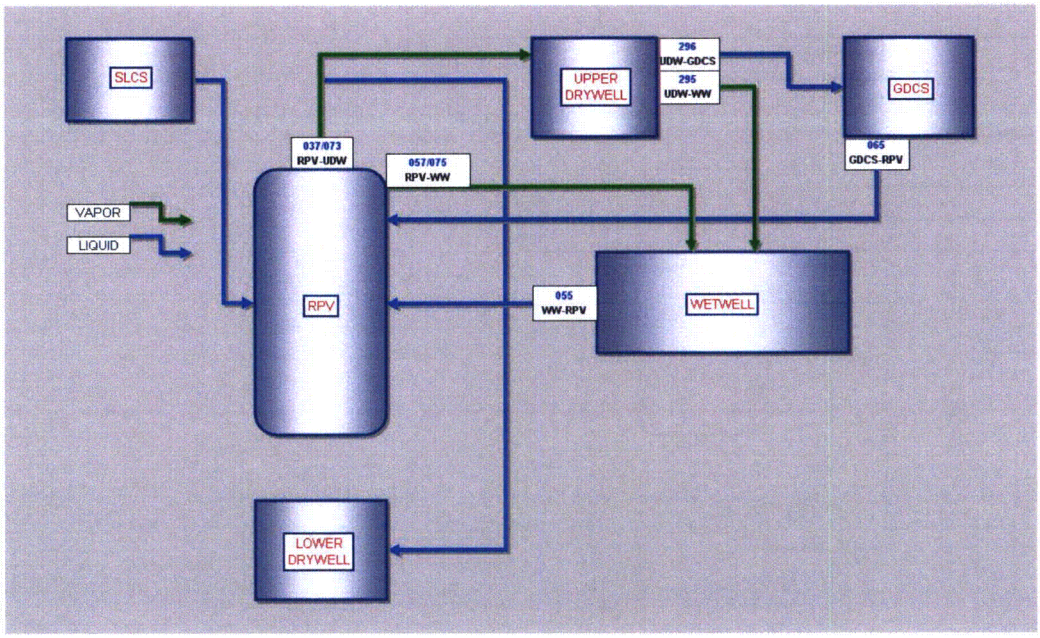

Estimation and Modeling of Effective Fission Product Decontamination Factor for ESBWR Containment – Part 2

Authors: Ilona Lindholm, Ari Auvinen, Yuko Enqvist, Karri Penttilä, Tuomo Sevón, Riitta Zilliacus

Confidentiality